Title
Exploring the Effects of Chimeric Antigen Receptor Sequence on CAR-T Cell Function by Rational Protein Design

Author
CHEN, XIMIN

Publication Date
2020

Peer reviewed|Thesis/dissertation

UNIVERSITY OF CALIFORNIA

Los Angeles

Exploring the Effects of Chimeric Antigen Receptor Sequence on CAR-T Cell Function by Rational Protein Design

A dissertation submitted in partial satisfaction of requirements for the degree

Doctor of Philosophy in Chemical Engineering

by

Ximin Chen

2020

ABSTRACT OF THE DISSERTATION

Exploring the Effects of Chimeric Antigen Receptor Sequence on CAR-T Cell Function by Rational Protein Design

by

Ximin Chen

Doctor of Philosophy in Chemical Engineering

University of California, Los Angeles, 2020

Professor Yvonne Y. Chen, Chair

Adoptive T-cell therapy has emerged as one of the most promising treatment modalities for cancer. CD19 chimeric antigen receptor (CAR)-T cell therapy has shown remarkable success in treating hematological malignancies, but robust clinical efficacy has not yet been observed with the vast majority of CARs targeting other tumor-associated antigens. Several recent reports suggest that antigen-independent, tonic signaling by CARs may be detrimental to T-cell function, and that the CD19 CAR's unique potency may be attributed to its lack of tonic signaling. Our goal is to study the impact of tonic signaling on CAR-T cell function and investigate protein engineering strategies to optimize non-CD19 CAR design. Here, we report that robust CAR-T cell function *in vivo* can be achieved by applying rational protein engineering to achieve a non-zero, calibrated level of tonic signaling. We also discovered a generalizable strategy to fine-tune CAR signaling by imposing structural changes through the insertion of alanine residues between the transmembrane and cytoplasmic domains of the CAR. The insertion of two alanines yielded superior CAR variants from a rituximab-based anti-CD20 CAR

and a 14g2a-based GD2 CAR. In addition, we found that CAR tonic signaling could be tuned through sequence hybridization of single-chain variable fragment (scFv) domains. A hybrid CAR incorporating a hybridized scFv sequence derived from the anti-CD20 antibodies rituximab and leu16 demonstrated superior anti-tumor function compared to both of the parental CARs, resulting in the first example of a CD20 CAR that outperformed a CD19 CAR in the Raji xenograft model to our knowledge. Through transcriptomic, epigenetic and metabolomic studies, we observed that CAR tonic signaling was associated with an upregulation of metabolic activity, which likely potentiates rapid effector function upon antigen stimulation, but could also lead to early exhaustion. Tuning of tonic-signaling intensity through alanine insertion and scFv hybridization yielded CARs that enable T cells to both quickly eliminate established tumors and maintain long-term tumor clearance *in vivo*. RNA-seq and ATAC-seq analysis further indicated that the two protein-engineering strategies explored in our study could yield synergistic effects on improving CAR-T cell function. Our study reveals the importance of tonic-signaling intensity tuning as a previously unknown feature of CAR-T cell biology, and provides generalizable strategies for novel, next-generation CAR design.

The dissertation of Ximin Chen is approved.

Harold G. Monbouquette

Junyoung O. Park

Anna Wu Work

Yvonne Y. Chen, Committee Chair

University of California, Los Angeles

2020

TABLE OF CONTENTS

LIST OF FIGURES

LIST OF SUPPLEMENTARY FIGURES AND TABLES

ACKNOWLEDGEMENT

First and foremost, I would like to express my sincere gratitude to my advisor Dr. Yvonne Chen for her guidance and unreserved support over the past six years. Her diligence, passion for science and excellent work ethics are truly admirable. She introduced me to the CAR-T cell therapy field, patiently helped me acquire all the basic experimental skills and taught me how to think as a scientist. As a mentor, her unceasing dedication and genuine suggestions guided me through numerous setbacks in my research projects and accelerated my personal growth. Through the years working with her, I acquired the right mindset to deal with the frustration and excitement of the uncertainty in research, learned to attend to details while not losing the big picture, and developed scientific literacy and a critical mind. I really appreciate her time, advice, encouragement, patience and funding which made my PhD experience productive and stimulating. It was a really rewarding experience to work with her, and she is a role model for me in many ways.

I am grateful to my thesis committee members, Drs. Anna M. Wu, Junyoung O. Park and Harold G. Monbouquette for their helpful suggestions and insightful comments on my research. I give my heartfelt thanks to Dr. Junyoung O. Park for his supervision on metabolomic studies to elucidate the mechanism of CAR-T cell function. I am thankful for Dr. Anna M. Wu and Dr. Kirstin A. Zettlitz for helpful discussions on anti-CD20 scFv sequences. Special thanks to my collaborators Dr. Xiangzhi Meng from Sun lab at UCLA for analyzing RNA-seq and ATAC-seq data and Aliya Lakhani from Park lab for assistance in data acquisition and analysis in metabolomic studies. Their fast turnaround in analysis enabled me to draft my manuscript and finish my research projects on time.

None of my work would be possible without the support of former and current members of the Chen lab. First, I wish to express my greatest appreciation to Dr. Mobina Khericha and Laurence Chen, for their numerous intellectual and experimental contributions. I thank Dr. ZeNan Chang and Dr. Christopher Ede for serving as great mentors in the lab, especially when I first

started. I thank Dr. Patrick Ho, Dr. Eugenia Zah and Dr. Meng-Yin Lin for being constant sources of useful technical discussion as well as having the patience to teach me new techniques in the lab. I would like to acknowledge Dr. Tasha Lin for her valuable clinical insights on my project as well as her constant supply of snacks. I am also grateful for Chris Nam, Andrew Hou, Amy Hong, Justin Clubb, Mobina Roshandell, Caitlin Harris, and Dr. Chris Walthers for their technical and emotional support, especially during the COVID-19 pandemic. I would like to acknowledge some undergraduate students, rotation students and staff members in the Chen lab who have worked with me – Emma Salvestrini, Amanda Shafer, Anya Alag, Yunfeng Ding, Demetri Nicolaou, Wallace Wennerberg, Jaimie Chen, Sabah Rahman, Brenda Ji and Paul Ayoub, who not only contributed to experiments used in this dissertation but also brought happiness to the whole lab.

In addition, I would like to extend my appreciation to several former and current graduate students from other research labs at UCLA for their collaboration and technical support. I would like to thank Dr. Duo Xu and Zheng Cao for their help in animal experiments, Dr. John Billingsley for his help editing my dissertation as well as Josh Bangayan, Suwen Li, Yang Zhou, Yanruide Li, Dr. Anjie Zhen for providing reagents, instruments, cell lines and other supplies. I would also like to thank my wonderful friends at UCLA for all the great memories that we have made and more exciting memories to come. Graduate school would not have been as enjoyable without them.

This thesis could not become a reality without help and support from many individuals and labs at UCLA. Dr. Willy Hugo and Katherine M. Sheu provided helpful guidance and discussions on RNA-seq data analysis, and Dr. Ying Zhen from UCLA QCB Collaboratory for assisting with analysis of amplicon sequencing data. I want to thank Suhua Feng, Marco Morselli, Shawn Cokus and Mahnaz Akhavan (UCLA BSCRC BioSequencing Core Facility), UCLA Molecular Instrument Center and UCLA MIC for their technical support. Many experiments in this dissertation were performed with instrumentation and computational resources from the Eli and Edythe Broad Center of Regenerative Medicine and Stem Cell Research – Molecular, Cell, and Developmental Biology Microscopy Core, the UCLA Jonsson Comprehensive Cancer Center (JCCC) Flow

Cytometry Core Facility supported by the National Institutes of Health (P30 CA016042), and the Hoffman2 Shared Cluster provided by the UCLA Institute for Digital Research and Education's Research Technology Group.

Last but not least, I would like to express my sincere gratitude to my family, in particular, my parents, for their support and unconditional love. In the past four and a half years, I wasn't able to go back home due to visa issues. My parents flew to the states three times a year to visit. Finally, I would like to thank my boyfriend Biao Xiang for his love and encouragement all the time.

This work kindly supported by grants from the Alliance for Cancer Gene Therapy and the Cancer Research Institute awarded to Yvonne Y. Chen as well as the UCLA Council on Research Faculty Research Grant awarded to Junyoung O. Park.

VITA

EDUCATION

2010 – 2014	University of California, San Diego, San Diego, CA B.S. Chemical Engineering

AWARDS

2019	American Association of Immunologists Poster Prize Immunology LA 2019
2020	Trainee Scholarship Keystone eSymposia – Advances in Cancer Immunotherapy

EXPERIENCE

09/2014 – 11/2020	Laboratory of Prof. Yvonne Chen, UCLA Rational Protein Engineering for Optimization of CAR-T Cell Therapy for Cancer
06/2013 – 09/2013	Laboratory of Dr. Dietrich Khlheyer, Juelich Research Center, Germany Performance analysis of microfluidic chromatographic separation device
09/2011 – 06/2013	Laboratory of Prof. Xiaohua Huang, UCSD Microfluidic device for single-cell capturing and analysis

TEACHING EXPERIENCE

Spring 2018	Graduate Teaching Assistant Course: Separation Process
Winter 2017, Fall 2015	Graduate Teaching Assistant Course: Molecular Biotechnology Laboratory

PUBLICATIONS

1. Ede C, **Chen X**, Lin M-Y, Chen YY. Quantitative analyses of core promoters enable precise engineering of regulated gene expression in mammalian cells. *ACS Synthetic Biology*. 2016;5(5):395-404.
2. Chang ZL, Lorenzini MH, **Chen X**, Tran U, Bangayan NJ, Chen YY. Rewiring T-cell responses to soluble factors with chimeric antigen receptors. *Nature Chemical Biology*. 2018;14(3):317-324
3. **Chen X**, Khericha M, Lakhani A, Meng X, Salvestrini E, Chen LC, Shafer A, Alag A, Ding Y, Nicolaou D, Park OJ, Chen YY. Rational tuning of CAR tonic signaling yields superior T-cell therapy for cancer. 2020. (*under review*)

PATENT

Yvonne Y. Chen, **Ximin Chen**. Anti-CD20 chimeric antigen receptors and related methods and compositions for the treatment of cancer. U.S. Provisional Patent Application No. 62/984,139 (2020)

PRESENTATIONS

1. **Ximin Chen** Emma Salvestrini, Demetri Nicolaou, Paul Ayoub, Yunfeng Ding, Anya Alag and Yvonne Chen. Investigation of tonic signaling behavior and their effect on CAR-T cells. *Keystone eSymposia – Advances in Cancer Immunotherapy*, August 18, 2020 (oral presentation)
2. **Ximin Chen** Emma Salvestrini, Demetri Nicolaou, Paul Ayoub, Yunfeng Ding, Anya Alag and Yvonne Chen. Investigation of tonic signaling behavior and their effect on CAR-T cells. *ImmunologyLA*, Skirball Cultural Center, Los Angeles, CA. June 28, 2019 (poster presentation)
3. **Ximin Chen** Emma Salvestrini, Demetri Nicolaou, Paul Ayoub, Yunfeng Ding, Anya Alag and Yvonne Chen. Investigation of tonic signaling behavior and their effect on CAR-T cells. *UCLA Biomedical/Life Science Innovation Day*, University of California Los Angeles May 22, 2019 (poster presentation)
4. **Ximin Chen**, Demetri Nicolaou, Yunfeng Ding and Yvonne Chen. Systematic investigation of parameters that affect *in vivo* CAR-T cell function. *Cell Therapies and Bioengineering Conference*, UCSF, San Francisco, CA, September 20, 2018 (oral presentation)
5. **Ximin Chen,** Yunfeng Ding and Yvonne Chen. Establishing a high-throughput screening platform for rapid isolation of high-performance chimeric antigen receptors. UCLA Chemical and Biomolecular Engineering Department, May 7, 2018 (oral presentation)

Chapter 1: Design parameters of chimeric antigen receptors (CARs) for adoptive cell therapy

CHIMERIC ANTIGEN RECEPTOR (CAR)-T CELL THERAPY

In recent decades, immunotherapy has provided numerous breakthroughs in cancer therapeutics, including cancer vaccines, antibody therapy, checkpoint blockade therapy, and adoptive cell therapy (ACT). ACT relies on the generation of T cells capable of eradicating tumor cells. Tumor-specific T cells may be tumor-infiltrating lymphocytes (TILs) isolated from tumors or patient-derived T cells that are genetically engineered to express chimeric antigen receptors (CARs). T cells can be expanded *ex vivo* and reinfused back into patients for tumor-cell lysis (Figure 1.1).

CAR-T cell therapy is recognized as a promising approach in immunotherapy and has gained tremendous success in cancer treatments over the course of several decades. To date, there are three CAR-T cell therapy products—axicabtagene ciloleucel (Yescarta, by Gilead) and tisagenleuluecel (Kymriah, by Novartis)—were approved by the FDA for certain CD19+ B-cell malignancies (Calmes-Miller, 2018; Gliead, 2020; Rose, 2017), suggesting that T-cell therapy is an advanced strategy in cancer therapeutics. Unlike T-cell receptor (TCR)-based adoptive T-cell therapy, CAR-T cells can recognize tumor antigens independent of the major histocompatibility complex (MHC). As such, CARs can be engineered to recognize a broader range of tumor associated antigens. CARs engineered to target CD19, a pan-B-cell marker, have achieved up to 90% complete remission rates in treating relapsed and/or refractory chronic lymphocytic leukemia (CLL), acute lymphocytic leukemia (ALL) and non-Hodgkin lymphoma (NHL) (Brentjens et al., 2013; Brentjens et al., 2011; Kalos et al., 2011; Kochenderfer et al., 2015; Kochenderfer et al., 2017; Maude et al., 2014; Neelapu et al., 2017; Schuster et al., 2017; Turtle et al., 2016). The success of CD19 CAR-T cell therapy has stimulated the translation of this

approach to target other malignancies. To date, CARs for over 60 tumor-associated targets have been evaluated in both preclinical and clinical settings (Arndt et al., 2020; MacKay et al., 2020). The next two leading candidates of CAR-T cell therapy are anti-CD22 and anti-B-cell maturation antigen (BCMA) (Brudno et al., 2018; Bu et al., 2018; D'Agostino et al., 2017). Despite the rapid increase in clinical trials of CAR-T cell therapy, the success of the CD19 CAR has not yet been replicated in CARs targeting other antigens.

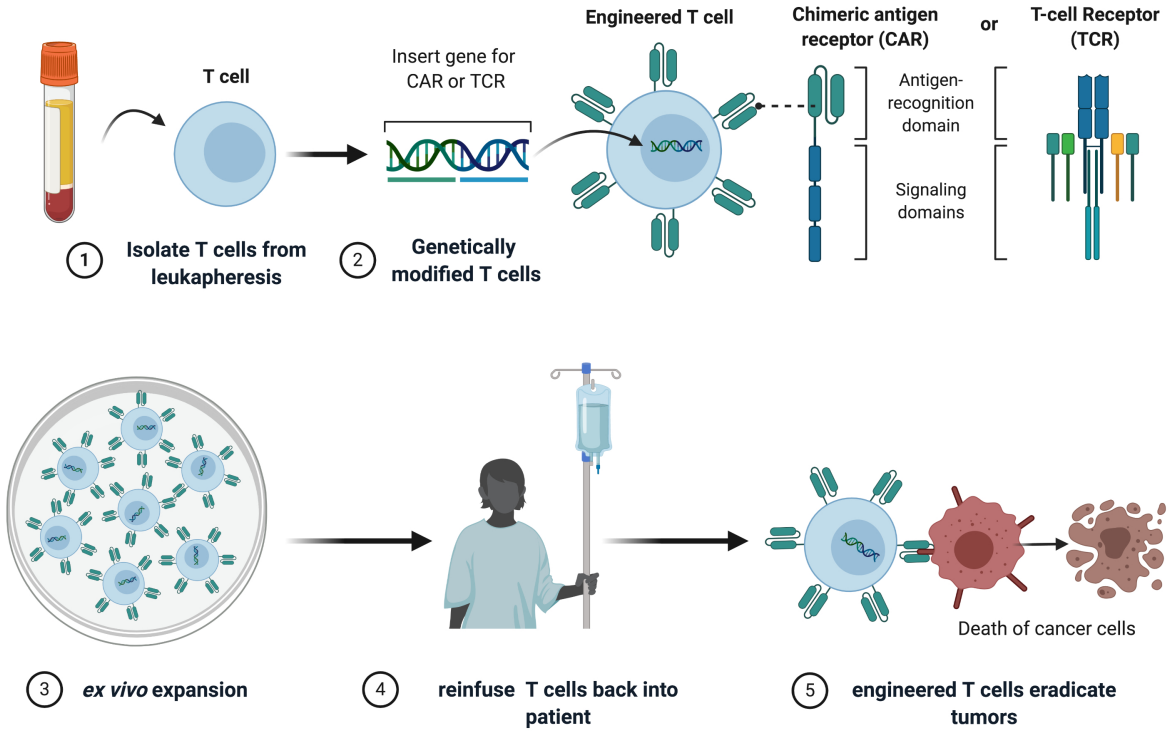

Figure 1.1. Adoptive T-cell therapy overview. T cells are isolated from patients' leukapheresis product, genetically engineered to express CARs or TCRs, expanded *ex vivo* and reinfused back into patients for tumor eradication. Figure was adapted from 'CAR-T Cell Therapy Overview' (BioRender.com, 2020)

CHIMERIC ANTIGEN RECEPTOR DESIGN

Following the introduction of CARs in the 1980s, the design of engineered CARs has evolved into four generations, depicted in Figure 1.2A. An antibody-derived single-chain variable fragment (scFv) is the most commonly used extracellular domain of CARs to facilitate antigen recognition. The extracellular domain provides antigen recognition and structural support for

CAR/antigen binding between T cells and target cells. Each scFv contains two types of regions: the framework region (FR) and the complementary determining region (CDR) (Figure 1.2B) (Chothia and Lesk, 1987; Chothia et al., 1989; Kabat and Wu, 1971; Martin, 1996). First-generation CARs consist of a scFv, a spacer region, and a transmembrane domain connecting an intracellular signaling domain derived from CD3ζ or FcRγ (Dotti et al., 2014; Sadelain et al., 2013). Second-generation and third-generation CARs are comprised of one or two additional intracellular costimulatory domains (CD28, 4-1BB, CD27, OX40, ICOS, etc) (Dotti et al., 2014; MacKay et al., 2020; Majzner and Mackall, 2019; Sadelain et al., 2013), respectively, for optimal T-cell activation and improved proliferation and persistence. Some preclinical and clinical data comparing second-generation and third-generation CARs suggest that certain third-generation CARs are superior while others are not (Abate-Daga et al., 2014; Guedan et al., 2018; Ramos et al., 2018). This mixed evidence suggests that the addition of an extra costimulatory domain is not always beneficial and can sometimes be detrimental to CAR-T cell function. One design of a fourth-generation CAR, known as “T cell redirected for universal cytokine killing” (TRUCK), is a second-generation CAR with the addition of a constitutive or inducible payload encoding for cytokines or chemokines that recruit other immune cells to eradicate tumors (Chmielewski and Abken, 2015; Dotti et al., 2014; MacKay et al., 2020). Another design of the fourth-generation CAR incorporates an inducible suicide gene in a second- or third-generation CAR, as a safety switch (Li et al., 2018). Most clinical trials use second-generation CARs (80%) and the most commonly used costimulatory domains are 4-1BB (54.5%) and CD28 (32.7%) (MacKay et al., 2020).

FACTORS THAT AFFECT CAR-T CELL PERFORMANCES

Despite increasing investment in understanding CAR design principles, the process of developing new CARs remains highly dependent on trial and error. New CAR variants are generated by combining extracellular spacers, transmembrane domains, cytoplasmic signaling

domains, and various ligand-binding domains and are tested empirically to determine final clinical candidates. Although this method can always yield functional candidates, it does not always yield optimal ones. Comparisons between CAR candidates are not truly head-to-head due to confounding factors, such as antigens, antigen density, spacer length, CAR expression level and costimulatory domains that contribute to CAR functionality.

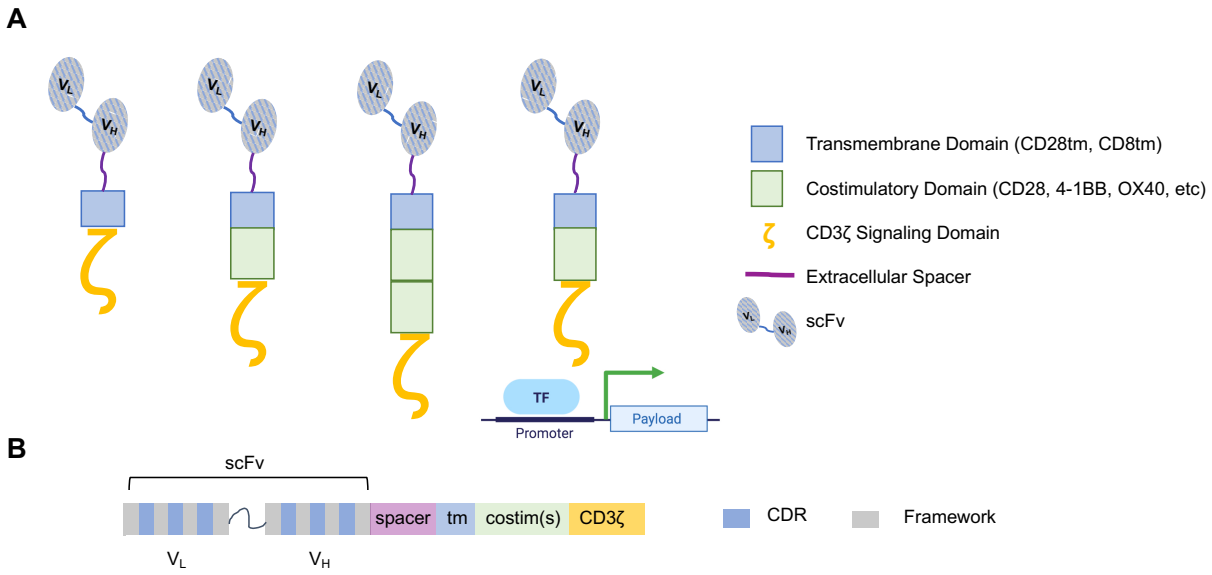

Figure 1.2 Chimeric antigen receptor design. (A) CARs consist of an extracellular domain, which is mainly derived from scFvs of antibodies, an extracellular spacer, a transmembrane domain, and intracellular domains. First-generation CARs contain only one signaling domain whereas second- and third-generation CARs have one to two costimulatory domains in addition to the CD3ζ signaling domain. Fourth-generation CARs combine a second-generation CAR and either a suicide gene as a safety switch or a gene cassette encoding for immunomodulators. (B) Both chains of the scFv contain three CDRs for epitope recognition and framework regions for structural support.

While CD28 and 4-1BB are the most commonly used costimulatory domains, as previously indicated, neither one has proven to be functionally superior to the other in different contexts. In one study, CD19 CAR-T cells expressing the CD28 costimulatory domain outperformed those with the 4-1BB costimulatory domain in targeting a tumor with low antigen density (Majzner et al., 2020). In another study, 4-1BB-CARs triggered T-cell proliferation and

persistence, but CD28-CARs exhibited stronger phosphorylation and effector T-cell activity shortly after stimulation (Salter et al., 2018; Song et al., 2011; Zhang et al., 2007). In short, a definitive conclusion indicating the superiority of either costimulatory domain has not been reached.

In addition to costimulatory domains, another parameter that needs to be taken into account when comparing CAR-T cell performance is the structural relationship between the CAR and its antigen. The affinity of the scFv can predict CAR-T cell function; CARs expressing a high affinity ROR1-specific scFv have superior performance to those expressing low affinity scFvs (Hudecek et al., 2013). However, CAR-T cell function does not increase indefinitely with increasing affinity of the scFv. Above a certain threshold, CARs are unaffected by the increase in affinity, which is likely because of the avidity of CAR-antigen interaction, e.g., formation of an immunological synapse. Moreover, the spacer length between the scFv and transmembrane domain also affects CAR-T cell function. For example, the recognized epitope for CD19 is membrane distal whereas the epitope for CD20 is membrane proximal (Hudecek et al., 2015; Zah et al., 2016). Therefore, CD19 CARs require a short spacer whereas CD20 CARs require a long spacer to obtain optimal T-cell activation. Lastly, antigen density also plays an important role in CAR-T cell efficacy (Majzner et al., 2020; Ramakrishna et al., 2019). Studies have shown tuning antigen density affects the efficacy of CD19, CD20, CD22, EGFR and Her2 targeting CAR-T cells (Caruso et al., 2015; Fry et al., 2018; Liu et al., 2015; Majzner and Mackall, 2018; Majzner et al., 2020; Majzner et al., 2019; Shah and Fry, 2019; Watanabe et al., 2015).

Decades of CAR studies offer valuable lessons. For example, T-cell exhaustion is one of the unfavorable properties in ACT. It is often characterized by expression of various surface markers, e.g., PD-1, LAG-3, PD-1, CTLA-4, associated with T-cell exhaustion, impaired proliferation, and loss of effector function, e.g., cytokine production and target-cell lysis (Wherry, 2011). Recent advances in omics tools have steered the field towards transcriptomic and epigenetic profiling to define T-cell exhaustion (Chen et al., 2019; Khan et al., 2019; McLane et

al., 2019). Over the past ten years, tonic signaling—antigen-independent signaling—has drawn a lot of attention. Several studies have suggested that tonic signaling, often linked with antigen-independent receptor clustering, induces premature T-cell exhaustion, which is detrimental to the CAR-T-cell therapeutic outcome (Frigault et al., 2015; Gomes-Silva et al., 2017; Guedan et al., 2018; Long et al., 2015; Milone et al., 2009; Watanabe et al., 2016). There are multiple CAR-intrinsic and extrinsic factors that have been reported to contribute to tonic signaling. Certain scFvs have been reported to cause tonic signaling. Frigault et al. have shown that anti-c-Met and anti-mesothelin CARs, in the context of second-generation CARs incorporating a CD28 costimulatory domain, have triggered a constitutive growth phenotype (Frigault et al., 2015). Replacing CD28 with ICOS or 4-1BB abrogates tonic signaling. Moreover, replacing the IgG4 spacer with a CD8α also reduces the constitutive growth phenotype. A study by Long et al. suggested that framework regions of a 14g2a based anti-GD2 CAR are responsible for antigen-independent receptor clustering, which induce premature T-cell exhaustion (Long et al., 2015). Watanabe et al. have shown that deletion of the CH2CH3 spacer reduced tonic T-cell signaling (Watanabe et al., 2016). When the long CH2CH3 spacer was replaced with a medium-length CH3 spacer, tonic signaling behavior was drastically decreased. Intracellular costimulatory domains also contribute to tonic CAR signaling. It has been shown that CD28 and 4-1BB facilitate tonic signaling within different contexts (Frigault et al., 2015; Gomes-Silva et al., 2017; Long et al., 2015; Milone et al., 2009). Taken together, tonic signaling cannot be attributed to a single component of a CAR. Instead, it is result of a combinatorial effect of features from multiple CAR domains. Emerging evidence suggests that there is an optimal configuration of all the components within a CAR to induce maximum CAR-T cell function, which fuels the interests to investigate rational CAR design.

ESTABLISHING A GENERALIZABLE STRATEGY FOR OPTIMAL CAR DESIGN

As CAR-T cell therapy matures, more and more efforts are being made to explore the structural properties and signaling propensities of CARs, and the focus of studies has shifted from trial-and-error empirical testing to fine-tuning and rational design. The focus of this dissertation is to explore generalizable strategies for designing new CAR variants and to elucidate the mechanistic signatures of functionally superior CARs. In Chapter 2, a high-throughput screening platform for rapid isolation of optimal CAR candidates has been constructed in a library screening platform. Certain CAR variants were enriched in an anti-CD20 CAR library after two rounds of screening based on tonic signaling phenotypes and proliferative potential. In addition to high-throughput library screening, rational design approaches were taken to modulate signaling intensity of CAR variants (Chapter 3). Minor sequence variations were shown to trigger differential CAR-T cell performance in both the CD20 and GD2 CAR. To understand the mechanistic basis of functionally superior CARs identified in the previous chapter, multiple omics studies were performed to identify the metabolic, transcriptomic and epigenetic differences of CAR candidates (Chapter 4).

REFERENCES

Abate-Daga, D., Lagisetty, K.H., Tran, E., Zheng, Z., Gattinoni, L., Yu, Z., Burns, W.R., Miermont, A.M., Teper, Y., Rudloff, U.*, et al.* (2014). A Novel Chimeric Antigen Receptor Against Prostate Stem Cell Antigen Mediates Tumor Destruction in a Humanized Mouse Model of Pancreatic Cancer. Human Gene Therapy *25*, 1003-1012.

Arndt, C., Fasslrinner, F., Loureiro, L.R., Koristka, S., Feldmann, A., and Bachmann, M. (2020). Adaptor CAR Platforms-Next Generation of T Cell-Based Cancer Immunotherapy. Cancers (Basel) *12*.

BioRender.com (2020). CAR-T Cell Therapy Overview, pp. https://app.biorender.com/biorender-templates

Brentjens, R.J., Davila, M.L., Riviere, I., Park, J., Wang, X., Cowell, L.G., Bartido, S., Stefanski, J., Taylor, C., Olszewska, M.*, et al.* (2013). CD19-targeted T cells rapidly induce molecular remissions in adults with chemotherapy-refractory acute lymphoblastic leukemia. Sci Transl Med *5*, 177ra138.

Brentjens, R.J., Riviere, I., Park, J.H., Davila, M.L., Wang, X., Stefanski, J., Taylor, C., Yeh, R., Bartido, S., Borquez-Ojeda, O.*, et al.* (2011). Safety and persistence of adoptively transferred autologous CD19-targeted T cells in patients with relapsed or chemotherapy refractory B-cell leukemias. Blood *118*, 4817-4828.

Brudno, J.N., Maric, I., Hartman, S.D., Rose, J.J., Wang, M., Lam, N., Stetler-Stevenson, M., Salem, D., Yuan, C., Pavletic, S.*, et al.* (2018). T Cells Genetically Modified to Express an Anti-B-Cell Maturation Antigen Chimeric Antigen Receptor Cause Remissions of Poor-Prognosis Relapsed Multiple Myeloma. J Clin Oncol *36*, 2267-2280.

Bu, D.X., Singh, R., Choi, E.E., Ruella, M., Nunez-Cruz, S., Mansfield, K.G., Bennett, P., Barton, N., Wu, Q., Zhang, J.*, et al.* (2018). Pre-clinical validation of B cell maturation antigen (BCMA) as a target for T cell immunotherapy of multiple myeloma. Oncotarget *9*, 25764-25780.

Calmes-Miller, J. (2018). FDA Approves Second CAR T-cell Therapy. Cancer Discov *8*, 5-6.

Caruso, H.G., Hurton, L.V., Najjar, A., Rushworth, D., Ang, S., Olivares, S., Mi, T., Switzer, K., Singh, H., Huls, H.*, et al.* (2015). Tuning Sensitivity of CAR to EGFR Density Limits Recognition of Normal Tissue While Maintaining Potent Antitumor Activity. Cancer Res *75*, 3505-3518.

Chen, Z., Ji, Z., Ngiow, S.F., Manne, S., Cai, Z., Huang, A.C., Johnson, J., Staupe, R.P., Bengsch, B., Xu, C.*, et al.* (2019). TCF-1-Centered Transcriptional Network Drives an Effector versus Exhausted CD8 T Cell-Fate Decision. Immunity *51*, 840-855 e845.

Chmielewski, M., and Abken, H. (2015). TRUCKs: the fourth generation of CARs. Expert Opin Biol Ther *15*, 1145-1154.

Chothia, C., and Lesk, A.M. (1987). Canonical structures for the hypervariable regions of immunoglobulins. J Mol Biol *196*, 901-917.

Chothia, C., Lesk, A.M., Tramontano, A., Levitt, M., Smith-Gill, S.J., Air, G., Sheriff, S., Padlan, E.A., Davies, D., Tulip, W.R.*, et al.* (1989). Conformations of immunoglobulin hypervariable regions. Nature *342*, 877-883.

D'Agostino, M., Boccadoro, M., and Smith, E.L. (2017). Novel Immunotherapies for Multiple Myeloma. Curr Hematol Malig Rep *12*, 344-357.

Dotti, G., Gottschalk, S., Savoldo, B., and Brenner, M.K. (2014). Design and development of therapies using chimeric antigen receptor-expressing T cells. Immunol Rev *257*, 107-126.

Frigault, M.J., Lee, J., Basil, M.C., Carpenito, C., Motohashi, S., Scholler, J., Kawalekar, O.U., Guedan, S., McGettigan, S.E., Posey, A.D., Jr.*, et al.* (2015). Identification of chimeric antigen receptors that mediate constitutive or inducible proliferation of T cells. Cancer Immunol Res *3*, 356-367.

Fry, T.J., Shah, N.N., Orentas, R.J., Stetler-Stevenson, M., Yuan, C.M., Ramakrishna, S., Wolters, P., Martin, S., Delbrook, C., Yates, B.*, et al.* (2018). CD22-targeted CAR T cells induce remission in B-ALL that is naive or resistant to CD19-targeted CAR immunotherapy. Nat Med *24*, 20-28.

Gliead (2020). U.S. FDA Approves Kite's Tecartus™, the First and Only CAR T Treatment for Relapsed or Refractory Mantle Cell Lymphoma.

Gomes-Silva, D., Mukherjee, M., Srinivasan, M., Krenciute, G., Dakhova, O., Zheng, Y., Cabral, J.M.S., Rooney, C.M., Orange, J.S., Brenner, M.K.*, et al.* (2017). Tonic 4-1BB Costimulation in Chimeric Antigen Receptors Impedes T Cell Survival and Is Vector-Dependent. Cell Rep *21*, 17-26.

Guedan, S., Posey, A.D., Jr., Shaw, C., Wing, A., Da, T., Patel, P.R., McGettigan, S.E., Casado-Medrano, V., Kawalekar, O.U., Uribe-Herranz, M.*, et al.* (2018). Enhancing CAR T cell persistence through ICOS and 4-1BB costimulation. JCI Insight *3*.

Hudecek, M., Lupo-Stanghellini, M.T., Kosasih, P.L., Sommermeyer, D., Jensen, M.C., Rader, C., and Riddell, S.R. (2013). Receptor affinity and extracellular domain modifications affect tumor recognition by ROR1-specific chimeric antigen receptor T cells. Clin Cancer Res *19*, 3153-3164.

Hudecek, M., Sommermeyer, D., Kosasih, P.L., Silva-Benedict, A., Liu, L., Rader, C., Jensen, M.C., and Riddell, S.R. (2015). The nonsignaling extracellular spacer domain of chimeric antigen receptors is decisive for in vivo antitumor activity. Cancer Immunol Res *3*, 125-135.

Kabat, E.A., and Wu, T.T. (1971). Attempts to locate complementarity-determining residues in the variable positions of light and heavy chains. Ann N Y Acad Sci *190*, 382-393.

Kalos, M., Levine, B.L., Porter, D.L., Katz, S., Grupp, S.A., Bagg, A., and June, C.H. (2011). T cells with chimeric antigen receptors have potent antitumor effects and can establish memory in patients with advanced leukemia. Sci Transl Med *3*, 95ra73.

Khan, O., Giles, J.R., McDonald, S., Manne, S., Ngiow, S.F., Patel, K.P., Werner, M.T., Huang, A.C., Alexander, K.A., Wu, J.E.*, et al.* (2019). TOX transcriptionally and epigenetically programs CD8(+) T cell exhaustion. Nature *571*, 211-218.

Kochenderfer, J.N., Dudley, M.E., Kassim, S.H., Somerville, R.P., Carpenter, R.O., Stetler-Stevenson, M., Yang, J.C., Phan, G.Q., Hughes, M.S., Sherry, R.M.*, et al.* (2015). Chemotherapy-refractory diffuse large B-cell lymphoma and indolent B-cell malignancies can be effectively treated with autologous T cells expressing an anti-CD19 chimeric antigen receptor. J Clin Oncol *33*, 540-549.

Kochenderfer, J.N., Somerville, R.P.T., Lu, T., Yang, J.C., Sherry, R.M., Feldman, S.A., McIntyre, L., Bot, A., Rossi, J., Lam, N.*, et al.* (2017). Long-Duration Complete Remissions of Diffuse Large B Cell Lymphoma after Anti-CD19 Chimeric Antigen Receptor T Cell Therapy. Mol Ther *25*, 2245-2253.

Li, J., Li, W., Huang, K., Zhang, Y., Kupfer, G., and Zhao, Q. (2018). Chimeric antigen receptor T cell (CAR-T) immunotherapy for solid tumors: lessons learned and strategies for moving forward. J Hematol Oncol *11*, 22.

Liu, X., Jiang, S., Fang, C., Yang, S., Olalere, D., Pequignot, E.C., Cogdill, A.P., Li, N., Ramones, M., Granda, B.*, et al.* (2015). Affinity-Tuned ErbB2 or EGFR Chimeric Antigen Receptor T Cells Exhibit an Increased Therapeutic Index against Tumors in Mice. Cancer Res *75*, 3596-3607.

Long, A.H., Haso, W.M., Shern, J.F., Wanhainen, K.M., Murgai, M., Ingaramo, M., Smith, J.P., Walker, A.J., Kohler, M.E., Venkateshwara, V.R.*, et al.* (2015). 4-1BB costimulation ameliorates T cell exhaustion induced by tonic signaling of chimeric antigen receptors. Nat Med *21*, 581-590.

MacKay, M., Afshinnekoo, E., Rub, J., Hassan, C., Khunte, M., Baskaran, N., Owens, B., Liu, L., Roboz, G.J., Guzman, M.L.*, et al.* (2020). The therapeutic landscape for cells engineered with chimeric antigen receptors. Nat Biotechnol *38*, 233-244.

Majzner, R.G., and Mackall, C.L. (2018). Tumor Antigen Escape from CAR T-cell Therapy. Cancer Discov *8*, 1219-1226.

Majzner, R.G., and Mackall, C.L. (2019). Clinical lessons learned from the first leg of the CAR T cell journey. Nat Med *25*, 1341-1355.

Majzner, R.G., Rietberg, S.P., Sotillo, E., Dong, R., Vachharajani, V.T., Labanieh, L., Myklebust, J.H., Kadapakkam, M., Weber, E.W., Tousley, A.M.*, et al.* (2020). Tuning the Antigen Density Requirement for CAR T-cell Activity. Cancer Discov *10*, 702-723.

Majzner, R.G., Theruvath, J.L., Nellan, A., Heitzeneder, S., Cui, Y., Mount, C.W., Rietberg, S.P., Linde, M.H., Xu, P., Rota, C.*, et al.* (2019). CAR T Cells Targeting B7-H3, a Pan-Cancer Antigen, Demonstrate Potent Preclinical Activity Against Pediatric Solid Tumors and Brain Tumors. Clin Cancer Res *25*, 2560-2574.

Martin, A.C. (1996). Accessing the Kabat antibody sequence database by computer. Proteins *25*, 130-133.

Maude, S.L., Frey, N., Shaw, P.A., Aplenc, R., Barrett, D.M., Bunin, N.J., Chew, A., Gonzalez, V.E., Zheng, Z., Lacey, S.F.*, et al.* (2014). Chimeric antigen receptor T cells for sustained remissions in leukemia. N Engl J Med *371*, 1507-1517.

McLane, L.M., Abdel-Hakeem, M.S., and Wherry, E.J. (2019). CD8 T Cell Exhaustion During Chronic Viral Infection and Cancer. Annu Rev Immunol *37*, 457-495.

Milone, M.C., Fish, J.D., Carpenito, C., Carroll, R.G., Binder, G.K., Teachey, D., Samanta, M., Lakhal, M., Gloss, B., Danet-Desnoyers, G.*, et al.* (2009). Chimeric receptors containing CD137 signal transduction domains mediate enhanced survival of T cells and increased antileukemic efficacy in vivo. Mol Ther *17*, 1453-1464.

Neelapu, S.S., Locke, F.L., Bartlett, N.L., Lekakis, L.J., Miklos, D.B., Jacobson, C.A., Braunschweig, I., Oluwole, O.O., Siddiqi, T., Lin, Y.*, et al.* (2017). Axicabtagene Ciloleucel CAR T-Cell Therapy in Refractory Large B-Cell Lymphoma. N Engl J Med *377*, 2531-2544.

Ramakrishna, S., Highfill, S.L., Walsh, Z., Nguyen, S.M., Lei, H., Shern, J.F., Qin, H., Kraft, I.L., Stetler-Stevenson, M., Yuan, C.M.*, et al.* (2019). Modulation of Target Antigen Density Improves CAR T-cell Functionality and Persistence. Clin Cancer Res *25*, 5329-5341.

Ramos, C.A., Rouce, R., Robertson, C.S., Reyna, A., Narala, N., Vyas, G., Mehta, B., Zhang, H., Dakhova, O., Carrum, G.*, et al.* (2018). In Vivo Fate and Activity of Second- versus Third-Generation CD19-Specific CAR-T Cells in B Cell Non-Hodgkin's Lymphomas. Mol Ther *26*, 2727-2737.

Rose, S. (2017). First-Ever CAR T-cell Therapy Approved in U.S. Cancer Discov *7*, OF1.

Sadelain, M., Brentjens, R., and Riviere, I. (2013). The basic principles of chimeric antigen receptor design. Cancer Discov *3*, 388-398.

Salter, A.I., Ivey, R.G., Kennedy, J.J., Voillet, V., Rajan, A., Alderman, E.J., Voytovich, U.J., Lin, C., Sommermeyer, D., Liu, L.*, et al.* (2018). Phosphoproteomic analysis of chimeric antigen receptor signaling reveals kinetic and quantitative differences that affect cell function. Sci Signal *11*.

Schuster, S.J., Svoboda, J., Chong, E.A., Nasta, S.D., Mato, A.R., Anak, O., Brogdon, J.L., Pruteanu-Malinici, I., Bhoj, V., Landsburg, D.*, et al.* (2017). Chimeric Antigen Receptor T Cells in Refractory B-Cell Lymphomas. N Engl J Med *377*, 2545-2554.

Shah, N.N., and Fry, T.J. (2019). Mechanisms of resistance to CAR T cell therapy. Nat Rev Clin Oncol *16*, 372-385.

Song, D.G., Ye, Q., Carpenito, C., Poussin, M., Wang, L.P., Ji, C., Figini, M., June, C.H., Coukos, G., and Powell, D.J. (2011). In Vivo Persistence, Tumor Localization, and Antitumor Activity of CAR-Engineered T Cells Is Enhanced by Costimulatory Signaling through CD137 (4-1BB). Cancer Research *71*, 4617-4627.

Turtle, C.J., Hanafi, L.A., Berger, C., Gooley, T.A., Cherian, S., Hudecek, M., Sommermeyer, D., Melville, K., Pender, B., Budiarto, T.M.*, et al.* (2016). CD19 CAR-T cells of defined CD4+:CD8+ composition in adult B cell ALL patients. J Clin Invest *126*, 2123-2138.

Watanabe, K., Terakura, S., Martens, A.C., van Meerten, T., Uchiyama, S., Imai, M., Sakemura, R., Goto, T., Hanajiri, R., Imahashi, N.*, et al.* (2015). Target antigen density governs the efficacy of anti-CD20-CD28-CD3 zeta chimeric antigen receptor-modified effector CD8+ T cells. J Immunol *194*, 911-920.

Watanabe, N., Bajgain, P., Sukumaran, S., Ansari, S., Heslop, H.E., Rooney, C.M., Brenner, M.K., Leen, A.M., and Vera, J.F. (2016). Fine-tuning the CAR spacer improves T-cell potency. Oncoimmunology *5*, e1253656.

Wherry, E.J. (2011). T cell exhaustion. Nat Immunol *12*, 492-499.

Zah, E., Lin, M.Y., Silva-Benedict, A., Jensen, M.C., and Chen, Y.Y. (2016). T Cells Expressing CD19/CD20 Bispecific Chimeric Antigen Receptors Prevent Antigen Escape by Malignant B Cells. Cancer Immunol Res *4*, 498-508.

Zhang, H., Snyder, K.M., Suhoski, M.M., Maus, M.V., Kapoor, V., June, C.H., and Mackall, C.L. (2007). 4-1BB is superior to CD28 costimulation for generating CD8+ cytotoxic lymphocytes for adoptive immunotherapy. J Immunol *179*, 4910-4918.

Chapter 2. Establishing a high-throughput screening platform for rapid isolation of optimal CAR variants

ABSTRACT

Chimeric antigen receptor (CAR)-T cell therapy has emerged as one of the most promising treatment modalities for cancer. Growing numbers of CAR candidates have been evaluated in both pre-clinical and clinical studies. In conventional CAR studies, a limited number of variants are built and characterized individually, which results in a labor-intensive development process. Here, we developed a high-throughput screening platform that enables phenotypic and functional screening of CAR libraries in primary T cells to isolate functionally superior variants. It has been reported that tonic signaling causes pre-mature T-cell dysfunction, which led to inferior *in vivo* performance of CAR-T cells. Thus, the elimination of clones that contributed to tonic signaling was incorporated in the screening platform. In addition, T-cell proliferation upon stimulation is indicative of a good therapeutic response. In this screening platform, our strategy was to isolate clones that exhibited antigen-dependent proliferative benefit without tonic signaling behaviors. An anti-CD20 library containing 1024 variants in the light chain (V_L) of scFv was generated and subjected to two rounds of screening based on expression of phenotypic markers on T cells that were indicative of tonic signaling and the CAR-T cells' ability to proliferate upon repeated antigen stimulation. Deep sequencing was performed to identify enriched variants from the final pool of T cells.

INTRODUCTION

CAR-T cell therapy has achieved remarkable success in recent decades. From 2014 to 2018, there was a 4-fold increase globally in clinical trials of CARs (MacKay et al., 2020). Standard CAR construction strategies are based on attaching limited sets of hinge regions and cytoplasmic signaling domains including co-stimulatory and signaling domains with ligand-binding moieties specific to the antigen of interest (MacKay et al., 2020; Sadelain et al., 2013). The most commonly used targeting domain – scFv – is derived from antibodies and different research labs have different preferences for the choice of the scFv. To date, the functional characterization of novel CAR candidates is performed empirically by evaluating their anti-tumor effect in primary T cells. In most of CAR studies, a small number of CAR variants are generated and evaluated individually. Thus, the process of CAR design requires substantial trial-and-error and individual assessment of CAR clones can be labor-intensive.

Indeed, a high-throughput screening platform for rapid isolation of lead candidates would be substantially beneficial to CAR development. Previously, studies on CAR library screening yielded functionally superior candidates, suggesting that this is a robust method to generate effective CAR variants (Di Roberto et al., 2020; Duong et al., 2013; Rydzek et al., 2019; Sommermeyer et al., 2017; Ying et al., 2019). A study by Sommermeyer *et al.* generated a panel of humanized anti-CD19 scFvs derived from humanization of the FMC63-based scFv and screened the libraries for their ability to bind to targets before evaluating their activities in CAR-T cell format (Sommermeyer et al., 2017). This CAR library screening study was based on the screening of scFv variants, which were later incorporated in CAR format for functional characterization. To study the effect of signaling molecules on CAR-T cell, Duong et al. constructed a CAR library by ligating a random number and order of signaling adaptors and costimulatory molecules, etc., from the TCR signaling pathway to the C terminus of the CD28 transmembrane domain. The library members were introduced into Jurkat cells and evaluated for their ability to trigger CD69 expression on Jurkat cells upon stimulation (Duong et al., 2013).

Rydzek and colleagues studied both CD19- and ROR-1 CAR libraries in a dual reporter cell line containing the nuclear factor κB (NF-κB) and nuclear factor of activated T cells (NFAT) response elements as a measurement of T-cell activation (Rydzek et al., 2019).

A critical aspect of library screening is to identify parameters that are conducive to T-cell function. It has been suggested that T-cell persistence and proliferation are associated with good clinical outcomes (Guedan et al., 2018). Recently, researches have shown that tonic signaling – antigen independent signaling – would cause premature T-cell exhaustion, which leads to T-cell dysfunction (Frigault et al., 2015; Gomes-Silva et al., 2017; Long et al., 2015; Watanabe et al., 2016). Various studies have incorporated tonic signaling as one of the methods for CAR-T cell characterization (Bloemberg et al., 2020; Mirzaei et al., 2019; Smith et al., 2019; Zheng et al., 2018), but it has not yet been incorporated into CAR library screening methods. Therefore, we were interested in evaluating tonic signaling as a parameter within a library-based screening platform.

There are multiple phenotypic and functional readouts that can be used to evaluate CAR tonic signaling, including antigen-independent T-cell expansion, cytokine production, up-regulation of inhibitory markers, constitutive phosphorylation of CD3ζ, and T-cell differentiation to effector phenotype (Frigault et al., 2015; Long et al., 2015). Among these properties, only a few can be implemented in the context of library screening. One of the measurements of tonic signaling is inhibitory marker expression without antigen stimulation. As previously described in the study by Long and colleagues, the tonically signaling GD2 CAR-T cells sustained elevated expression of the inhibitory markers PD-1, TIM-3 and LAG-3, which are associated with an exhausted T-cell phenotype (Long et al., 2015). Thus, exhaustion-related phenotypic markers can be readily incorporated in a high-throughput screening setting.

In this study, we were interested in using a CAR targeting CD20 antigen for platform validation. CD19 and CD20 are both highly expressed on a wide range of B-cell malignancies, in particular, lymphoma (Johnson et al., 2009; Kehrl et al., 1994). CD20 expresses at a slightly

higher level than CD19 in the lymph node according to the NCBI database. However, consistent clinical success is only achieved in CARs targeting CD19 (Grigor et al., 2019; Guedan et al., 2018; Majzner and Mackall, 2019; Yamamoto et al., 2019). CARs targeting CD20 have achieved some clinical efficacy in phase I/II trials, though not as promising as the CD19 CAR (Till et al., 2012; Zhang et al., 2016). In addition, there are multiple clinical reports suggesting CD19-antigen loss or downregulation after treatment of CD19 CAR-T cells (Majzner and Mackall, 2019), but this phenomenon is rarely reported in CD20 CAR-T cell therapy, which indicates that CD20 might be a better target. Therefore, optimization of CD20 CARs may provide a promising alternative to patients that do not benefit from CD19 CAR-T cell therapy. Moreover, engineering a CD20 CAR would enable side-by-side comparisons of efficacy with the "gold-standard" CD19 CAR in the same disease model.

Unlike previous studies to screen for scFv binding, we proposed to construct an scFv library which would be incorporated into the CAR format for downstream analysis. The impact of scFv affinity on CAR-T cell performance is still poorly understood and thus purely screening for a good binder may not fully recapitulate performance in the CAR format. Therefore, high-affinity scFv variants do not necessarily translate into superior CARs. In fact, these variants may increase the risk of causing serious adverse effect due to on-target, off-tumor toxicities when CAR-expressing T cells recognize lowly expressed antigens on healthy cells (Liu et al., 2015; Morgan et al., 2010; Richman et al., 2018). The high-affinity 4D5-scFv based HER2 CAR-T cells have been reported to trigger fatal pulmonary toxicity and cytokine release syndrome (CRS) due to recognition of low level HER2 expression on healthy lung tissues (Morgan et al., 2010). Similarly, a 14g2a-based CAR with enhanced affinity was generated by incorporating the E101K mutation onto the scFv and triggered a stronger antitumor effect in T cells against $GD2^{+}$ neuroblastoma xenografts *in vivo* compared to the CAR-T cells without the mutation (Richman et al., 2018). However, the improvement in *in vivo* anti-tumor efficacy led to substantial T-cell infiltration and proliferation in the brain, which was associated with subsequent lethal

neurotoxicity (Liu et al., 2015; Richman et al., 2018). Liu et al. also suggested that high-affinity CARs recognized antigens that expressed at any levels including both cancerous and normal cells, which could lead to on-target, off-tumor toxicities (Liu et al., 2015). Moreover, high-affinity CARs stimulate a strong T-cell activation signal, which might lead to early T-cell exhaustion and the loss of T-cell effector function (Engels et al., 2012).

Here, we primarily focus on the scFv's effect on CARs. As previously shown, certain framework regions contributed to constitutive signaling (Long et al., 2015). To further study the cause of tonic signaling, the framework regions (FRs) and the complementarity determining regions (CDRs) of GD2- and CD19-scFv were swapped to generate new CAR variants. Despite one hybrid CAR failing to express on the surface, the CAR-T cells comprising CD19 CDRs and GD2 FRs exhibited elevated levels of the tonic signaling phenotype compared to the parental CD19 CAR-T cells, which suggested that certain framework regions of the scFv caused the antigen-independent T-cell signaling. We hypothesize that amino acid variations on scFv could impact T-cell function, and therefore sought to study the sequence-dependent properties of scFvs that impact the CAR-T cell functionality. It is unclear the specific residues on framework regions that cause differential T-cell performance; thus a library-based method could let us validate more combinations of residues than running functional tests on individual CAR candidates.

In addition to implementing the evaluation of tonic signaling propensities, T-cell proliferation, one of the indicators of a positive therapeutic outcome, was also considered as part of the screening pipeline. Thus, in this study, we developed a high-throughput platform that enabled direct phenotypic and functional readouts of anti-CD20 CAR variants in primary T cells to isolate clones that exhibited a low tonic signaling profile and demonstrated favorable proliferation.

METHODS

Construction of an anti-CD20 library

Degenerate oligonucleotides were synthesized by IDT with one position limited to two amino acid between FMC63- and Leu16-based scFvs. Barcodes were cloned near the mutated gene and had at least ten times more diversity than the library to ensure unique barcodes for each variant. PCR product of the library were digested and inserted into the retroviral or AAV backbone.

Cell line maintenance

HEK 293T, Raji and Jurkat Clone E6–1 cell lines were obtained from ATCC. The Jurkat cell line with a 4xNFAT-dsEGFP reporter was a gift from Dr. Arthur Weiss (University of California, San Francisco). The Jurkat cell lines with 3x or 6x NFAT-mCherry-PEST reporter were cloned in house by attaching three or six copies of NFAT binding elements downstream of the IL-2 minimal promoter to drive expression of mCherry linked with a degradation tag PEST. The Jurkat cell line with an EGFP NFκB reporter was a gift from Dr. Xin Lin (MD Anderson). The TM-LCL cell line, an Epstein-Barr virus (EBV)-transformed lymphoblastoid cell line, was a gift from Dr. Michael Jensen (Seattle Children's Research Institute). K562 cells were a gift from Dr. Michael C. Jensen (Seattle Children's Research Institute). $CD19^{+}CD20^{+}$ K562 cells were generated as previously described (Zah et al., 2016). Jurkat cell lines 4x-NFAT-d2EGFP reporter, or NFκB-GFP reporter, and primary human T cells, Raji, and K562 cells were cultured in RPMI-1640 (Lonza) with 10% heat-inactivated FBS (HI-FBS; ThermoFisher). HEK 293T cells were cultured in DMEM (HyClone) supplemented with 10% HI-FBS.

Viral production

Retroviral production Retroviral supernatants were produced by transient co-transfection of HEK 293T cells with plasmids encoding CARs, and pRD114/pHIT60 virus-packaging plasmids (gifts from Dr. Steven Feldman), using linear polyethylenimine (PEI, 25 kDa; Polysciences).

Supernatants were collected 48 and 72 hours later and pooled after removal of cell debris by a 0.45 μm membrane filter.

Adeno-associated viral production Three million HEK293T cells were seeded in 9 mL of DMEM + 10% HI-FBS in 10-cm dishes with total 18 dishes. Twenty-four hours later, cells were transfected with a plasmid containing the CD20 library in the AAV backbone along with two viral packaging helper plasmidspXX6 and pHelper (gifts from Dr. David Schaffer) using linear PEI. Seventy-two hours post-transfection, cells were harvested from the dishes and resuspended in AAV lysis buffer (50 mM Tris, 150 mM NaCl, pH 8.2) at 800 μL per dish. Cells were treated with 10 U/mL benzonase (EMD Millipore) followed by three freeze-thaw cycles for complete lysis. Supernatants were collected and overlayed at the top of an iodixanol (Stemcell Technologies) density gradient that were at 15%, 25%, 40% and 54% density, respectively. Phenol red was added to every other layer. AAV lysates were centrifuged at 30,000 rpm for 18 hrs at 4 °C. Purified AAV supernatants were harvested at the interfacial layer between 40% and 54% iodixanol, followed by buffer exchanged into PBS +0.01% Tween-20.

SpCas9 protein generation and purification

SpCas9 sequences were obtained from Addgene (plasmid 42230, pX330 vector) and subcloned into the pET28a vector expression system for transformation into the BL21DE3 *E. coli* strain. SpCas9 expression was induced by IPTG when *E. coli* reached an OD_{600} of 0.4-0.7. Bacteria were harvested at stationary phase followed by sonication to obtain cell lysate. Proteins from lysates were purified by a Ni-NTA column (Genesee) and concentrations were measured via Bradford assay (Bio-Rad).

Cell line and human primary T cell generation

Retroviral transduction Healthy donor blood was obtained from the UCLA Blood and Platelet Center. $CD8^+$ T cells were isolated using RosetteSep Human $CD8^+$ T Cell Enrichment Cocktail

(StemCell Technologies) following the manufacturer's protocol. T cells were stimulated with CD3/CD28 Dynabeads (ThermoFisher) at a 3:1 cell-to-bead ratio on Day 0 (day of isolation) and transduced with retroviral supernatant on Day 2 and Day 3. Dynabeads were removed on Day 7. T cells were cultured in RPMI-1640 supplemented with 10% HI-FBS and fed with recombinant human IL-2 (ThermoFisher) and IL-15 (Miltenyi) every 2 days to final concentrations of 50 U/mL and 1 ng/mL, respectively. For library screening, target populations were enriched by fluorescence-activated cell sorting (FACS) on FACSAria (II) (BD Bioscience) at the UCLA Flow Cytometry Core Facility.

Site-specific integration via CRISPR/Cas9 Freshly isolated $CD8^+$ T cells were activated with CD3/CD28 Dynabeads (ThermoFisher) at 3:1 cell-to-bead ratio. Seventy-two hours post-activation, dynabeads were removed and recovered for 4 hours prior to editing by CRISPR/Cas9. Chemically synthesized sgRNAs targeting the TRAC locus (C*A*G*GGUUCUGGAUAUCUGUGUUUUAGAGCUAGAAAUAGCAAGUUAAAAUAAGGCUAGUCCGUUAUCAACUUGAAAAAGUGGCACCGAGUCGGUGCUU*U*U*) were purchased from Synthego and resuspended in Tris-HCl buffer. SpCas9 protein was added to sgRNA at a 1:1 molar ratio (300 pmol of each) to generate ribonucleoprotein (RNP) complex. Five million human $CD8^+$ T cells were mixed with the RNP complex in 100 µL of nucleofection solution (Mirus Bio). The RNP and cell mixture was nucleofected using program T-017 of the Amaxa Nucleofector 2b Device (Lonza) following the manufacturer's protocol. Cells were incubated at room temperature for 10 min prior to adding complete RPMI + 10% HI-FBS supplemented with IL-2 and IL-15 at 50 U/mL and 1 ng/mL, respectively. AAV were added T-cell culture and incubated at 37°C for 48 hours.

T-cell enrichment with repeated stimulation

CAR^+ T cells were seeded at 3 x 10^6 cells/well in 12-well plates and coincubated with target cells at a 2:1 E:T ratio. Gamma-irradiated TMLCL target cells (1.5 x 10^6 cells/well) were added

every two days to stimulate T cells and a total of two stimulations were performed. The target cell population was enriched by FACS sorting.

Antibody staining for flow-cytometry analysis

EGFRt expression was measured with biotinylated cetuximab (Eli Lilly; biotinylated in-house), followed by PE-conjugated streptavidin (Jackson ImmunoResearch #016-110-084). CAR expression was quantified by surface epitope staining using Flag tag (DYKDDDDK tag, APC, clone L5, BioLegend #637308). Antigen-independent activation-marker expression of CAR-T cells was evaluated by antibody staining for CD107a (Pacific Blue, clone H4A3, BioLegend 328624.) CD137 (PE/Cy7, clone 4B4-1, BioLegend #309818) and PD-1 (FITC, clone EH12.2H7, BioLegend #329904) on Day 11 (i.e., 11 days after Dynabead addition and 4 days after Dynabead removal). All samples were analyzed on a MACSQuant VYB flow cytometer (Miltenyi), and the resulting data were analyzed using the FlowJo software (TreeStar).

Amplicon library construction and analysis

Genomic DNA was isolated from cells using DNeasy kit (Qiagen) following the manufacture's protocol. Amplicon-seq libraries were generated using a modified 2-round PCR protocol as previously described (Klindworth et al., 2013). In short, locus-specific primers flanking the barcode and V_L region with 5' adapter sequences added to allow subsequent PCR were used to amplify regions of interest on genomic DNA. Both rounds of PCR used 2X KAPA HiFi HotStart ReadyMix (KAPA Biosystems). The first round of target amplification used 25 cycles with 12.5 nm genomic DNA input, 1 μM of primers and 2xKAPA HiFi HotStart ReadyMix in a 25 μL reaction. Forward primer (P5) and reverse primer (P7) sequences are 5' - TCGTCGGCAGCGTCAGATGTGTATA AGAGACAGAGCCCTCACTCCTTCTCTAGGCG and 5' - GTCTCGTGGGCTCGGAGATGTGT ATAAGAGACAGGGAGCCACCACCGCTAGTACTG, respectively. AmPure XP beads (Beckman Coulter) were used to size select target DNA

sequences containing added adaptors on the 5' end. In a second round of PCR adding sequencing indexes, 5 µL of sample from the prior step was used as template along with 1 µM primers and PCR mastermix. Water was added to bring up the reaction volume to 50 µL. A total of 8 cycles of PCR was performed followed by AMPure beads selection. The final product was run on a TapeStation D1000 DNA chip to verify the size. Fastq files from RNA-seq were quality-examined by FastQC (Linux, v0.11.8). Reads were processed by cutadapt (Linux, v1.18) to remove reads with low quality (quality score < 33) and to trim adapters. A barcode lookup table containing the NNKNNKttagNNKNNKaatgNNKNNK barcode and their corresponding sequences were extracted using Matlab. Raw counts for each variant sequence were recorded.

RESULT

Identifying parameters that distinguish CARs with differential performance

T-cell activation is triggered by phosphorylation of CD3ζ on T-cell receptors (TCR) or chimeric antigen receptors (CAR) which leads to a series of downstream signal transduction events (Hartman and Groves, 2011). The activation of signaling adaptor proteins induces activation of various transcription factors, for example, the NFAT and NF-κB, etc. Various studies have used Jurkat cells with a NFAT and/or NF-κB reporter to evaluate TCR- or CAR- based T-cell activation (Albrecht et al., 2002; Chang et al., 2018; Lin and Weiss, 2003; Rydzek et al., 2019).

In our study, we sought to adapt this easy-to-use NFAT/NF-κB reporter system to screen for lead CAR candidate in library setting. To validate the system, we first tested the reported response using two CARs of known function. The FMC63-based CD19 CAR with a short extracellular spacer (later referred to as CD19S) is a well-known CAR with a robust and superior function, and the Leu16-based CD20 CAR with a long extracellular spacer (later referred to as CD19L) is robust but functionally inferior to the CD19 CAR (Zah et al., 2016)(Figure 2.1A). The idea was to see if these two CARs triggered differential activation of the reporter output, which thus allowed a clear separation among CAR candidates.

CD19S and CD20L CARs were introduced retrovirally into the 4xNFAT-d2EGFP Jurkat reporter cell lines, which contained four copies of the NFAT response element as previously described (Lin and Weiss, 2003). Two CAR-Jurkat cell lines were co-incubated with $CD19^{+}/CD20^{+}$ K562 cells at a 3:1 E:T ratio for 24 hours to stimulate EGFP signaling through NFAT activation (Figure 2.1B). However, there was not a significant difference between these two CAR-T cell lines tested. We reasoned that the duration of CAR stimulation was too long such that all

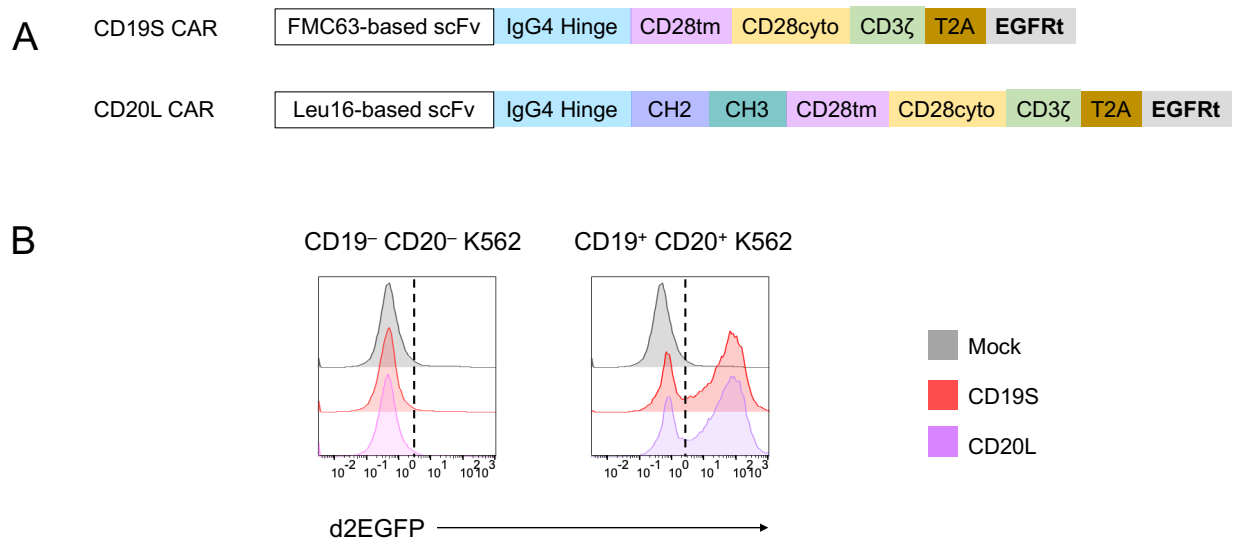

Figure 2.1 NFAT Jurkat reporter responses triggered by CD19 and CD20 CARs in 24hr
(A) CD19S and CD20L CAR schematic.
(B) CD19S and CD20L CAR-Jurkat cell lines were co-incubated with parental K562 ($CD19^{-}$ /$CD20^{-}$) and $CD19^{+}/CD20^{+}$ K562 cells at 3:1 E:T ratio for 24 hours. NFAT reporter output measured by EGFP intensity were quantified by flow cytometry.

signals reached the maximum; thus, there was no difference between CARs with differential performance. Previous studies have suggested that NFAT activation happens within hours after TCR activation (Rudolf et al., 2014). Thus, to capture early activation of NFAT without signal saturation, we tested the NFAT reporter output at 5 and 9 hours and used multiple stimulation conditions (Figure 2.2). However, due to high sensitivity of the reporter system, the use of 4xNFAT-d2EGFP reporter did not reflect the activity of differentially performing CAR variants.

Alternatively, we turned to investigate another reporter system NF-κB for its ability to distinguish cells with different anti-tumor efficacy. The NF-κB Jurkat bearing CD19S or CD20L CARs were stimulated with $CD19^+/CD20^+$ K562 cells. Similar to the NFAT reporter, the NF-κB reporter failed to separate CD19S and CD20L CAR (Figure 2.3). Both reporter systems allowed robust detection of CAR mediated activation of downstream transcription factors, yet the separation of CARs was not achieved. Therefore, we sought to find additional parameters that enabled clear identification of functionally superior variants.

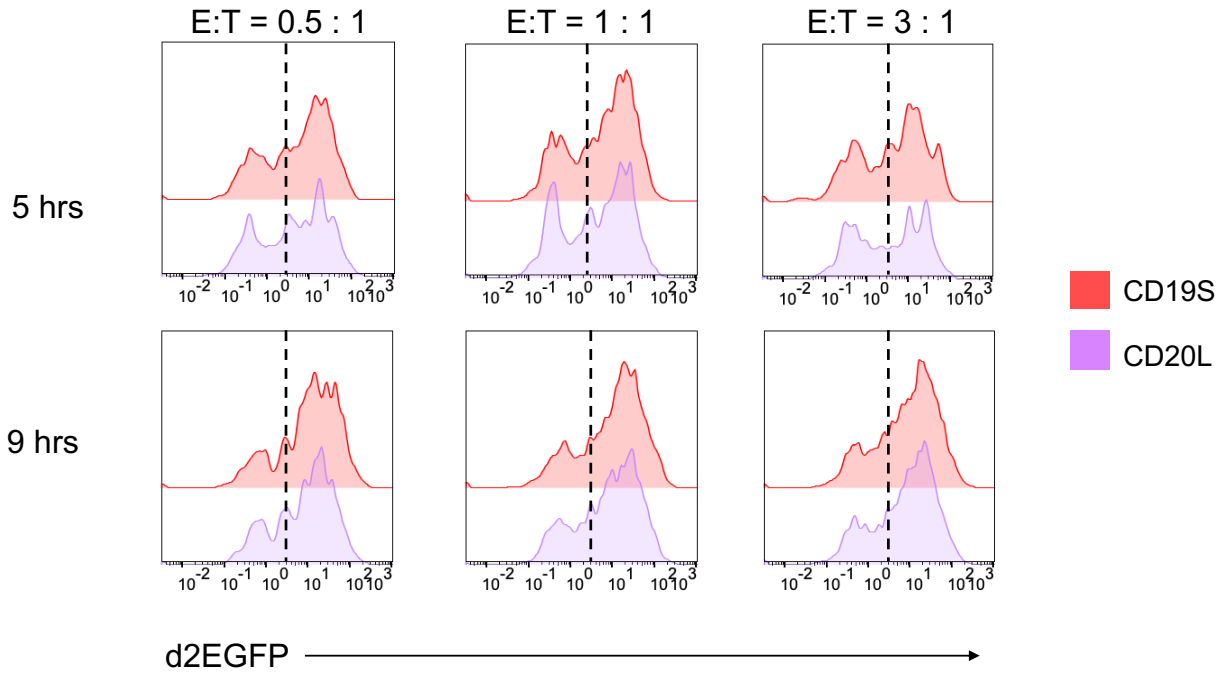

Figure 2.2 Early activation of NFAT Jurkat reporter triggered by CD19 and CD20 CARs
CD19S and CD20L CAR-Jurkat cell lines were co-incubated with parental K562 ($CD19^-/CD20^-$) and $CD19^+/CD20^+$ K562 cells at 0.5:1, 1:1, 3:1 E:T ratio for 5 hr and 9 hrs. NFAT reporter output measured by EGFP intensity were quantified by flow cytometry.

Phenotypic markers are easy to implement in library screening pipelines. Tonically signaling CAR-T cells upregulate inhibitory markers as well as T-cell activation markers on their surface (Long et al., 2015), which make them perfect parameters for use in high-throughput screening. In order to identify phenotypic outputs of CAR-T cells that exhibit antigen-

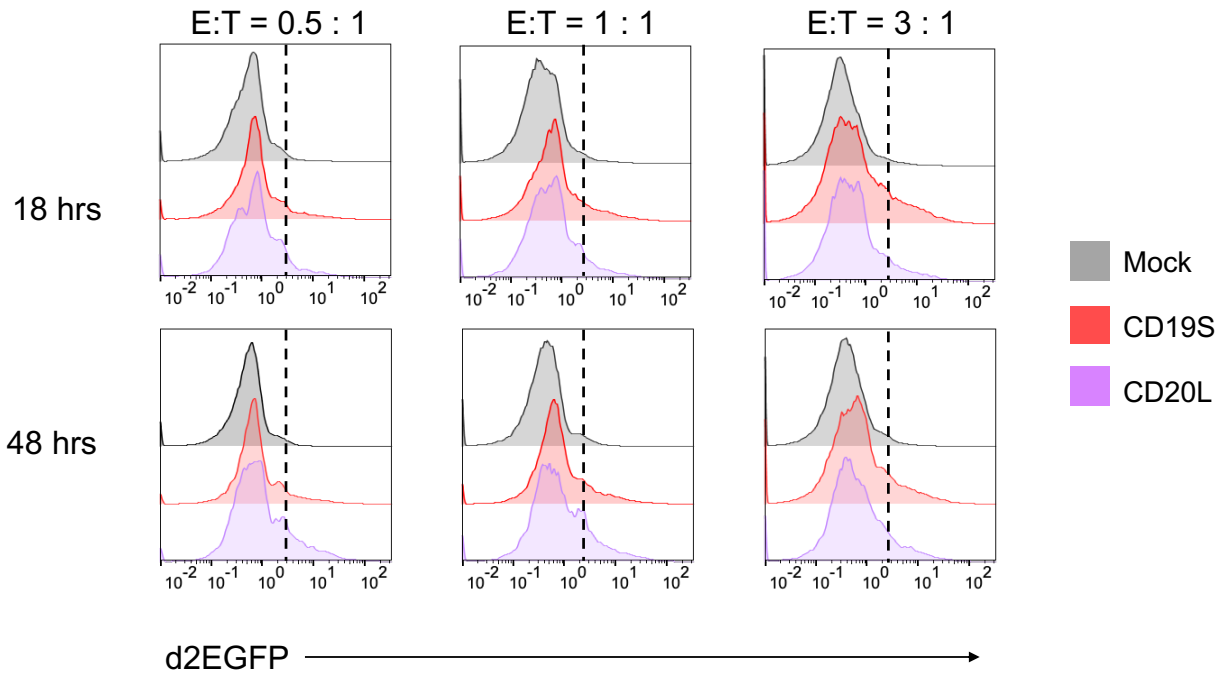

Figure 2.3 CD19 and CD20 CARs trigger similar level of NF-κB activation CD19S and CD20L CAR-Jurkat cell lines were co-incubated with parental K562 ($CD19^-/CD20^-$) and $CD19^+/CD20^+$ K562 cells at 0.5:1, 1:1, 3:1 E:T ratio for 5 hr and 9 hrs. NF-κB reporter output measured by EGFP intensity were quantified by flow cytometry.

independent signaling, we had compared GD2, which was reported to have tonic signaling behavior, and CD19 CAR-T cells in the absence of antigen and evaluated their expression of surface markers (Figure 2.4). In most activation/exhaustion marker expressions, there were distinct differences between GD2 and CD19 CAR-T cells. Specifically, CD107a, CD137 and PD-1 were significantly upregulated in the tonically signaling GD2 CAR-T cells and thus made them good indicators of T-cell tonic signaling in our high-throughput screening pipeline.

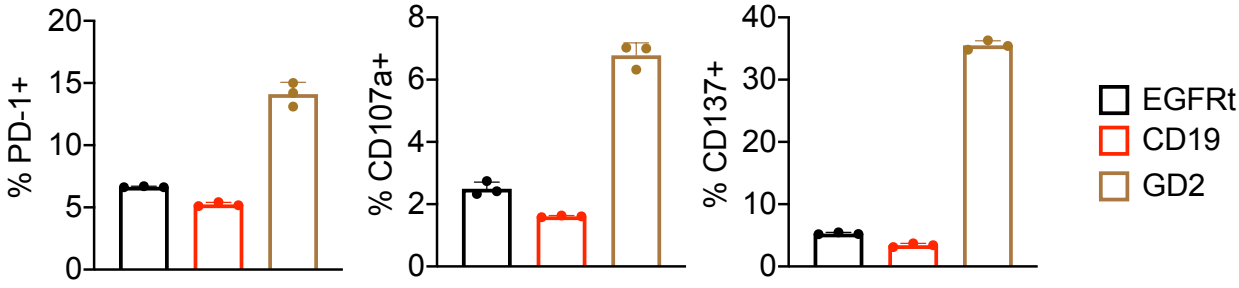

Figure 2.4 GD2 CAR-T cells upregulate surface markers that associated with tonic signaling Freshly isolated CD8 T cells were stimulated with dynabeads and retrovirally transduced to express EGFRt only, CD19s CAR or a 14g2a-based GD2 CAR. Initial stimulation

by dynabeads were removal on Day 7. Four days post dynabeads removal, GD2 CAR-T cells upregulated PD-1, CD107a and CD137 compared to CD19 CAR-T cells and cells expressing only the transduction marker EGFRt.

T-cell proliferation upon antigen stimulation is also another important characteristic of CAR function. We hypothesized that functionally superior CAR-T cells would be preferentially enriched in a mixed culture with stimulation, which allowed identification of lead candidates in library screening. To evaluate our hypothesis, CD19S and CD20L CARs containing CD28 costimulatory domains were mixed in the culture and stimulated with tumor cells. Mixed T-cell culture stimulated by $CD19^{+}/CD20^{+}$ TMLCL allowed better separation of CARs with different performance level compared to Raji stimulated culture (Figure 2.5). Therefore, TMLCL was used for our next optimization study.

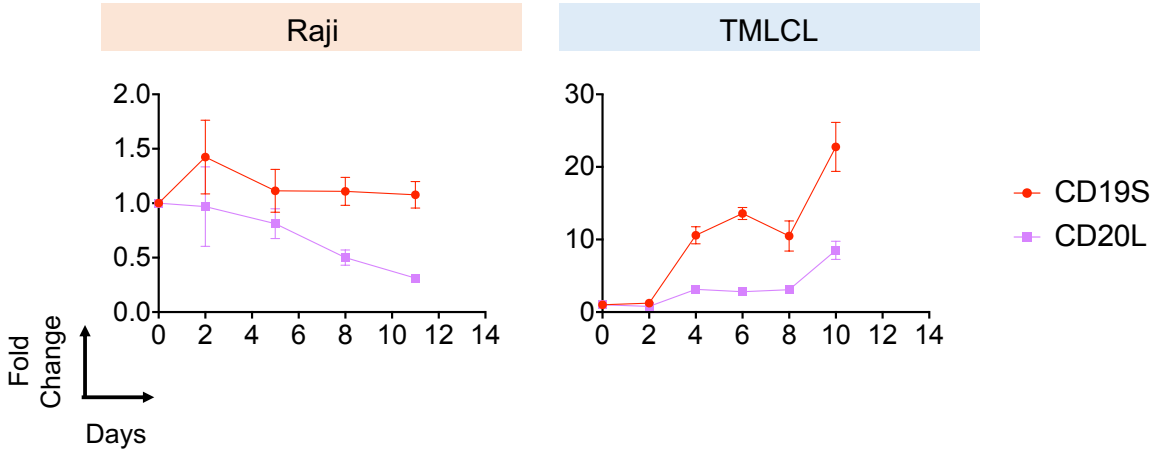

Figure 2.5. **TMLCL allows better separation of CARs with differential performance** CD8 T cells expressing CD19S or CD20L CAR were incubated with γ-irradiated Raji or TMLCL cells at 1:1 E:T ratio with exogenous cytokines IL-2 and IL-15 at 50 U/mL and 1 ng/mL, respectively. Cell counts were monitored every two days by flow cytometry.

To further improve the resolution of different CARs in the T-cell expansion assay, we included the CD20S CAR – a CD20 CAR expressing a short extracellular spacer – in addition to the CD19S and CD20L CARs in the mixed culture study. It has been reported that CD20 requires a long spacer to obtain optimal target recognition and superior anti-tumor function (Zah et al., 2016) (Figure 2.6A). TMLCL cells were added to a long-term mixed culture containing

CD19S, CD20L and CD20S CAR-T cells at 1:1, 1:3.5 and 1:7 E:T ratios with different amounts (10%, 50% or 100%) of the regular level of exogenous cytokines (regular level: IL-2 and IL15 were 50 U/ml and 1 ng/mL, respectively). As the E:T ratio decreased, the separation of CAR-T cell lines decreased. Cytokine concentration did not affect separation of CAR-T cell lines based on their relative function (Figure 2.6B). Going forward, a 1:1 E:T ratio and regular cytokine level were used in the screening pipeline.

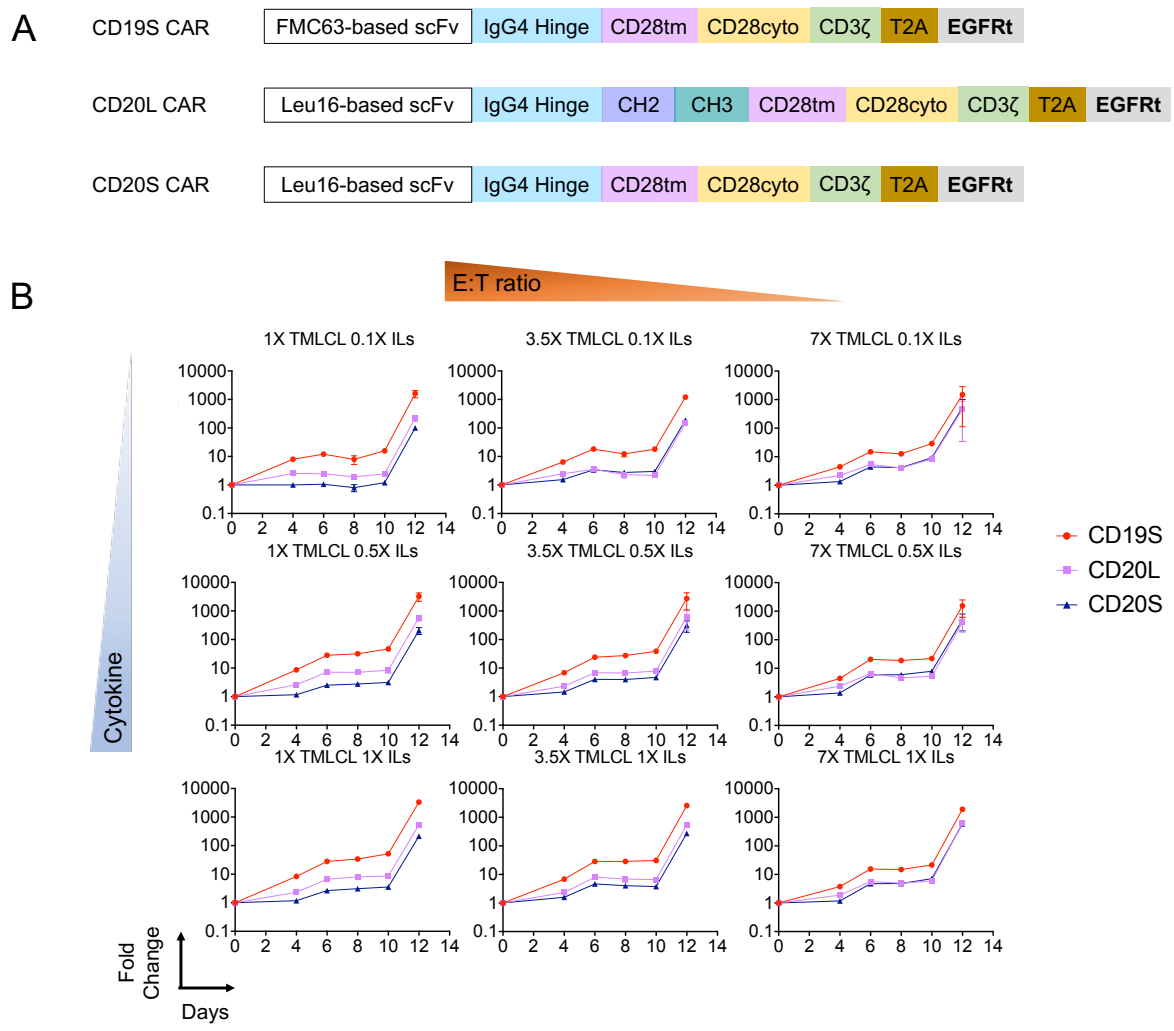

Figure 2.6. Optimization of co-incubation condition for better separation of CARs with differential performance

(A) CD19S, CD20L and CD20S CAR shematic.

(B) CD8 T cells expressing CD19S, CD20L or CD20S CAR were incubated with γ-irradiated TMLCL cells at 1:1 (1X), 1: 3.5 (3.5X) or 1:7 (7X) E:T ratio with 0.1X, 0.5X or 1X exogenous

cytokines (1X ILs indicated regular cytokine level at which IL-2 and IL-15 were 50 U/mL and 1 ng/mL, respectively). Cell counts were monitored every two days by flow cytometry.

Construction of an anti-CD20 library based on framework region mutations

FMC63-based CD19 CAR-T cells have consistently achieved promising preclinical and clinical outcomes, which was attributed to their minimal tonic signaling behavior. To facilitate library generation and study sequence-function relationship, we decided to use the “gold-standard” FMC63 scFv-based CD19 CAR as the template to guide the library design of a CD20 CAR library. As previously reported, certain framework regions cause oligomerization of CARs, which was hypothesized to be the contributor to tonic signaling (Long et al., 2015). In this study, we attempted to engineer the CD20 CAR to as close to CD19 CAR as possible in terms of sequence variation in the framework region such that the newly generated variants could remain intact and bind to the CD20 antigen while exhibiting minimal tonic signaling.

Our goal was to construct a library of CARs that had mutations in FRs that were different between the Leu16- and FMC63-based scFv to evolve the CD20 CAR in the direction of the CD19 CAR. To probe the effect of the framework regions on CAR performance, we rationally designed a CAR library containing mutations in certain framework region residues. Since there is a combinatorial effect of residues at different locations, simply changing every position to match the amino acid with the CD19 scFv might not yield functionally superior variants and instead the new variant could be deleterious. Therefore, we decided to toggle the residues that are different between FRs on two scFvs to get the best combination that leads to a high-performing CAR candidate. To achieve that, Leu16-based CD20 CAR framework regions (FR) were compared against FMC63-based CD19 CAR FRs using the EMBL-EBI sequence analysis tool to identify residues that are different between two FRs (Madeira et al., 2019) (Figure 2.7). The specific residues in the framework region that had been modified for the library should not be part of or contribute to the formation of the secondary structures of the scFvs and CDR

loops. It has been reported that certain residues on the scFv, e.g., vernier zone residues and chain-packing residues at the V_L/V_H interface, are known to modulate antigen-binding by affecting the conformation of CDR loops (Chothia et al., 1985; Foote and Winter, 1992; Makabe et al., 2008; Safdari et al., 2013). Therefore, in our library construction, we retained those critical residues from Leu16 scFv to minimize the potential loss of binding to the antigen. After identifying the conserved residues at the V_L/V_H interface and vernier zone of the CD20 CAR, residues from the CD20 FR were kept. Residues that were different between the two scFvs and did not belong vernier zone, V_L/V_H interface or in the core of the proteins, would be toggled between the two scFvs.

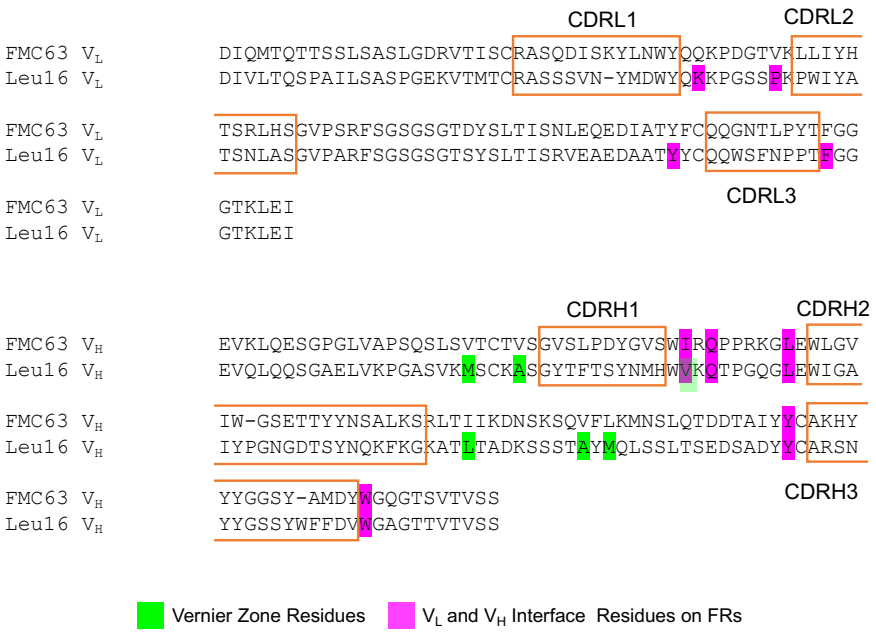

Figure 2.7 Alignments of FMC63-based CD19 and Leu16-based CD20 scFv Light chain and heavy chain sequences of FMC63 and Leu16 were aligned using EMBL-EBI sequence analysis tool. CDR regions were identified using abYsis and were boxed in orange. Residues that belonged to vernier zones (green) or contributed to V_L / V_H Interface (magenta) were highlighted.

In addition, we wanted to avoid generating CAR variants that exhibit tonic signaling behavior. We hypothesized that tonic CAR signaling was caused by receptor aggregation without stimulation. Therefore, to mitigate tonic signaling, we focused on the residues that were "facing out", i.e., had potential interactions with other molecules on cell surface. Core residues

were kept the same to retain protein folding. After applying the criteria listed above, we had 22 and 38 residues that required mutation on the light and heavy chains, respectively, from which we would generate 1.15 x 10^8 variants and it would be impossible to screen in mammalian cells. To reduce the size of the library, we did not apply changes to those positions that couldn't be encoded in degenerate oligos for only two desired amino acids (one from leu16 scFv and one from FMC63 scFv) (Figure 2.8A,B). The library created from the above guideline contains 2^{24} (10^7) variants, which was too cumbersome to manipulate in primary T cells. Therefore, we decided to split it into two sub-libraries (V_H and V_L libraries) containing 1.6 x 10^4 and 1024 variants, respectively. Libraries with mutations in framework regions were constructed by SOE PCR-based degenerate oligonucleotide assembly. Each variant residue was limited to two amino acids.

Figure 2.8 Proposed design of CD20 scFv library DNA sequences of light chain (**A**) and heavy chain (**B**) were shown. Point mutations indicated the degeneracy of oligos that enabled coding for two amino acids in certain positions.

After constructing the library, it was very important to evaluate its diversity and ensure no variant loss. The diversity of the library was evaluated by colony-counting in a small-scale transformation reaction as previously described (Glanville et al., 2009; Jiao et al., 2017; Robin

and Martineau, 2012; Tanaka and Rabbitts, 2010). The diversity of the library was calculated by counting the total number of positive clones (evaluated by colony PCR and then scaled up). Importantly, to achieve full coverage, we used ten times the number of positive clones to the total variant number as previously suggested (Fowler et al., 2014).

Vector copy number per cell is one of the most important metrics in library screening. To ensure the average integration of one copy of the transgene per cells, cells were transduced with retrovirus with an efficiency of 30% or lower to generate an average of one copy of the transgene per cell (Kustikova et al., 2003). Most peripheral human T cells only express a single αchain on the cell surface (Rybakin et al., 2014). Therefore, site-specific integration of the transgene into the TRAC locus by CRISPR/Cas9 with subsequent homologous direct repair (HDR) via AAV offers an alternative means of achieving one copy of transgene insertion per cell.

Rapid isolation of CAR variants with differential performances in polyclonal culture

The workflow of the high-throughput screening platform is depicted in Figure 2.9. Libraries were introduced into human CD8 T cells and were subjected to two rounds of screening to eliminate tonically signaling clones as well as enriching for clones with highly proliferative potential. A pilot screening was done using the retroviral based V_L library (Figure 2.8A) and enrichment was evaluated at each step of screening, including the raw library containing plasmid and cells from pre-sort, post-tonic signaling elimination and post-T-cell expansion.

The CD20 library based on framework variations was introduced into primary CD8 T cells through retroviral transduction at a MOI of 0.5. Cells were stimulated with dynabeads and exogeneous cytokines (IL-2 and IL-15 at 50 U/mL and 1 ng/mL, respectively) for seven days prior to dynabead removal. In the first-round screening at four days post-dynabead removal, cells that upregulated CD107a, CD137 and PD-1 were eliminated by FACS to remove clones that were associated with a tonic signaling phenotype (Figure 2.10). In the second-round of

screening, we looked for CAR-T cells' ability to proliferate upon repeated antigen exposure to allow downstream high-throughput sequencing for enrichment analysis. Sorted cells were stimulated with γ-irradiated TMLCL target cells at a 1:1 E:T ratio on day of co-incubation setup and two days after the first stimulation.

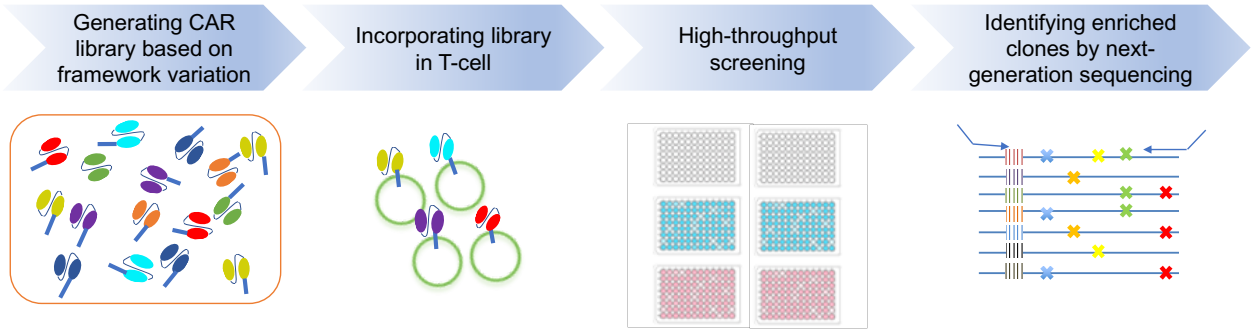

1. Negative selection to eliminate T cells that have antigen-independent expression of exhaustion markers.
2. Positive selection to enrich for CAR-T cells that proliferate upon antigen stimulation.
3. Identification of enriched variants through amplicon sequencing of the gDNA from T cells post-screen.

Figure 2.9 Proposed workflow of high-throughput screening of CD20 library CD8 T cells expressing the CD20 library went into two rounds of screening for isolation of lead candidates. The first round of selection was to eliminate T cells that exhibited antigen-independent expression of exhaustion markers. The second round was a positive selection to enrich for CAR-T cells that proliferated upon antigen stimulation. Enriched variants were identified through amplicon sequencing.

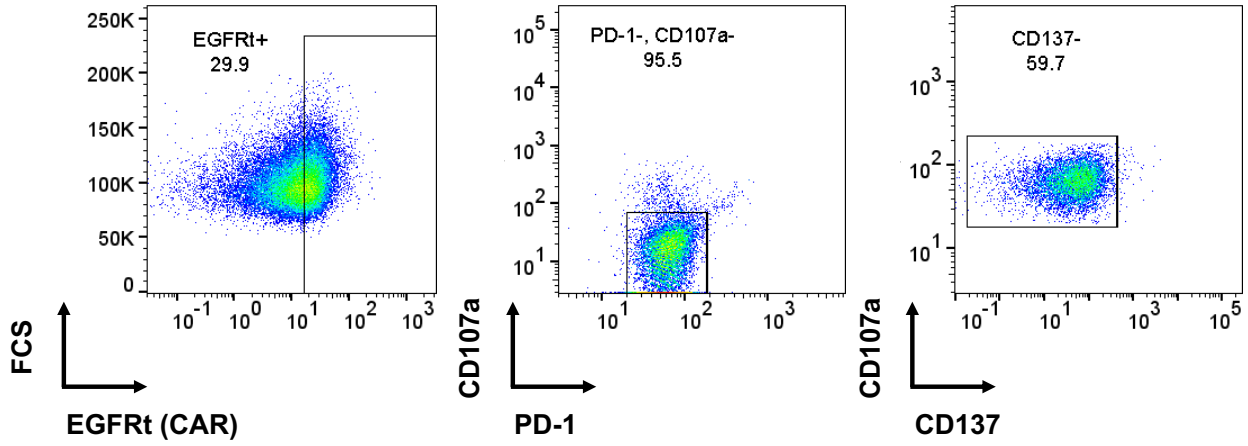

Figure 2.10 Negative selection to eliminate CAR-T cells exhibiting tonic signaling phenotype CD8 T cells retrovirally transduced to express CD20 V_L library were sorted for $EGFRt^+$ to isolate the transduced population, followed by enrichment of the $PD\text{-}1^-CD107a^-CD137^-$ population.

Four days after the initial stimulation, genomic DNA was extracted from the T cells to assess for T-cell clonal expansion by amplicon sequencing. We followed the previously reported protocol to identify enriched protein variants using high-throughput DNA sequencing (Fowler et al., 2014). Raw counts from each of the three populations were calculated by normalization to library size and adjusted for differences among three libraries. To identify enrichment, we plotted column-based z-score heatmaps to show frequency distribution of 30 clones with the highest enrichment and 30 clones with lowest enrichment after two rounds of sorting (Figure 2.11A,B). After each round of sorting, we compared the count to the initial population without undergoing screening. Contrary to expectation, cells sorted by tonic signaling markers did not eliminate any diversity, nor did it strongly enrich or deplete most clones – indicating that sorting through tonic signaling was not an effective method or the choice of surface markers was not fully reflective of tonic signaling behavior. After T-cell expansion upon antigen stimulation, there were differential enrichments and deletion of certain clones (Figure 2.1A,B; Supplementary Table 1-2). In particular, the top three clones were strongly enriched at the final library (Supplementary Table 1) and the last eight were completely eliminated (Supplementary Table 1). The purpose of library screening is to have a pipeline that enables stepwise elimination of diversity and ultimately enriches for the lead candidates. In our study, the choice of tonic signaling markers did not provide a clean result to eliminate non-functional candidates. Thus, we mainly relied on the growth-based assay. However, CAR-T cell function cannot be fully explained by only one set of readouts, which made it less reliable than measurement of polyfunctionality. Therefore, we chose not to pursue this method because it only relied on T-cell expansion to enrich for clones.

A

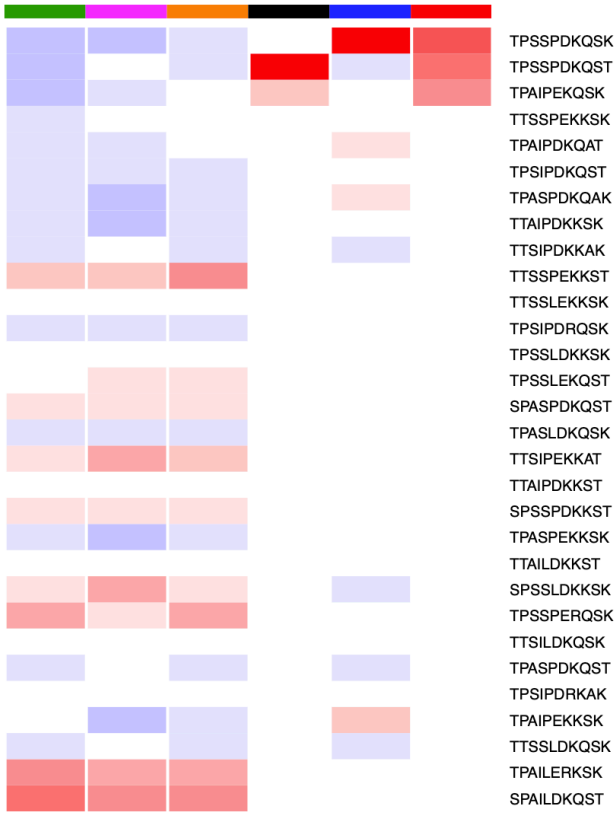

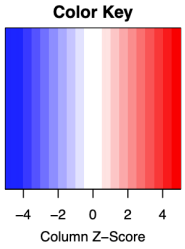

Count: unsorted
Count: post-sort 1st round
Count: post-sort 2nd round
Fold Change: 1st sort to unsorted
Fold Change: 2nd sort to 1st sort
Fold Change: 2nd sort to unsorted

B

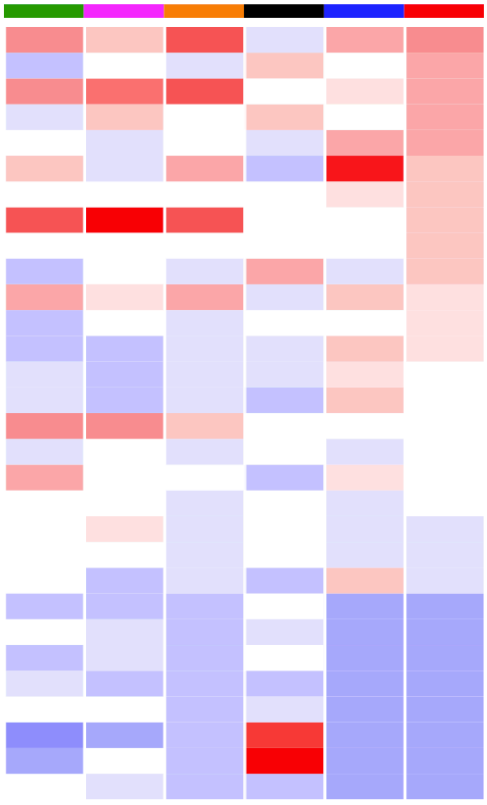

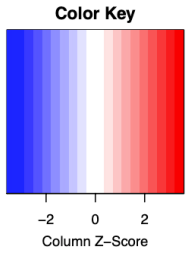

Count: unsorted
Count: post-sort 1st round
Count: post-sort 2nd round
Fold Change: 1st sort to unsorted
Fold Change: 2nd sort to 1st sort
Fold Change: 2nd sort to unsorted

Figure 2.11 Elimination of tonic signaling phenotype does not correlate with final enrichment T cells containing the library of CAR variants had undergone two consecutive steps of screening to remove tonically signaling clones and to enrich for highly proliferative clones. Genomic DNA was extracted from T cells to assess T-cell clonal expansion by amplicon sequencing. Raw count of each variant was normalized to the total read count of the library to calculate relative frequency. Relative frequencies of each clone before stimulation (unsorted), post-tonic signaling elimination (post-sort 1st round) and post-T cell expansion (post-sort 2nd round) were shown as column z-score in the first three columns. The last three columns were fold enrichments between unsorted and sorted samples from the 1st or the 2nd sorting step. Thirty variants that represented the highest (A) or the lowest (B) enrichment in the final library were shown.

In library screening scenarios, controlling vector copy number to one is essential to include only one genomic insertion per cell. Though a literature search, we have found retroviral transduction at MOI of 0.5 generally resulted in 30% or lower transduction efficiency of certain cells, which was expected to generate cells containing an average one copy of the transgene (Kustikova et al., 2003). Further validation of copy number, e.g., ddPCR, is required for accurate quantification in the pooled library. We had tried ddPCR using the primer/probe sets targeting WPRE elements on the MSCV retroviral backbone. However, the results of vector copy number and corresponding transduction efficiency varied from donor to donor despite the use of the same batch of retrovirus and same MOI. Due to high experimental variability, we were unable to accurately estimate total copies of transgene per cells. It is likely that there were multiple variants in one T cell through retroviral transduction in our abovementioned pilot study. Therefore, a more robust method, for example, site-specific integration of CAR libraries into a locus that only contains one copy of the gene. The CRISPR/Cas9 system shows high repeatability and efficiency in site-specific integration of transgenes (Eyquem et al., 2017; Roth et al., 2020; Roth et al., 2018). We had successfully knocked in our library into the TRAC locus. In our attempt, we demonstrated efficient site-specific integration into TRAC locus via CRISPR/Cas9 and AAV (Figure 2.12). Further characterization still needs to be made after finding new parameters for the screening platform.

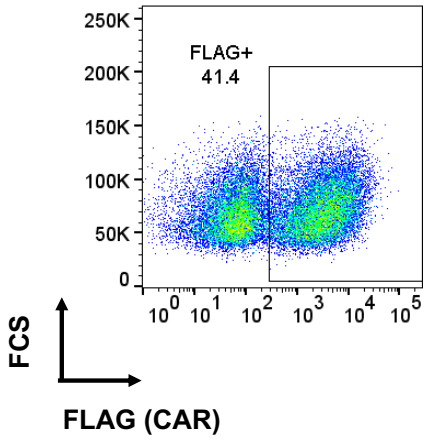

Figure 2.12 Site-specific integration of library into TRAC locus and eliminating T-cells with tonic signaling phenotype CD20 V_L library was site-specifically integrated and sorted for CAR^+ population ($FLAG^+$), followed by enrichment of $PD\text{-}1^-CD107a^-CD137^-$ population.

DISCUSSION

A growing number of CAR candidates have been generated and characterized in recent decades. Increasing cases of clinical trials indicate the success of finding lead CAR candidates. However, most studies evaluated CARs individually, which makes the characterization process labor-intensive. To accelerate the process of CAR identification, we established a high-throughput screening platform for rapid isolation of functionally superior CARs.

In this study, a library containing 1024 CAR variants was successfully integrated into human CD8 T cells via retrovirus or CRISPR/Cas9-mediated site-specific integration into the TRAC locus without loss of diversity. Through a series of optimizations, we identified a growth-based method to enrich for highly proliferative T-cell clones, enabling separation of CAR variants with differential expansion potential upon antigen stimulation. We were able to use the high-throughput amplicon sequencing to identify enrichment and depletion of certain clones, which still require further individual validation *in vitro* and *in vivo*.

Despite showing differential enrichments and deletions of certain clones after T-cell expansion upon antigen stimulation, our library had several limitations. It was generated only

based on framework variation in the V_L region, which limited the number of potential candidates. Light and heavy chains work together to provide target-recognition and antitumor function; thus, the combinatorial effect of residues on both chains remained elusive. In the future, efforts are needed to optimize integration of libraries with high diversity into in primary T cells.

Recent studies have demonstrated the use of NFAT and NF-κB reporter systems to predict CAR function (Albrecht et al., 2002; Chang et al., 2018; Lin and Weiss, 2003; Rydzek et al., 2019). Upon stimulation, CAR recruits phosphorylated ZAP-70, which induces downstream signaling proteins to activate NFAT and NF-κB. The activation of these transcription factors turns on a programed reporter output. We have observed CAR-induced activation in NFAT or NF-κB responsive Jurkat cell lines as early as 5 hr, but the systems were unable to provide clean separation of differentially performing CARs.

By multiple rounds of screening, we hoped to reduce the diversity of the library and have enrichment of certain clones. However, our result showed that elimination of clones expressing PD-1, CD107a and CD137 did not reduce library diversity, indicating that this set of markers might not fully recapitulate CAR tonic signaling. It also suggested the need to assess CAR tonic signaling using multiple parameters. T cells expressing the same CAR variant have a gradient expression of phenotypic markers when being cultured individually. Depletion of cells that exhibited tonic signaling phenotype in a pooled culture might only eliminate a subpopulation of cells with high expression but did not completely eliminate all cells that contained the same variant. Furthermore, the fact that negative screening of tonic signaling did not eliminate any clones implies that tonic signaling may not be completely detrimental to cells. It is conceivable that basal signaling could prime T-cells and prepare them to rapidly respond to target stimulation. Thus, we would like to explore the impact of tonic signaling on CAR-T cells.

In summary, we report an approach to establish a high-throughput screening platform to isolate lead CAR candidates based on tonic signaling and antigen-depending T-cell expansion in primary T cells. The system allows screening for 1024 CAR candidates in a pooled culture

and we believe that it is scalable to higher diversity. One of our finding indicates that tonic signaling might not be detrimental to CAR performance. In our next study, we would like to evaluate the effect of tonic signaling on CAR-T cells and sought to find alternative methods to engineer CD20 CARs for optimal performance.

REFERENCES

Albrecht, B., D'Souza, C.D., Ding, W., Tridandapani, S., Coggeshall, K.M., and Lairmore, M.D. (2002). Activation of nuclear factor of activated T cells by human T-lymphotropic virus type 1 accessory protein p12(I). J Virol *76*, 3493-3501.

Bloemberg, D., Nguyen, T., MacLean, S., Zafer, A., Gadoury, C., Gurnani, K., Chattopadhyay, A., Ash, J., Lippens, J., Harcus, D.*, et al.* (2020). A High-Throughput Method for Characterizing Novel Chimeric Antigen Receptors in Jurkat Cells. Mol Ther Methods Clin Dev *16*, 238-254.

Chang, Z.L., Lorenzini, M.H., Chen, X., Tran, U., Bangayan, N.J., and Chen, Y.Y. (2018). Rewiring T-cell responses to soluble factors with chimeric antigen receptors. Nat Chem Biol *14*, 317-324.

Chothia, C., Novotny, J., Bruccoleri, R., and Karplus, M. (1985). Domain association in immunoglobulin molecules. The packing of variable domains. J Mol Biol *186*, 651-663.

Di Roberto, R.B., Castellanos-Rueda, R., Frey, S., Egli, D., Vazquez-Lombardi, R., Kapetanovic, E., Kucharczyk, J., and Reddy, S.T. (2020). A Functional Screening Strategy for Engineering Chimeric Antigen Receptors with Reduced On-Target, Off-Tumor Activation. Mol Ther.

Duong, C.P., Westwood, J.A., Yong, C.S., Murphy, A., Devaud, C., John, L.B., Darcy, P.K., and Kershaw, M.H. (2013). Engineering T cell function using chimeric antigen receptors identified using a DNA library approach. PLoS One *8*, e63037.

Engels, B., Chervin, A.S., Sant, A.J., Kranz, D.M., and Schreiber, H. (2012). Long-term persistence of CD4(+) but rapid disappearance of CD8(+) T cells expressing an MHC class I-restricted TCR of nanomolar affinity. Mol Ther *20*, 652-660.

Eyquem, J., Mansilla-Soto, J., Giavridis, T., van der Stegen, S.J., Hamieh, M., Cunanan, K.M., Odak, A., Gonen, M., and Sadelain, M. (2017). Targeting a CAR to the TRAC locus with CRISPR/Cas9 enhances tumour rejection. Nature *543*, 113-117.

Foote, J., and Winter, G. (1992). Antibody framework residues affecting the conformation of the hypervariable loops. J Mol Biol *224*, 487-499.

Fowler, D.M., Stephany, J.J., and Fields, S. (2014). Measuring the activity of protein variants on a large scale using deep mutational scanning. Nat Protoc *9*, 2267-2284.

Frigault, M.J., Lee, J., Basil, M.C., Carpenito, C., Motohashi, S., Scholler, J., Kawalekar, O.U., Guedan, S., McGettigan, S.E., Posey, A.D., Jr.*, et al.* (2015). Identification of chimeric antigen receptors that mediate constitutive or inducible proliferation of T cells. Cancer Immunol Res *3*, 356-367.

Glanville, J., Zhai, W., Berka, J., Telman, D., Huerta, G., Mehta, G.R., Ni, I., Mei, L., Sundar, P.D., Day, G.M.*, et al.* (2009). Precise determination of the diversity of a combinatorial antibody library gives insight into the human immunoglobulin repertoire. Proc Natl Acad Sci U S A *106*, 20216-20221.

Gomes-Silva, D., Mukherjee, M., Srinivasan, M., Krenciute, G., Dakhova, O., Zheng, Y., Cabral, J.M.S., Rooney, C.M., Orange, J.S., Brenner, M.K.*, et al.* (2017). Tonic 4-1BB Costimulation in Chimeric Antigen Receptors Impedes T Cell Survival and Is Vector-Dependent. Cell Rep *21*, 17-26.

Grigor, E.J.M., Fergusson, D., Kekre, N., Montroy, J., Atkins, H., Seftel, M.D., Daugaard, M., Presseau, J., Thavorn, K., Hutton, B.*, et al.* (2019). Risks and Benefits of Chimeric Antigen Receptor T-Cell (CAR-T) Therapy in Cancer: A Systematic Review and Meta-Analysis. Transfus Med Rev *33*, 98-110.

Guedan, S., Ruella, M., and June, C.H. (2018). Emerging Cellular Therapies for Cancer. Annu Rev Immunol *37*, 145-171.

Hartman, N.C., and Groves, J.T. (2011). Signaling clusters in the cell membrane. Curr Opin Cell Biol *23*, 370-376.

Jiao, L., Liu, Y., Zhang, X., Liu, B., Zhang, C., and Liu, X. (2017). Site-saturation mutagenesis library construction and screening for specific broad-spectrum single-domain antibodies against multiple Cry1 toxins. Appl Microbiol Biotechnol *101*, 6071-6082.

Johnson, N.A., Boyle, M., Bashashati, A., Leach, S., Brooks-Wilson, A., Sehn, L.H., Chhanabhai, M., Brinkman, R.R., Connors, J.M., Weng, A.P.*, et al.* (2009). Diffuse large B-cell lymphoma: reduced CD20 expression is associated with an inferior survival. Blood *113*, 3773-3780.

Kehrl, J.H., Riva, A., Wilson, G.L., and Thevenin, C. (1994). Molecular mechanisms regulating CD19, CD20 and CD22 gene expression. Immunol Today *15*, 432-436.

Klindworth, A., Pruesse, E., Schweer, T., Peplies, J., Quast, C., Horn, M., and Glockner, F.O. (2013). Evaluation of general 16S ribosomal RNA gene PCR primers for classical and next-generation sequencing-based diversity studies. Nucleic Acids Res *41*, e1.

Kustikova, O.S., Wahlers, A., Kuhlcke, K., Stahle, B., Zander, A.R., Baum, C., and Fehse, B. (2003). Dose finding with retroviral vectors: correlation of retroviral vector copy numbers in single cells with gene transfer efficiency in a cell population. Blood *102*, 3934-3937.

Lin, J., and Weiss, A. (2003). The tyrosine phosphatase CD148 is excluded from the immunologic synapse and down-regulates prolonged T cell signaling. J Cell Biol *162*, 673-682.

Liu, X., Jiang, S., Fang, C., Yang, S., Olalere, D., Pequignot, E.C., Cogdill, A.P., Li, N., Ramones, M., Granda, B.*, et al.* (2015). Affinity-Tuned ErbB2 or EGFR Chimeric Antigen Receptor T Cells Exhibit an Increased Therapeutic Index against Tumors in Mice. Cancer Res *75*, 3596-3607.

Long, A.H., Haso, W.M., Shern, J.F., Wanhainen, K.M., Murgai, M., Ingaramo, M., Smith, J.P., Walker, A.J., Kohler, M.E., Venkateshwara, V.R.*, et al.* (2015). 4-1BB costimulation ameliorates T cell exhaustion induced by tonic signaling of chimeric antigen receptors. Nat Med *21*, 581-590.

MacKay, M., Afshinnekoo, E., Rub, J., Hassan, C., Khunte, M., Baskaran, N., Owens, B., Liu, L., Roboz, G.J., Guzman, M.L.*, et al.* (2020). The therapeutic landscape for cells engineered with chimeric antigen receptors. Nat Biotechnol *38*, 233-244.

Madeira, F., Park, Y.M., Lee, J., Buso, N., Gur, T., Madhusoodanan, N., Basutkar, P., Tivey, A.R.N., Potter, S.C., Finn, R.D.*, et al.* (2019). The EMBL-EBI search and sequence analysis tools APIs in 2019. Nucleic Acids Res *47*, W636-W641.

Majzner, R.G., and Mackall, C.L. (2019). Clinical lessons learned from the first leg of the CAR T cell journey. Nat Med *25*, 1341-1355.

Makabe, K., Nakanishi, T., Tsumoto, K., Tanaka, Y., Kondo, H., Umetsu, M., Sone, Y., Asano, R., and Kumagai, I. (2008). Thermodynamic consequences of mutations in vernier zone residues of a humanized anti-human epidermal growth factor receptor murine antibody, 528. J Biol Chem *283*, 1156-1166.

Mirzaei, H.R., Jamali, A., Jafarzadeh, L., Masoumi, E., Alishah, K., Fallah Mehrjardi, K., Emami, S.A.H., Noorbakhsh, F., Till, B.G., and Hadjati, J. (2019). Construction and functional

characterization of a fully human anti-CD19 chimeric antigen receptor (huCAR)-expressing primary human T cells. J Cell Physiol *234*, 9207-9215.

Morgan, R.A., Yang, J.C., Kitano, M., Dudley, M.E., Laurencot, C.M., and Rosenberg, S.A. (2010). Case report of a serious adverse event following the administration of T cells transduced with a chimeric antigen receptor recognizing ERBB2. Mol Ther *18*, 843-851.

Richman, S.A., Nunez-Cruz, S., Moghimi, B., Li, L.Z., Gershenson, Z.T., Mourelatos, Z., Barrett, D.M., Grupp, S.A., and Milone, M.C. (2018). High-Affinity GD2-Specific CAR T Cells Induce Fatal Encephalitis in a Preclinical Neuroblastoma Model. Cancer Immunol Res *6*, 36-46.

Robin, G., and Martineau, P. (2012). Synthetic customized scFv libraries. Methods Mol Biol *907*, 109-122.

Roth, T.L., Li, P.J., Blaeschke, F., Nies, J.F., Apathy, R., Mowery, C., Yu, R., Nguyen, M.L.T., Lee, Y., Truong, A.*, et al.* (2020). Pooled Knockin Targeting for Genome Engineering of Cellular Immunotherapies. Cell *181*, 728-744 e721.

Roth, T.L., Puig-Saus, C., Yu, R., Shifrut, E., Carnevale, J., Li, P.J., Hiatt, J., Saco, J., Krystofinski, P., Li, H.*, et al.* (2018). Reprogramming human T cell function and specificity with non-viral genome targeting. Nature *559*, 405-409.

Rudolf, R., Busch, R., Patra, A.K., Muhammad, K., Avots, A., Andrau, J.C., Klein-Hessling, S., and Serfling, E. (2014). Architecture and expression of the nfatc1 gene in lymphocytes. Front Immunol *5*, 21.

Rybakin, V., Westernberg, L., Fu, G., Kim, H.O., Ampudia, J., Sauer, K., and Gascoigne, N.R. (2014). Allelic exclusion of TCR alpha-chains upon severe restriction of Valpha repertoire. PLoS One *9*, e114320.

Rydzek, J., Nerreter, T., Peng, H., Jutz, S., Leitner, J., Steinberger, P., Einsele, H., Rader, C., and Hudecek, M. (2019). Chimeric Antigen Receptor Library Screening Using a Novel NF-kappaB/NFAT Reporter Cell Platform. Mol Ther *27*, 287-299.

Sadelain, M., Brentjens, R., and Riviere, I. (2013). The basic principles of chimeric antigen receptor design. Cancer Discov *3*, 388-398.

Safdari, Y., Farajnia, S., Asgharzadeh, M., and Khalili, M. (2013). Antibody humanization methods - a review and update. Biotechnol Genet Eng Rev *29*, 175-186.

Smith, E.L., Harrington, K., Staehr, M., Masakayan, R., Jones, J., Long, T.J., Ng, K.Y., Ghoddusi, M., Purdon, T.J., Wang, X.*, et al.* (2019). GPRC5D is a target for the immunotherapy of multiple myeloma with rationally designed CAR T cells. Sci Transl Med *11*.

Sommermeyer, D., Hill, T., Shamah, S.M., Salter, A.I., Chen, Y., Mohler, K.M., and Riddell, S.R. (2017). Fully human CD19-specific chimeric antigen receptors for T-cell therapy. Leukemia *31*, 2191-2199.

Tanaka, T., and Rabbitts, T.H. (2010). Protocol for the selection of single-domain antibody fragments by third generation intracellular antibody capture. Nat Protoc *5*, 67-92.

Till, B.G., Jensen, M.C., Wang, J., Qian, X., Gopal, A.K., Maloney, D.G., Lindgren, C.G., Lin, Y., Pagel, J.M., Budde, L.E.*, et al.* (2012). CD20-specific adoptive immunotherapy for lymphoma using a chimeric antigen receptor with both CD28 and 4-1BB domains: pilot clinical trial results. Blood *119*, 3940-3950.

Watanabe, N., Bajgain, P., Sukumaran, S., Ansari, S., Heslop, H.E., Rooney, C.M., Brenner, M.K., Leen, A.M., and Vera, J.F. (2016). Fine-tuning the CAR spacer improves T-cell potency. Oncoimmunology *5*, e1253656.

Yamamoto, T.N., Kishton, R.J., and Restifo, N.P. (2019). Developing neoantigen-targeted T cell-based treatments for solid tumors. Nat Med *25*, 1488-1499.

Ying, Z., Huang, X.F., Xiang, X., Liu, Y., Kang, X., Song, Y., Guo, X., Liu, H., Ding, N., Zhang, T.*, et al.* (2019). A safe and potent anti-CD19 CAR T cell therapy. Nat Med *25*, 947-953.

Zah, E., Lin, M.Y., Silva-Benedict, A., Jensen, M.C., and Chen, Y.Y. (2016). T Cells Expressing CD19/CD20 Bispecific Chimeric Antigen Receptors Prevent Antigen Escape by Malignant B Cells. Cancer Immunol Res *4*, 498-508.

Zhang, W.Y., Wang, Y., Guo, Y.L., Dai, H.R., Yang, Q.M., Zhang, Y.J., Zhang, Y., Chen, M.X., Wang, C.M., Feng, K.C.*, et al.* (2016). Treatment of CD20-directed Chimeric Antigen Receptor-modified T cells in patients with relapsed or refractory B-cell non-Hodgkin lymphoma: an early phase IIa trial report. Signal Transduct Target Ther *1*, 16002.

Zheng, W., O'Hear, C.E., Alli, R., Basham, J.H., Abdelsamed, H.A., Palmer, L.E., Jones, L.L., Youngblood, B., and Geiger, T.L. (2018). PI3K orchestration of the in vivo persistence of chimeric antigen receptor-modified T cells. Leukemia *32*, 1157-1167.

SUPPLEMENTARY FIGURES

Supplementary Table 1. Normalized count of the 30 variants representing the most enriched clones in the final library (ranked by final enrichment after T-cell expansion from unsorted population) First column indicates the amino acid at each of the 10 locations of the library. Columns two to four were normalized counts for three libraries where raw counts were normalized by library size and divided by total read count per library. Column five to seven were enrichment between unsorted, and the two sorted populations. Values shown in the table were used to generate the heatmap shown in Figure 2.11A.

Variant	Count of Unsorted	Count of Tonic Signaling Sorted	Count of Expansion Sorted	Enrichment after Tonic Signaling Sorted (Tonic Signaling Count normalized to Unsorted)	Enrichment from Tonic Signaling Sorted to Expansion (Expansion Count normalized to Tonic Signaling Count)	Enrichment after Expansion (Expansion Count normalized to Unsorted Count)
TPSSPDKQSK	0.000004	0.000016	0.000265	4.14	16.13	66.71
TPSSPDKQST	0.000004	0.000214	0.000218	53.78	1.02	54.93
TPAIPEKQSK	0.000008	0.000132	0.000377	16.55	2.87	47.48
TTSSPEKKSK	0.000032	0.000197	0.000496	6.21	2.51	15.60
TPAIPDKQAT	0.000028	0.000099	0.000412	3.55	4.17	14.80
TPSIPDKQST	0.000020	0.000099	0.000203	4.96	2.06	10.20
TPASPDKQAK	0.000024	0.000038	0.000200	1.61	5.20	8.37
TTAIPDKKSK	0.000024	0.000077	0.000172	3.22	2.24	7.19
TTSIPDKKAK	0.000032	0.000269	0.000218	8.45	0.81	6.87
TTSSPEKKST	0.000207	0.000515	0.001388	2.49	2.69	6.72
TTSSLEKKSK	0.000087	0.000340	0.000543	3.89	1.60	6.21
TPSIPDRQSK	0.000032	0.000143	0.000197	4.48	1.38	6.18
TPSSLDKKSK	0.000127	0.000203	0.000727	1.59	3.58	5.71
TPSSLEKQST	0.000151	0.000488	0.000858	3.23	1.76	5.68
SPASPDKQST	0.000171	0.000411	0.000911	2.41	2.22	5.33
TPASLDKQSK	0.000056	0.000164	0.000296	2.95	1.80	5.33
TTSIPEKKAT	0.000195	0.000641	0.000986	3.29	1.54	5.06
TTAIPDKKST	0.000083	0.000236	0.000387	2.82	1.64	4.63
SPSSPDKKST	0.000195	0.000460	0.000889	2.36	1.93	4.56
TPASPEKKSK	0.000044	0.000077	0.000197	1.75	2.56	4.49
TTAILDKKST	0.000123	0.000307	0.000533	2.49	1.74	4.33
SPSSLDKKSK	0.000191	0.000718	0.000805	3.76	1.12	4.22
TPSSPERQSK	0.000286	0.000438	0.001188	1.53	2.71	4.15
TTSILDKQSK	0.000103	0.000230	0.000427	2.23	1.86	4.14
TPASPDKQST	0.000048	0.000389	0.000197	8.16	0.50	4.12
TPSIPDRKAK	0.000131	0.000186	0.000537	1.42	2.88	4.09
TPAIPEKKSK	0.000076	0.000055	0.000306	0.73	5.58	4.05
TTSSLDKQSK	0.000056	0.000203	0.000225	3.64	1.11	4.04
TPAILERKSK	0.000302	0.000691	0.001210	2.29	1.75	4.01
SPAILDKQST	0.000370	0.000773	0.001463	2.09	1.89	3.96

Supplementary Table 2. Normalized count of the 30 variants representing the least enriched clones in the final library (ranked by final enrichment after T-cell expansion from unsorted population) The first column indicates the amino acid at each of the 10 locations in the library. Columns two to four were normalized counts for three libraries where raw counts were normalized by library size and divided by total read count per library. Columns five to seven were enrichment between unsorted, and the two sorted populations. Values shown in the table were used to generate heatmap shown in Figure 2.11B.

Variant	**Count of Unsorted**	**Count of Tonic Signaling Sorted**	**Count of Expansion Sorted**	**Enrichment after Tonic Signaling Sorted** (Tonic Signaling Count normalized to Unsorted)	**Enrichment from Tonic Signaling Sorted to Expansion** (Expansion Count normalized to Tonic Signaling Count)	**Enrichment after Expansion** (Expansion Count normalized to Unsorted Count)
SPSILDKQSK	0.000644	0.000493	0.000019	0.77	0.04	0.03
TTSIPDRQSK	0.000111	0.000214	0.000003	1.92	0.01	0.03
TPASPERKAK	0.000672	0.000691	0.000019	1.03	0.03	0.03
TTSSPDRKSK	0.000238	0.000455	0.000006	1.91	0.01	0.03
TPAILDKQST	0.000246	0.000164	0.000006	0.67	0.04	0.03
TPSILDKQST	0.000501	0.000203	0.000012	0.40	0.06	0.02
TTSIPEKQSK	0.000262	0.000247	0.000006	0.94	0.03	0.02
TPAILERQST	0.000815	0.001036	0.000019	1.27	0.02	0.02
TPAILDKQAT	0.000274	0.000356	0.000006	1.30	0.02	0.02
TPSSPDRKST	0.000143	0.000318	0.000003	2.22	0.01	0.02
TTSSLDRKSK	0.000588	0.000384	0.000012	0.65	0.03	0.02
TTSILDKQST	0.000151	0.000214	0.000003	1.42	0.01	0.02
TPAIPDKQAK	0.000155	0.000104	0.000003	0.67	0.03	0.02
TPSILDKKSK	0.000207	0.000126	0.000003	0.61	0.02	0.02
TPAIPDRQSK	0.000211	0.000110	0.000003	0.52	0.03	0.01
TPASPERKSK	0.000644	0.000619	0.000009	0.96	0.02	0.01
TPASLEKQAK	0.000238	0.000296	0.000003	1.24	0.01	0.01
TPSSPEKKAT	0.000584	0.000252	0.000006	0.43	0.02	0.01
TPSSPEKQAT	0.000298	0.000296	0.000003	0.99	0.01	0.01
TTSSPDRKAK	0.000302	0.000422	0.000003	1.40	0.01	0.01
TPSIPDRKSK	0.000302	0.000285	0.000003	0.94	0.01	0.01
TPASPDKKST	0.000314	0.000110	0.000003	0.35	0.03	0.01
TTSSPDKKAK	0.000099	0.000137	0.000000	1.38	0.00	0.00
TTSSPDKQST	0.000242	0.000186	0.000000	0.77	0.00	0.00
TTSIPDKQAK	0.000163	0.000181	0.000000	1.11	0.00	0.00
TPASPDKKSK	0.000175	0.000088	0.000000	0.50	0.00	0.00
TPASPDRQAK	0.000366	0.000219	0.000000	0.60	0.00	0.00
TPSSPEKQSK	0.000016	0.000055	0.000000	3.45	0.00	0.00
TPSSPEKQST	0.000056	0.000219	0.000000	3.94	0.00	0.00
TPSIPDKKAT	0.000362	0.000170	0.000000	0.47	0.00	0.00

Chapter 3: Calibration of CAR Tonic Signaling Through Rational Protein Engineering Yields Superior T-Cell Therapy for Cancer

ABSTRACT

The clinical success of the CD19 chimeric antigen receptor (CAR)-T cell therapy has demonstrated the potential of engineered immune cells as a novel class of cancer therapeutics. A wide variety of additional antigens have been targeted by CARs in both preclinical and clinical settings. However, the CD19 CAR remains unique in its strong and consistent therapeutic efficacy. The success has not yet been replicated in CARs targeting other antigens. Several recent reports suggest that antigen-independent, tonic signaling by CARs may be a critical contributor to CAR-T cell exhaustion, and that the CD19 CAR's unique potency may be due to its relative lack of tonic signaling. To this end, we sought to study the effects of tonic signaling and to investigate strategies to generate CAR variants with improved *in vivo* functions. Here, we systematically explore the effect of CAR protein sequence and structure on CAR-T cell function. Specifically, our results suggest that tonic signaling is not detrimental to CAR-T cell function. We found two protein engineering methods to tune CAR tonic signaling to low but non-zero levels, which resulted in robust CAR-T cell function *in vivo*. In addition, the generation of novel CARs yielded several variants that outperform the CD19 CAR in a Raji xenograft. To elucidate the mechanism of functional superiority of certain CAR variants, we performed transcriptomic, epigenetic and metabolomic analysis on CARs with known performance levels. We found high-performing CAR-T cells exhibited non-zero tonic signaling behavior, and upregulated memory and interferon-γ associated genes. Furthermore, we observed that metabolic activity at rest is strongly associated with CAR tonic signaling. In summary, our work establishes methodologies for tonic signaling calibration through rational protein engineering to improve next-generation CAR design.

INTRODUCTION

Tonic signaling of CAR-T cells has been extensively studied in recent years. Multiple studies were performed by comparing the FMC63-based CD19 CAR with CARs targeting other antigens to evaluate tonic signaling propensity (Frigault et al., 2015; Long et al., 2015), The consistent success of the CD19 CAR is partly attributed to its lack of tonic signaling. In the study comparing CARs targeting disialoganglioside (GD2) and CD19, Long et al. showed that GD2 CAR-T cells triggered antigen-independent signaling, which they believed was the cause of the inability of GD2 CAR-T cells to eradicate tumors as efficiently as CD19 CAR-T cells. Spontaneous clustering of receptors was shown to be associated with tonic signaling of GD2 CAR-T cells.

Calibration of receptor signaling by modification of the intracellular domain has been widely adopted and proved to be effective in calibrating signaling intensity of receptors. The deletion of different immunoreceptor tyrosine-based activation motifs (ITAMs) on CD3ζ induced differential CAR-T cell performance, which supports the theory that accessibility of ITAM domains affects T-cell signaling (Feucht et al., 2019). In addition, Ying et al. demonstrated that CARs with different physical conformations can trigger differential *in vivo* outcomes, which further solidifies the potential benefits of tuning CAR signaling by reorientation of receptors (Ying et al., 2019). In this study, our goal was to identify robust protein engineering strategies that enable the development of CAR candidates with superior anti-tumor function.

Insertion of alanine residues has been widely adopted strategy proven effective in calibrating signaling intensity of receptor signaling, particularly in relation to studies of the erythropoietin receptor (EpoR) (Brown et al., 2005; Constantinescu et al., 2001; Greiser et al., 2002; Liu et al., 2008; Scheller et al., 2018). We hypothesized that the structural alteration of intracellular signaling domains of CARs would change the accessibility of downstream signaling molecules and thus induce differential signaling, which affects T-cell performance at rest and upon stimulation. It is conceivable that structural changes of the CARs would change the level

of exposure of their intracellular domains – costimulatory domains, e.g., CD28 and 4-1BB, and signaling domain CD3ζ – and induce differential signaling. To apply this method in CAR engineering, we proposed a strategy to fine tune CAR-T cells' *in vivo* performance by imposing structural changes on their intracellular domains through inserting one to four alanine residues between the transmembrane and costimulatory domains. Each alanine residue would introduce a 109° rotation of CAR's intracellular domains.

Each scFv is comprised of a light chain and a heavy chain and each chain contains complementarity-determining regions (CDRs) and framework regions (FRs) to provide both antigen recognition and structural support. In addition to alanine insertion, we have also evaluated the possibility to hybridize scFv via FR grafting. Grafting functional frameworks to CDRs is a conventional method for humanization in antibody studies (Jones et al., 1986; Krauss et al., 2003; Queen et al., 1989; Willuda et al., 1999). Previously, it has been reported that FRs of 14g2a scFv caused T-cell tonic signaling and that grafting of 14g2a FRs into FMC63-based CD19 scFv promoted T-cell exhaustion (Long et al., 2015). From the same study, grafting the FRs of the FMC63-based scFv to 14g2a scFv was expected to generate variants with a reduced tonic signaling phenotype, yet yielded a hybrid CAR that did not express on the cell surface. Even though FR grafting to CDRs sometimes generated variants with impaired function, it was not fully established whether or not scFv hybridization could resulted in CAR variants with improved function. In this study, we examined the scFv hybridization method and evaluated its effect on tuning CAR signaling.

Here, we report that a low but non-zero level of tonic signaling can enhance CAR-T cell function by facilitating rapid anti-tumor response while avoiding premature T-cell exhaustion. Furthermore, we outlined two rational protein engineering methods – insertion of torsional linkers and the sequence hybridization of FRs and CDRs from different antibodies – which can be used to tune the level of basal T-cell activation for generation of functionally superior candidates.

In our study, a rituximab based, anti-CD20 CAR comprising a CD28 costimulatory domain with a two-alanine insertion outperformed the parental CAR without alanine in a Raji xenograft. Therefore, alanine-induced structural change may provide a generalizable method for optimizing CARs. In addition, scFv hybridization of CAR containing framework regions from a tonically signaling rituximab CAR and complementarity determining regions from a non-tonically signaling Leu16 CAR yielded a robust CAR with a superior anti-tumor effect against Raji xenografts and retained low-levels of T-cell activation at rest. Similar to activating effector-like cells, we found that CAR-T cells that exhibited tonic signaling behavior triggered strong metabolic activity at rest, in particular, glycolysis and glutaminolysis. These results suggest that tonic signaling does not deterministically predict CAR-T cell dysfunction, and minute changes in the scFv sequence can significantly impact the efficacy of CAR-T cells.

MATERIALS AND METHODS

Construction of anti-CD20 scFvs and CARs

Plasmids encoding scFv sequences of rituximab and GA101 were generous gifts from Dr. Anna M. Wu (Zettlitz et al., 2017) (UCLA and City of Hope). DNA sequence encoding the ofatumumab scFv was codon optimized and synthesized by Integrated DNA Technologies (IDT; Coralville, IA). Plasmid encoding scFv derived from the leu16 monoclonal antibody (mAb) was a generous gift from Dr. Michael C. Jensen (Seattle Children's Research Institute) (Jensen et al., 1998). V_L and V_H sequences of anti-GD2 scFv were identified from the 14g2a mAb (PDB code 4TUJ) using abYsis (Swindells et al., 2017). Anti-CD20 CARs were constructed by assembling an scFv (in V_L-V_H orientation), an extracellular IgG4 hinge-CH2-CH3 spacer containing the L235E N297Q mutation (Hudecek et al., 2015), CD28 transmembrane and cytoplasmic domain, CD3ζ cytoplasmic domain, and a T2A "self-cleaving" sequence followed by a truncated epidermal growth factor receptor (EGFRt) with the MSCV backbone. EGFRt was used as a transduction

and sorting marker. The abovementioned anti-CD20 CAR constructs were used as templates to generate CAR-HaloTag fusion proteins for microscopy imaging of CAR clustering.

Cell line generation and maintenance

HEK 293T and Raji cells were obtained from ATCC. K562 cells were a gift from Dr. Michael C. Jensen (Seattle Children's Research Institute). $CD19^+CD20^+$ K562 cells were generated as previously described (Zah et al., 2016). Luciferase-expressing CHLA-255 cell line (CHLA-255-Luc) was a gift from Dr. Shahab Asgharzadeh (Children's Hospital of Los Angeles). CHLA-255-Luc-EGFP cells were generated by retroviral transduction of CHLA-255-Luc to express EGFP, and EGFP+ cells were enriched by fluorescence-activated cell sorting (FACS) on FACSAria (II) (BD Bioscience) at the UCLA Flow Cytometry Core Facility. HEK 293T cells were cultured in DMEM (HyClone) supplemented with 10% heat-inactivated FBS (HI-FBS; ThermoFisher). CHLA-255-Luc-EGFP cells were cultured in IMDM (ThermoFisher) with 10% HI-FBS. Primary human T cells, Raji, and K562 cells were cultured in RPMI-1640 (Lonza) with 10% HI-FBS.

Retrovirus production and generation of human primary CAR-T cells

Retroviral supernatants were produced by transient co-transfection of HEK 293T cells with plasmids encoding anti-CD20 CAR or control constructs, and pRD114/pHIT60 virus-packaging plasmids (gifts from Dr. Steven Feldman), using linear polyethylenimine (PEI, 25 kDa; Polysciences). Supernatants were collected 48 and 72 hours later and pooled after removal of cell debris by a 0.45 μm membrane filter. Healthy donor blood was obtained from the UCLA Blood and Platelet Center. $CD8^+$ T cells were isolated using RosetteSep. Human $CD8^+$ T Cell Enrichment Cocktail (StemCell Technologies) following manufacturer's protocol. Peripheral blood mononuclear cells (PBMCs) were isolated from a Ficoll-Paque PLUS (GE Healthcare) density gradient. $CD14^-/CD25^-/CD62L^+$ naïve/memory T cells ($T_{N/M}$) were enriched from PBMCs using magnetic-activated cell sorting (MACS; Miltenyi). T cells were stimulated with CD3/CD28

Dynabeads (ThermoFisher) at a 3:1 cell-to-bead ratio on Day 0 (day of isolation) and transduced with retroviral supernatant on Day 2 and Day 3. Dynabeads were removed on Day 7. T cells were cultured in RPMI-1640 supplemented with 10% HI-FBS and fed with recombinant human IL-2 (ThermoFisher) and IL-15 (Miltenyi) every 2 days to final concentrations of 50 U/mL and 1 ng/mL, respectively.

Cytokine production quantification

Fifty thousand CAR+ T cells on Day 13 or 14 were incubated with 25,000 EGFP-expressing parental K562 ($CD19^{-}CD20^{-}$) or $CD19^{+}CD20^{+}$ K562 target cells at a 2:1 effector-to-target (E:T) ratio in 96-well U-bottom plate. To control for cell density while accounting for differences in transduction efficiency, untransduced T cells were added as necessary to reach the same number of total T cells per well. After a 48-hour co-incubation, cells were spun down at 300 xg for 2 min. Supernatant was harvested and cytokine levels were quantified by ELISA (BioLegend).

Proliferation assay

T cells were stained with 1.25 μM CellTrace Violet (ThermoFisher) and 40,000 CAR^{+} T cells were seeded in each well in 96-well U-bottom plates with parental K562 or $CD19^{+}CD20^{+}$ K562 cells at a 2:1 E:T ratio. Untransduced T cells were added to wells as needed to normalize for differing transduction efficiencies and ensure the total number of T cells per well was consistent throughout. Cultures were passaged as needed, and CTV dilution was analyzed on a MACSQuant VYB flow cytometer after a 4-day co-incubation.

Cytotoxicity assay with repeated antigen challenge

CAR^{+} T cells were seeded at 4 x 10^{5} cells/well in 24-well plate and coincubated with target cells at a 2:1 E:T ratio. Untransduced T cells were added to wells as needed to normalize for differing

transduction efficiencies and ensure the total number of T cells per well was consistent throughout. Cell counts were quantified by a MACSQuant VYB flow cytometer every 2 days prior to addition of fresh target cells (2 x 10^5 cells/well).

Antibody staining for flow-cytometry analysis

EGFRt expression was measured with biotinylated cetuximab (Eli Lilly; biotinylated in-house), followed by PE-conjugated streptavidin (Jackson ImmunoResearch #016-110-084). CAR expression was quantified by surface epitope staining using Flag tag (DYKDDDDK tag, APC, clone L5, BioLegend #637308), HA (FITC, clone GG8-1F3.3.1, Miltenyi #130-120-722), or with anti-Fc (Alexa Fluor 488, Jackson ImmunoResearch #709-546-098). Antigen-independent activation-marker expression of CAR-T cells was evaluated by antibody staining for CD137 (PE/Cy7, clone 4B4-1, BioLegend #309818) and CTLA-4 (PE/Cy7, clone BNI3, BioLegend #369614) on Days 18 (i.e., 18 days after Dynabead addition and 11 days after Dynabead removal). Antibodies for PD-1 (APC, clone EH12.2H7, BioLegend #329908), and LAG-3 (APC, clone 3DS223H, ThermoFisher #17-2239-42) were used to evaluate T-cell subtype and exhaustion status. T-cell and tumor-cell persistence *in vivo* were monitored by antibody staining of retro-orbital blood samples. Samples were treated with red blood cell lysis solution (10X, Miltenyi) following manufacturer's protocol. The remaining cellular content was stained with anti-human CD45 (PacBlue or PECy7, clone HI30, BioLegend #304029 or #304016) and biotinylated cetuximab, followed by PE-conjugated streptavidin. All samples were analyzed on a MACSQuant VYB flow cytometer (Miltenyi), and the resulting data were analyzed using the FlowJo software (TreeStar).

Confocal microscopy

Jurkat cells transduced with CAR-HaloTag fusion protein were seeded at 10,000 cells per well in 50 μL RPMI-1640 + 10% HI-FBS in one well of a 48-well flat-bottom glass plate (MatTek).

Scanning confocal imaging was acquired with a Zeiss LSM 880 laser scanning confocal microscope with AiryScan and a 63X 1.4 NA oil objective.

***In vivo* studies**

Six- to 8- week old NOD/SCID/IL-2Rγ^{null} (NSG) mice were obtained from UCLA Department of Radiation and Oncology. The protocol was approved by UCLA Institutional Animal Care and Used Committee. For evaluation of CD19 and CD20 CAR-T cells, each mouse was administered 0.5 x 10^5 EGFP$^+$ firefly luciferase (ffLuc)-expressing Raji cells by tail-vein injection. Six to nine days later, 1.5 x 10^6 – 5 x 10^6 CAR$^+$ T cells or cells expressing EGFRt only (negative control) were injected via tail vein to tumor-bearing mice after confirming tumor engraftment. A second dose at 0.5 x 10^6 and a third dose at 2 x 10^6 of tumor cells were administered in a subset of studies as noted in the text and figures. In the study of GD2 CAR-T cells, each mouse was administered with 3.5 x 10^6 CHLA-255-Luc-EGFP cells by tail-vein injection. Upon confirmation of CHLA-255 tumor engraftment (17 days post tumor injection), 2 x 10^6 CAR$^+$ T cells were injected via tail vein to tumor-bearing mice. Details of tumor dose, T-cell dose, tumor re-challenge were indicated in the text and figures. Tumor progression/regression was monitored with an IVIS Illumina III LT Imaging System (PerkinElmer). Blood samples were harvested via retro-orbital bleeding 3 days post T-cell injection and every 10 days thereafter. Mice were euthanized at the humane endpoint. Bone marrow, spleen and liver were collected after euthanasia. Tissues were ground and passed through a 100-μm filter followed by red-blood-cell lysis prior to flow-cytometry analysis.

ATAC-seq library construction and data analysis

ATAC-seq libraries were constructed as previously described (Buenrostro et al., 2013; Corces et al., 2017). In brief, 30,000 – 50,000 viable T cells per mouse from MACS sort were washed once with PBS and lysed in 50 μL Resuspension Buffer (RSB) buffer (10 mM Tris-HCL, pH 7.4,

10 mM NaCl, 3 mM $MgCl_2$) with 0.1% IGEPAL CA-630, 0.1% Tween-20, and 0.01% digitonin. Samples were washed with 1 mL RSB buffer containing 0.1% Tween-20 and centrifuged at 500 xg for 10 minutes at 4 °C. Pelleted nuclei were resuspended in 25 µL Tn5 transposition mix (12.5 µL 2X Tagment DNA buffer, 1.25 µL Tn5 transposase, and 11.25 µL sterile water; Illumina) and stored in a shaking incubator at 37°C and 500 RPM for one hour. Transposition reaction was purified with DNA Clean & Concentrator kit (Zymo Research). DNA fragments were PCR-amplified using NEB Q5 MasterMix and custom primers as previously described (Buenrostro et al., 2013). Libraries were size selected by AmPure beads (Beckman Coulter) and quantified by TapeStation. Libraries were sequenced on the Illumina NovaSeq S1 platform at the High Throughput Sequencing core at UCLA Broad Stem Cell Research Center with 50-bp paired-end reads. Fastq files from ATAC-seq were quality examined by FastQC (Linux, v0.11.8). Reads were processed by cutadapt (Linux, v1.18) to remove reads with low quality (quality score < 33) and to trim adapters. Trimmed reads were aligned to mm10 reference genome using Bowtie2 (Linux, v2.2.9) to eliminate contaminating reads from mouse cells. Non-murine reads were subsequently mapped to hg38 genome by Bowtie2, and sam files were converted to bam files by samtools (Linux, v1.9). Peaks were called independently for each replicate using MACS2 (Linux, v2.1.2) on the aligned reads, and subsequently merged by bedtools (v2.26.0). Reads assigned to each peak were counted by f*eatureCounts* function in subread (Linux, v1.6.3). To visualize chromatin accessible sites, peaks called from MACS2 were visualized in IGV (v2.8.0). Fold enrichments (calculated by MACS2) of peaks within –1 kb to 1 kb of the transcription start site (TSS) indicate accessibility of promoter regions.

Bulk RNA-seq and gene set enrichment analysis (GSEA)

Total RNA was extracted from 200,000 – 700,000 MACS-sorted CAR-T cells using Qiagen RNeasy Plus Mini kit. mRNAs were isolated using NEBNext Poly(A) mRNA Magnetic Isolation Module (New England BioLabs). RNA-seq libraries were generated using NEBNext Ultra II

Directional RNA Library Prep Kit (New England BioLabs) following manufacturer's protocol. Fastq files from RNA-seq were quality-examined by FastQC (Linux, v0.11.8). Reads were processed by cutadapt (Linux, v1.18) to remove reads with low quality (quality score < 33) and to trim adapters. Trimmed reads were aligned to mm10 reference genome using Tophat2 (Linux, v2.1.0) to remove the contaminated reads from mouse cells. Non-murine reads were mapped to hg38 genome by Tophat2. Reads assigned to each gene were counted by *featureCounts* function in subread package (Linux, v1.6.3) with ensembl 38 gene sets as references. Genes without at least 8 reads mapped in at least one sample were considered below reliable detection limit and eliminated. Read counts were normalized by Trimmed Mean of M-values method (TMM normalization method in edgeR running on R v3.6.3) to yield RPKM (reads per millions per kilobases) values, and differential expression was calculated using the package edgeR. Gene ontology analysis was performed using GSEA software (v4.1.0, Broad Institute) and BubbleGUM (v1.3.19) (Spinelli et al., 2015). Expression values of differentially expressed genes were input to the program and using a curated list of 2493 T-cell–relevant gene sets selected from current MSigDB gene sets (Supplemental Data File 3). Heatmaps for differentially expressed genes were generated using *pheamap* and *ggplot2* packages in R (version 3.6.3). Volcano plots were generated using *ggplot2* in R (version 3.6.3).

Metabolite extraction and analysis

Cells were initially cultured in RPMI-1640 supplemented with 10% HI-FBS. At 24 to 72 hours before metabolite extraction, culture media were changed to RPMI containing 10% FBS or dialyzed FBS (dFBS) with 2 g/L 1,2-^{13}C-glucose. Cell culture media were collected from each cell line every 24 hours to evaluate nutrient uptake and consumption. Four volumes of 100% HPLC-grade methanol were added to one volume of media and centrifuged at 17,000 xg and 4°C for 5 minutes to precipitate cell debris. Clear supernatants were harvested and analyzed by liquid chromatography followed by mass spectrometry (LC-MS). To provide accurate estimation

of nutrient uptake and consumption, partial media change was performed every 24 hours to avoid nutrient depletion. Twenty-four or 72 hours after switching to labeled-glucose media, intracellular metabolite extraction was performed as previously described (Bennett et al., 2008; Park et al., 2019). In brief, cells were transferred onto nylon membrane filters (0.45 μm; Millipore) and vacuumed to remove media. Each filter was quickly soaked in 400 μL cold extraction solvent (HPLC-grade acetonitrile:methanol:water 40:40:20, v/v) in one well of a 6-well plate. The plates were incubated at –20°C for 20 minutes. Cell extracts were subsequently transferred to 1.7 mL microcentrifuge tubes and centrifuged at 17,000 xg in 4°C for 5 minutes. Supernatants were lyophilized and reconstituted in HPLC-grade water normalized to total cell count (50 μL per 1 million cells). Both methanol-treated media samples and intracellular metabolite extracts were analyzed by reversed-phase ion-pairing liquid chromatography (Vanquish UPLC; Thermo Fisher Scientific) coupled to a high-resolution orbitrap mass spectrometer (Q-Exactive plus Orbitrap; Thermo Fisher Scientific) at the Molecular Instrumentation Center (MIC) in UCLA. Metabolites were identified by comparing mass-to-charge (m/z) ratio and retention time to previously validated standards. Samples were detected in both negative-ion mode and positive-ion mode. Negative-ion mode was separated into two subgroups—nlo and nhi—to obtain data with m/z ratio from 60 to 200 and 200 to 2000, respectively. LC-MS data were processed using Metabolomic Analysis and Visualization Engine (MAVEN) (Clasquin et al., 2012). Labeling fractions were corrected for the naturally occurring abundance of ^{13}C. Concentration of metabolites in culture media was quantified at 24 and 72 hr by normalizing ion counts from LC-MS measurement to controls with known concentrations. Uptake and secretion rates were calculated by subtracting sample concentration from fresh media and normalizing to viable cell count (positive values indicated secretion and negative values indicated uptake). A mole balance was performed to account for media change from cell cultures. Calculation accounted for 10–20% of media evaporation every 24 hours.

Statistical Analysis

Statistical tests including two-tailed, unpaired, two-sample Student's *t* test and log-rank Mentel-Cox test were performed using GraphPad Prism V8. One-way ANOVA test for differential gene analysis in RNA-seq was performed with *glmQLFTest* function in edgeR.

RESULTS

scFv sequence alters CAR tonic signaling

To study tonic signaling of CAR-T cells, the "gold standard" CD19 CAR is often used to compare with CARs targeting other antigens. However, there are confounding factors of comparisons across different CARs: different antigens, different structural relationships between CAR and antigen, framework region, antigen density, method of introduction of CAR to T cells, spacer length, CAR expression level, co-stimulatory domains, etc. In this study, we hypothesized that minor changes in amino acid sequence of the ligand-binding scFv domain of a CAR significantly alter CAR function that is independent of binding affinity and target-antigen identify. We first started out using an anti-CD20 CAR that enabled benchmarking against the CD19 CAR *in vivo*. Second, clinical outcomes of CD20 CAR-T cell therapy have not yet been as successful as those for CD19 CAR-T cell therapy, leaving room for improvement. It has been previously reported that the CD19 antigen is very easy to lose which dampens the clinical outcome in treating some B-cell malignancies (Majzner and Mackall, 2019). Thus, optimization of CD20 CARs for better cancer treatment will draw high clinical interests.

To study the effect of minute changes in scFv sequences on CAR-T cell function, we constructed CARs using scFvs derived from four different mAbs of CD20 (Supplementary Table 1) that exhibited similar binding affinity (Mossner et al., 2010; Reff et al., 1994; Uchiyama et al., 2010) and similar complementarity determining region (CDR) structures predicted by abYsis (Martin and Thornton, 1996; Swindells et al., 2017). Three of the scFvs (Leu16, rituximab, and GA101) bind overlapping epitopes on the major extracellular loop of CD20, while ofatumumab

binds both the minor and major loops of CD20 (Klein et al., 2013; Niederfellner et al., 2011; Rufener et al., 2016; Teeling et al., 2006) (Figure 3.1A; Supplementary Figure 3.S1A). To eliminate confounding factors such as differences in binding affinity and binding-epitope location, all four CARs have identical extracellular spacers, transmembrane domains, and cytoplasmic signaling domains. This allows us to attribute the functional differences to the scFv sequence. To better explore the potential relationship between the scFv sequence and CAR tonic signaling, we chose to incorporate CD28 as the co-stimulatory domain, as CD28-containing CARs have previously been reported to be more prone to tonic signaling than 4-1BB-containing CARs (Frigault et al., 2015; Long et al., 2015).

All four CD20 CARs were efficiently expressed on the surface of primary human T cells (Supplementary Figure 3.S1B) and triggered comparable *ex vivo* T-cell expansion (Supplementary Figure 3.S1C). In response to repeated antigen stimulation, all CAR-T cell variants demonstrated the ability to lyse target cells and proliferate, and exhibited comparable *in vitro* cytotoxicity (Supplementary Figure S1D). However, in terms of *in vivo* anti-tumor function, the four CD20 CAR-T cells exhibited distinct performance against Raji xenografts (Figure 1B,D). Rituximab CAR-T cells showed the strongest initial tumor control (Figure 1B, C). Two weeks after T-cell administration, all CAR-T cells failed to control tumor outgrowth and mice treated with rituximab CAR-T cells exhibited the fastest tumor growth as indicated by the shortest tumor doubling rates (Figure 1D), which suggested early functional exhaustion of rituximab CAR-T cells. To evaluate T-cell dysfunction *in vivo*, persistent T cells were harvested from animal organs, specifically, the liver, spleen, bone marrow and brain. All mice had detectable CAR-T cells and tumors at the time of euthanasia (Supplementary Figure 3.S2A,B). All CAR-T cells expressed high inhibitory markers PD-1 and LAG-3 (Supplementary Figure 3.S2C,D), which suggested their dysfunction by the end of the study.

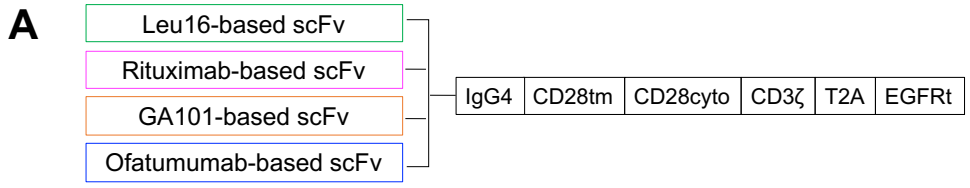

Antibody	Kd	CDRL1	CDRL2	CDRL3	CDRH1	CDRH2
Leu 16	N/A	1/10A	1/7A	1/9A	1/10A	2/10A
Rituximab	4.5 ~ 5.45 nM	1/10A	1/7A	1/9A	1/10A	2/10A
GA101	4.0 nM	4/16A	1/7A	1/9A	1/10A	2/10A
Ofatumumab	4.76 +/- 0.99 nM	2/11A	1/7A	1/9A	1/10A	3/10B

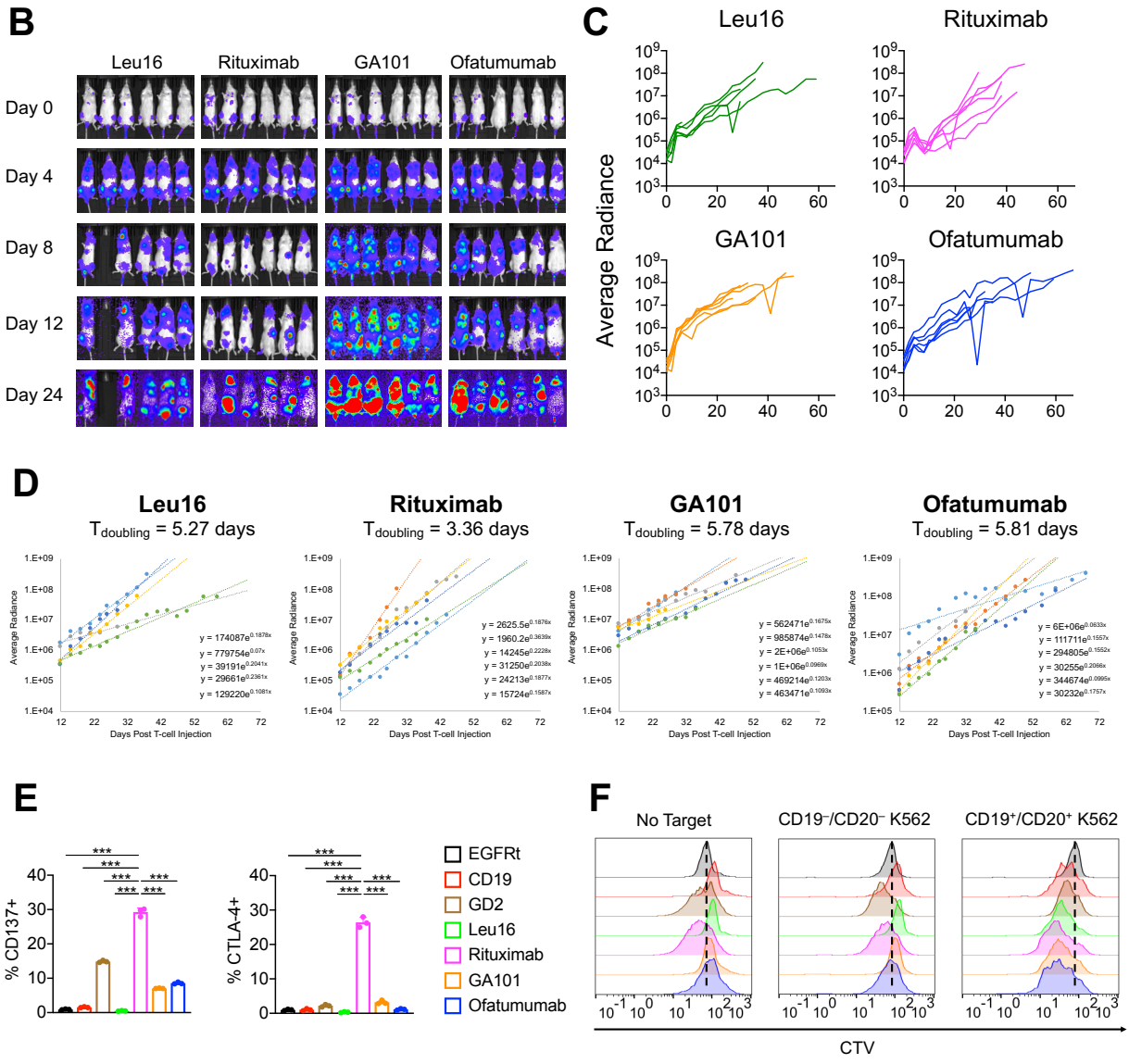

Figure 3.1. scFv sequence alters tonic signaling and CAR-T cell metabolism
(A) Schematic of a panel of 2nd-generation anti-CD20 CARs composed of scFvs derived from four different monoclonal antibodies fused to an IgG4 spacer, CD28 transmembrane and

cytoplasmic domains, and CD3ζ signaling domain. The CAR is further fused via a self-cleaving T2A peptide to a truncated EGFR (EGFRt), which was used as transduction marker (top). K_D values and CDR structure-family designations of the four antibodies from which scFvs were derived (bottom). FR and CDR sequences and structure-family designations were determined as previously described (Chothia and Lesk, 1987; Chothia et al., 1989; Kabat and Wu, 1971; Martin and Thornton, 1996).
(B–C) NSG mice were injected intravenously (i.v.) with 0.5 x 10^6 firefly-luciferase–expressing Raji cells 6 days prior to treatment with 5 x 10^6 CD20-targeting CAR-T cells delivered i.v.
(B) Tumor progression was monitored by bioluminescence imaging (n = 6 mice per group). Minimum and maximum values on the radiance-intensity scale are 5 x 10^4 and 1 x 10^7, respectively.
(C) Average radiance (p/sec/cm^2/sr) of individual animals for each test group.
(D) NSG mice were engrafted with firefly-luciferase–expressing Raji cells and treated with CD20 CAR-T cells as described in Figure 1B. Tumor burden was measured by bioluminescence imaging, and the tumor growth rate between Day 12 post T-cell injection and the humane end point was quantified by fitting exponential regression curves to each individual animal's tumor progression data. The average doubling time ($T_{doubling}$) for tumor signal among the mice (n = 6) in each group is shown above each plot.
(E) Activation and exhaustion maker expression on CAR^+ T cells were evaluated 11 days post Dynabead removal, without CD20 antigen stimulation. Data bars indicate the means of technical triplicates ± 1 standard deviation (S.D.). Results are representative of three independent experiments using T-cells derived from three different healthy donors. Unless otherwise noted, *p* values were determined by unpaired, two-tailed, two-sample Student's t-test; * $p<0.05$, ** $p<0.01$, *** $p<0.001$, n.s. not statistically significant.
(F) A 4-day T-cell proliferation assay on CAR^+ T cells with CellTrace Violet (CTV) dye in the absence or presence of target cells (on-target, $CD19^+/CD20^+$ K562 cells; off-target, parental K562 cells) at 2:1 effector-to-target (E:T) ratio. Data shown are representative of five independent experiments from five different healthy donors.

This evidence indicates that rituximab CAR-T cells are initially functional but could not sustain persistent anti-tumor function. In our study, we are interested in studying the causes of such behavior and evaluating design strategies to improve the long-term effect of CARs. To evaluate the potential driving forces that might cause early dysfunction of rituximab CAR-T cells, we reasoned the tonic signaling may drive T-cell dysfunction due to constitutive signaling. Without antigen stimulation, rituximab CAR-T cells up-regulated the activation marker CD137 (Figure 3.1E,F) and inhibitory marker CTLA-4 and exhibited antigen-independent T-cell proliferation that was even stronger than T cells expressing the 14g2a-based GD2 CAR, which is known to have tonic signaling behavior (Long et al., 2015).

Taken together, in the absence of antigen stimulation, rituximab CAR-T cells are basally activated to initiate T-cell effector function, which may explain rituximab CAR-T cells' rapid

tumor control at early time points *in vivo*. Even though rituximab CAR-T cells provided strong initial tumor control, the lack of complete tumor eradication suggested that continuous T-cell signaling without an antigen might be the cause of their loss of tumor control. Thus, our finding suggested that tonic signaling does not necessarily indicate suboptimal T-cell performance and there is a potential calibrated tonic signaling level that is conducive to CAR-T cell function. Next, we wanted to evaluate this possibility and explore other design parameters other than the choice of scFv to tune the level of tonic signaling of CARs for generation of CAR variants that enable rapid response against tumor without compromising long-term efficacy.

Structural alterations of the signaling domain enable calibration of CAR-T cell signaling

Receptor dimerization has been shown to trigger CAR signaling (Chang et al., 2018). It has been reported that CAR clustering in the absence of antigen-stimulation via scFv interaction is one of the causes of premature T-cell signaling, which causes suboptimal T-cell function (Long et al., 2015). However, in our study, all four CD20 CARs expressed uniformly on the T-cell surface in the absence of stimulation (Supplementary Figure 3.S3). Thus, more work is required to evaluate what causes tonic signaling and how to precisely calibrate this property in order to tune T-cell function. In T-cell activation, initiation of phosphorylation of ITAMs on CD3ζ recruits downstream adaptor proteins and kinases. The conformation of receptor chains affects the accessibility of these adaptor molecules, which impact the activation and signaling of cells (Hartman and Groves, 2011). Multiple models on TCR signaling proposed mechanisms involving conformational changes altering accessibility of ITAM to phosphorylation, which affects T-cell signaling (Love and Hayes, 2010; Smith-Garvin et al., 2009). We hypothesized that changes in the intracellular structure of CARs leads to differential accessibility of downstream signaling molecules to ITAM and the costimulatory domain, thus altering T-cell signaling. When multiple CAR molecules come into close proximity, each CAR molecule affects other molecules' ability to recruit downstream signaling adaptors due to rotations of intracellular costimulatory

and signaling domains. As such, we hypothesized that CARs adopt a physical conformation that enables optimal signal transduction. Therefore, we sought to find a design method that enables calibrating of CAR signaling in the presence and absence of antigen stimulation.

In this study, the widely-adopted alanine-insertion method was used to evaluate the impact of structural changes on both the tonic and antigen-dependent signaling propensity in CARs as well as to generate better performing CAR variants. To introduce structural change into the intracellular domain, one to four alanines were inserted between the transmembrane and cytoplasmic domains of CD28 in the rituximab-based CAR, with each alanine introducing a fixed-angle rotation of the protein of 109° (Figure 3.2A, Supplementary Figure 3.S4A).

All rituximab CAR variants with zero to four alanines incorporated in the intracellular domains expressed well on the T-cell surface (Supplementary Figure 3.S4B) and exhibited similar expansion and *in vitro* cytotoxicity upon repeated stimulation by $CD20^+$ Raji cells (Supplementary Figure 3.S4C). To evaluate the effect of alanine insertion on tonic signaling, we found that alanine incorporation caused reduction in antigen-independent T-cell proliferation and TNFα production compared to the original rituximab CAR-T cells (Figure 3.2B,C) without affecting the expression of the activation and exhaustion markers at rest (Supplementary Figure 3.S4D). When tested *in vivo*, rituximab CAR-T cells with one, two, or four alanines inserted demonstrated a stronger anti-tumor effect than T cells expressing the parental or other alanine-insertion variants in the Raji xenograft (Figure 3.2.D,E). In particular, mice treated with T cells expressing the two-alanine rituximab CAR showed a 2.1-fold increase in median survival compared to mice treated with the original rituximab CAR-T cells (55 days vs. 26 days; Figure 3.2E). Taken together, alanine insertion significantly reduced basal CAR-T cell activation, with the optimal structure of the rituximab CAR having a 218° rotation of its intracellular domain with two alanines inserted.

To expand the scope of the alanine strategy to CARs targeting other antigens, we used the 14g2a-based GD2 CAR as our candidate. All five alanine-insertion variants of GD2 CAR-T

cells expressed well on the T-cell surface (Supplementary Figure 3.S5A,B) and exhibited similar anti-tumor responses upon repeated antigen stimulation *in vitro* (Supplementary Figure 3.S5C). Consistent with results from the CD20 CAR panel (Figure 3.2D), T cells expressing GD2 CARs containing one, two, or four alanines outperformed GD2 CARs with zero or three alanines inserted in the CHLA-255 metastasis neuroblastoma xenograft (Supplementary Figure 3.5SD).

To evaluate the impact of alanine insertion on *in vivo* T-cell persistence, livers and spleens were collected for analysis at the time of euthanasia. CARs with two alanines incorporated again demonstrated the ability to trigger better T-cell persistence. These results indicate that second-generation CARs containing the CD28 transmembrane domain and cytoplasmic domain adopt the optimal conformation with a two-alanine insertion.

These promising results demonstrate that better-performing CAR variants can be obtained by altering intracellular structure with alanine insertions. However, despite significant improvement in animal survival, alanine-insertion in CAR-T cells failed to achieve complete tumor clearance. Next, we sought to explore additional engineering methods that could further optimize CAR-T cell function.

ScFv sequence hybridization further improves CAR-T cell anti-tumor function

Despite having a 91% similarity in scFv sequences and identical complementarity-determining region (CDR) structures (Figure 3.1A; Supplementary Figure 3.S1A), the Leu16 and rituximab based anti-CD20 CARs demonstrated disparate tonic signaling behavior and *in vivo* activity (Figure 3.1B-F; Supplementary Figure 3.S1D). Therefore, minute changes in the scFv sequence can significantly impact the signaling propensity and the efficacy of CAR-T cells.

Due to high similarity in sequences and disparate signaling dynamics *in vitro* and *in vivo*, Leu16 and rituximab scFvs were used to perform scFv hybridization. We constructed two hybrid CD20 CARs (RFR-LCDR, LFR-RCDR) which consisted of swapping FRs and CDRs from a non-

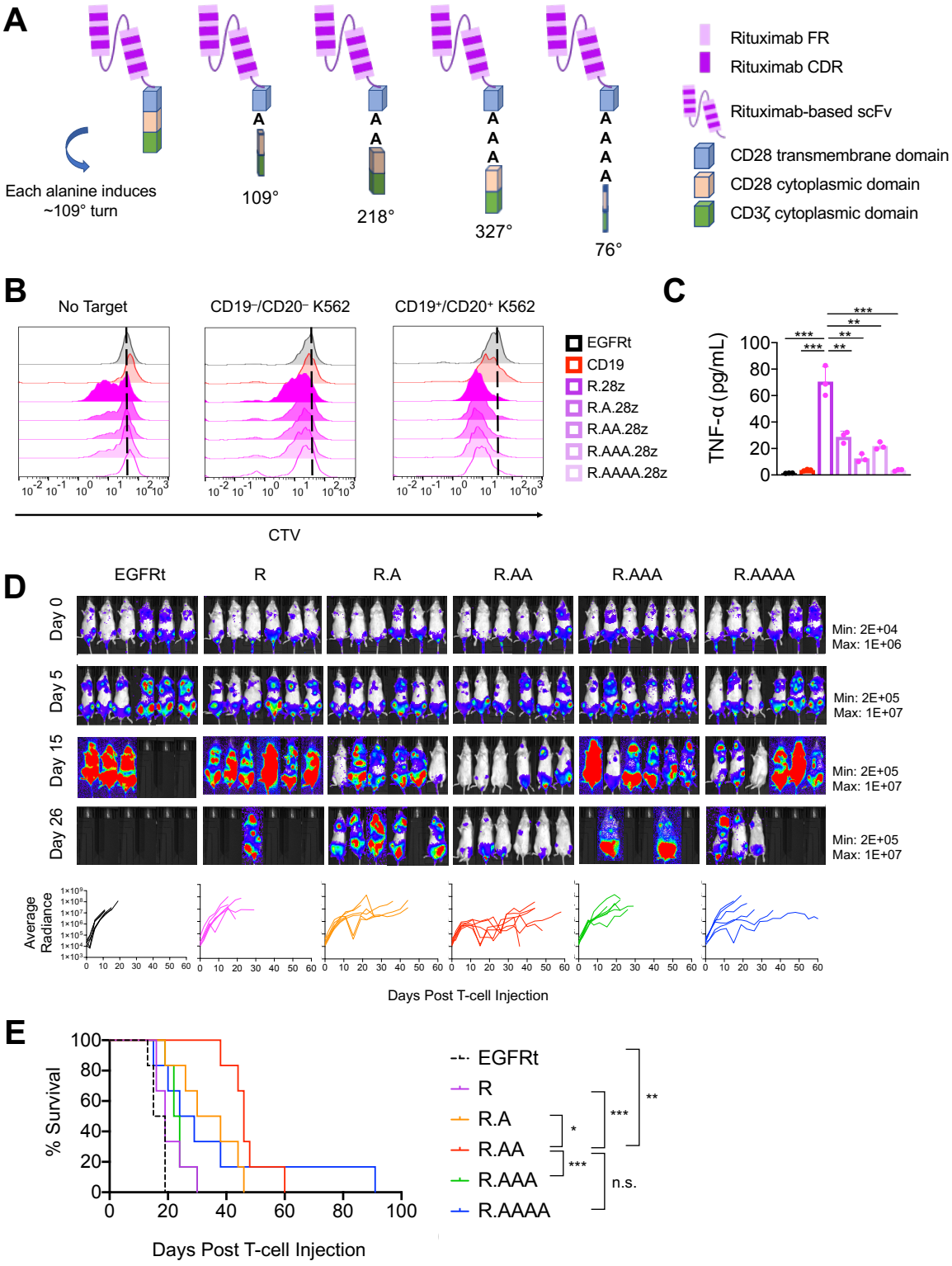

Figure 3.2. Torsional reorientation of signaling domain tunes CAR-T cell activity
(A) Schematic of alanine incorporation into the Rituximab-based CAR.

(B) A 4-day T-cell proliferation assay with CellTrace Violet (CTV) dye in the absence or presence of target cells at 2:1 E:T ratio. Data shown are representative of three independent experiments from three different healthy donors.
(C) TNF-α production of CAR-T cells was measured 7 days post Dynabead removal, without CD20 antigen stimulation. Results are representative of three independent experiments from three different healthy donors. *p<0.05, **p<0.01, ***p<0.001, n.s. not statistically significant.
(D,E) NSG mice were injected intravenously with 0.5 x 10^6 firefly-luciferase–expressing Rajicells followed by two doses of CAR^+ T cells 6 days (1.35 x 10^6 cells) and 12 days (1.5 x 10^6 cells) later; n = 6 mice per group.
(D) Tumor progression was monitored by bioluminescence imaging (top). Average radiance (p/sec/cm2/sr) of individual animals are shown for each group (bottom).
(E) Kaplan-Meier survival curve. Statistical significance was determined by log-rank (Mantel-Cox) test. *p<0.05, **p 0.01, ***p<0.001, n.s. not statistically significant.

tonic-signaling CAR (Leu16) and a tonic-signaling CAR (rituximab) (Figure 3.3A; Supplementary Table 3) to evaluate whether or not the new CAR variants demonstrated calibrated signaling both at rest and upon antigen stimulation as well as improved *in vivo* function.

Both hybrid CAR variants expressed well on the surface of T cells (Supplementary Figure 3.S6). In a serial antigen challenge assay, the RFR-LCDR CAR demonstrated improved T-cell cytotoxicity that was comparable to CD19 CAR-T cells and stronger than both of the parental CARs while LFR-RCDR was completely non-functional (Figure 3.3B). In the absence of antigen stimulation, we had confirmed that RFR-LCDR CAR-T cells triggered upregulation of exhaustion and activation markers that was at levels similar to the tonically signaling rituximab CAR-T cells. Unlike rituximab CAR-T cells, T cells expressing the RFR-LCDR CAR did not trigger antigen-independent T-cell proliferation, indicating a calibrated, non-zero level of T-cell activation at rest (Figure 3.3C,D). LRF-RCDR was excluded for future analysis because it was non-functional. These findings suggested that the RFR-LCDR CAR exhibited moderate tonic signaling but showed better *in vitro* cytotoxicity. It is consistent with our hypothesis that a non-zero level of tonic signaling is required to trigger overall better CAR-T cell performance.

Next, we sought to study whether or not scFv hybridization and alanine-insertion would synergize to further improve CAR-T cell function. We constructed RFR-LCDR with two alanine residues inserted between its transmembrane and costimulatory domains, which was later

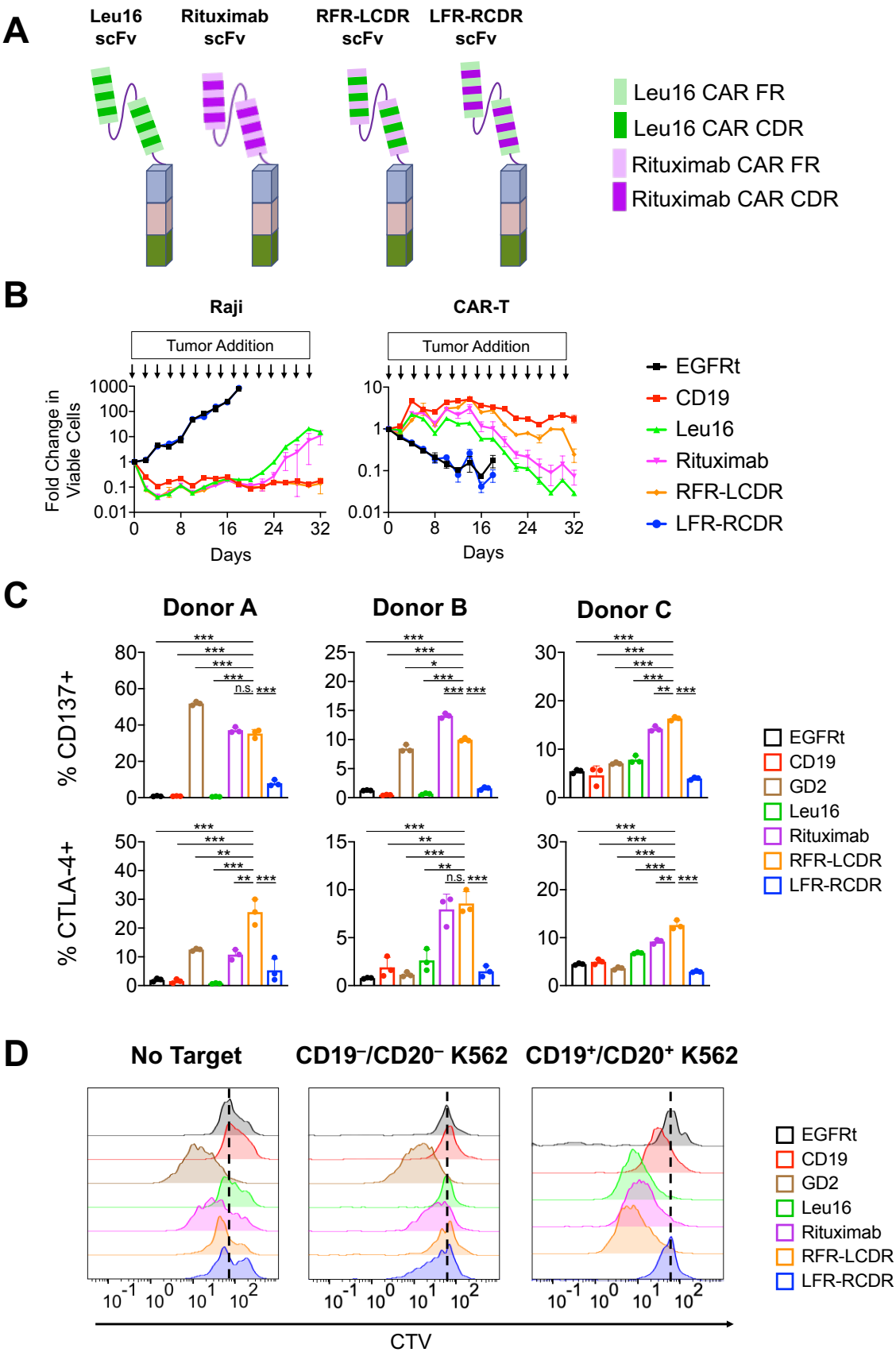
A
Leu16 scFv
Rituximab scFv
RFR-LCDR scFv
LFR-RCDR scFv
Leu16 CAR FR
Leu16 CAR CDR
Rituximab CAR FR
Rituximab CAR CDR
B
Raji
CAR-T
Tumor Addition
Tumor Addition
Fold Change in Viable Cells
Days
Days
EGFRt
CD19
Leu16
Rituximab
RFR-LCDR
LFR-RCDR
C
Donor A
Donor B
Donor C
% CD137+
% CTLA-4+
EGFRt
CD19
GD2
Leu16
Rituximab
RFR-LCDR
LFR-RCDR
D
No Target
CD19⁻/CD20⁻ K562
CD19⁺/CD20⁺ K562
CTV
EGFRt
CD19
GD2
Leu16
Rituximab
RFR-LCDR
LFR-RCDR

Figure 3.3. scFv sequence hybridization yields functionally superior CAR variant
(A) Schematic of scFv sequence hybridization in CAR molecules. The Framework regions (FR) and complementarity-determining regions (CDRs) of Leu16- and rituximab-derived scFvs were intermixed to yield two new CAR variants.
(B) RFR-LCDR hybrid CAR-T cells show superior anti-tumor function and T-cell proliferation upon repeated antigen challenge. CAR-T cells were challenged with Raji cells ($CD19^+/CD20^+$) at a 2:1 E:T ratio every two days. T-cell and target-cell counts were quantified by flow cytometry. Data shown are the means of technical triplicates ± 1 S.D. Results are representative of three independent experiments from three different healthy donors.
(C) Activation and exhaustion maker expression was evaluated 11 days post Dynabead removal, without CD20 antigen stimulation. Data bars indicate the means of technical triplicates ± 1 S.D. Results are representative of three independent experiments from three different healthy donors. **p*<0.05, ***p*<0.01, ****p*<0.001, n.s. not statistically significant.
(D) A 4-day CAR-T cell proliferation assay with CellTrace Violet (CTV) dye in the absence or presence of target cells at 2:1 E:T ratio.

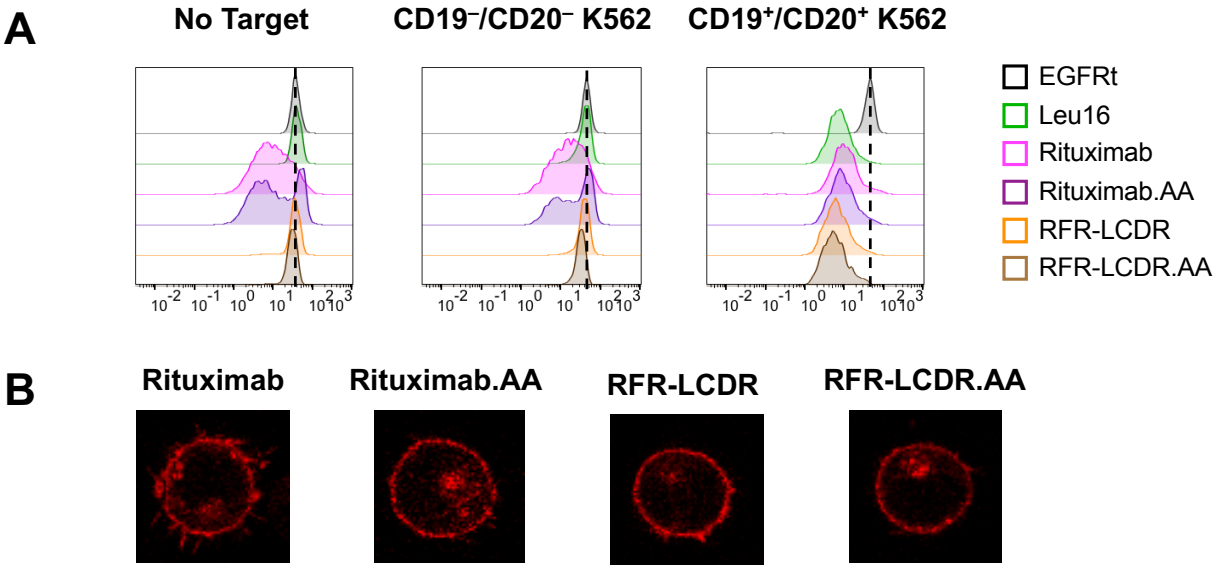

Figure 3.4. scFv sequence hybridization with or without torsional reorientation in CAR protein demonstrate similar *in vitro* performance
(A) A 4-day CAR-T cell proliferation assay with CellTrace Violet (CTV) dye in the absence or presence of target cells at 2:1 E:T ratio.
(B) Jurkat cells transduced with CAR-HaloTag fusion proteins were stained with the red fluorescent dye tetramethylrhodamine (TMR) and imaged by confocal microscopy. CAR molecules are uniformly distributed on cell surface in the absence of antigen stimulation.

referred to as RFR-LCDR.AA CAR. The newly generated RFR-LCDR hybrid CAR was compared side-by-side with both of the parental CARs, as well as the new AA version.

All CAR-T cells efficiently produced Th1 cytokines and proliferated upon antigen stimulation, suggesting their ability to recognize and respond to tumor challenge (Figure 3.4A;

Supplementary Figure 3.S7A,B). Both the hybrid CAR and rituximab CAR showed uniform receptor distribution on cell surface with or without the two-alanine insertion (Figure 3.4B). ScFv hybridization significantly decreased TNF-α production and increased IL-2 production in the absence of antigen stimulation compared to rituximab CAR-T cells, and alanine insertion did not have a strong impact on the cytokine production profile (Supplementary Figure 3.S7B).

To evaluate *in vivo* performance of the hybrid CAR, we tested its anti-tumor effect along with its parental CAR constructs (Leu16, rituximab) and the gold-standard CD19 CAR in a Raji xenograft (Figure 3.5A). In the *in vivo* study where the split doses of T cells were used, alanine insertion substantially improved the rituximab CAR-T cells (Figure 3.5B,C). Both hybrid CARs demonstrated efficient tumor eradication at an early timepoint with or without alanine insertion (Figure 3.5B,C). With the two-alanine insertion, RFR-LCDR.AA CAR-T cells exhibited faster tumor clearance and demonstrated better *in vivo* T-cell persistence in peripheral blood (Figure 3.5D), despite marginal improvement compared to the parental RFR-LCDR CAR-T cells. Both CAR-T cell lines remained in complete tumor control after tumor re-challenge to mice whereas the gold-standard CD19 CAR treated mice relapsed and eventually reached the humane endpoint, which represents the first example of a CD20 CAR that outperformed the CD19 CAR *in* B-cell lymphoma xenografts. To further validate the benefit of alanine insertion in the hybrid CAR, we performed a second *in vivo* study where T cells were injected as a single dose and tumor cells were challenged at escalating doses (Figure 3.5E). Rituximab.AA, RFR-LCDR, and RFR-LCDR.AA CAR-T cells all conferred T-cell persistence before and after each tumor re-challenge, with RFR-LCDR.AA CAR-T cells showing the highest level of CAR-T cells in peripheral blood (Figure 3.5F,G). Both hybrid CAR variants conferred complete protection to the animals throughout the study. Taken together, these results suggest that tonic signaling does not deterministically predict CAR-T cell dysfunction. ScFv hybridization yielded a hybrid CAR that retained a tonic signaling phenotype but exhibited markedly improved *in vivo* function, which suggested that calibration of tonic signaling could improve CAR-T cell function.

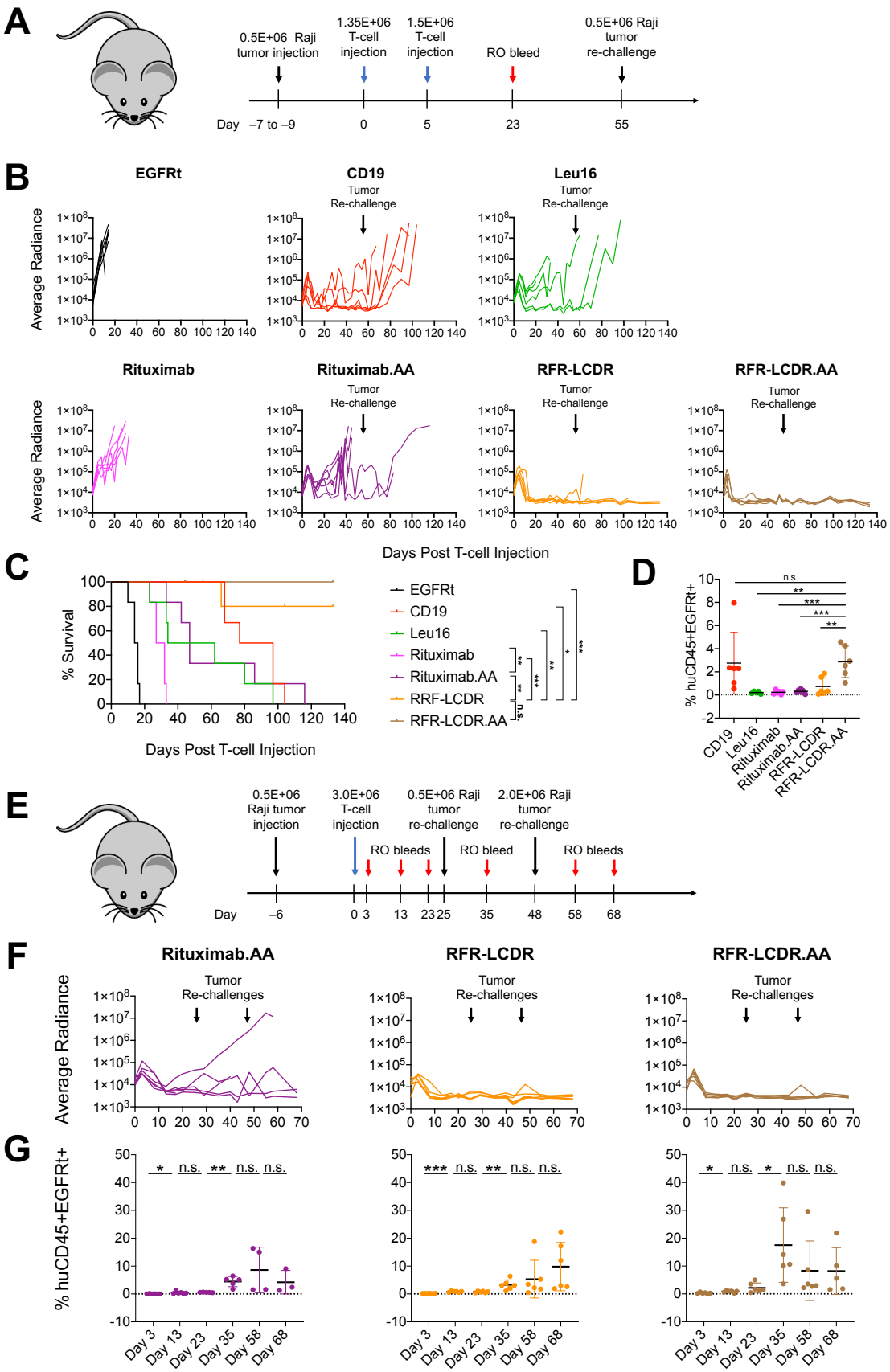
A
0.5E+06 Raji tumor injection
1.35E+06 T-cell injection
1.5E+06 T-cell injection
RO bleed
0.5E+06 Raji tumor re-challenge
Day –7 to –9
0
5
23
55
B
EGFRt
CD19
Leu16
Rituximab
Rituximab.AA
RFR-LCDR
RFR-LCDR.AA
Tumor Re-challenge
Average Radiance
Days Post T-cell Injection
C
% Survival
Days Post T-cell Injection
EGFRt
CD19
Leu16
Rituximab
Rituximab.AA
RRF-LCDR
RFR-LCDR.AA
D
% huCD45+EGFRt+
n.s.
CD19
Leu16
Rituximab
Rituximab.AA
RFR-LCDR
RFR-LCDR.AA
E
0.5E+06 Raji tumor injection
3.0E+06 T-cell injection
0.5E+06 Raji tumor re-challenge
2.0E+06 Raji tumor re-challenge
RO bleeds
RO bleed
RO bleeds
Day –6 0 3 13 23 25 35 48 58 68
F
Rituximab.AA
RFR-LCDR
RFR-LCDR.AA
Tumor Re-challenges
Average Radiance
G
% huCD45+EGFRt+
Day 3
Day 13
Day 23
Day 35
Day 58
Day 68

Figure 3.5. scFv hybridization in combination with torsional reorientation in CAR protein further enhance CAR-T cell function *in vivo*
(A–D) NSG mice were injected intravenously with firefly-luciferase–expressing Raji cells followed by two doses of CAR^+ T cells, and one Raji tumor rechallenge.
(A) Schematic of *in vivo* experiment (n = 6 mice per group).
(B) Tumor signal in individual animals quantified by bioluminescence imaging.
(C) Kaplan-Meier survival curve. Log-rank (Mantel-Cox) test was performed for pair-wise comparisons. **p*<0.05, ***p*<0.01, ****p*<0.001, n.s. not statistically significant.
(D) Frequency of human $CD45^+EGFRt^+$ cell in peripherical blood collected from mice at Day 23 after first dose of T-cell infusion.
(E–G) NSG mice were injected intravenously with firefly-luciferase expressing Raji cells followed by a single dose of CAR^+ T cells. Mice were re-challenged twice with Raji cells, on Day 25 and Day 45 post T-cell injection.
(E) Schematic of *in vivo* experiment (n = 6 mice per group).
(F) Tumor signal in individual animals quantified by bioluminescence imaging.
(G) Frequency of human $CD45^+EGFRt^+$ cell in peripherical blood collected from mice over time. **p*<0.05, ***p*<0.01, ****p*<0.001, n.s. not statistically significant.

Functionally superior CAR-T cells promote strong memory phenotype *in vivo*

To elucidate the mechanism of functionally superiority of certain CARs, we performed epigenetic and transcriptomic analysis on CAR-T cells with differential *in vivo* performance. NSG mice were engrafted with Raji cells and a dose of 2.85 million CAR^+ T cells (Figure 3.6A-B). We harvested CAR-T cells from mice 9 days post T-cell infusion in Raji xenograft. Cells recovered from animal organs were enriched for $huCD45^+$ and $EGFRt^+$ and subjected for ATAC-seq and RNA-seq. We noticed distinct different transcriptomic and epigenetic profiles of rituximab CAR-T cells compared to the others. Rituximab CAR-T cells had around 20 to 40 differentially expressed gene (DEG) from Leu16 and RFR-LCDR, but there were 280 differentially expressed gene from RFR-LCDR.AA, suggesting that RFR-LCDR.AA were the most functionally distinct from rituximab CAR (Figure 3.7A-B).

Among three groups of DEG, rituximab CAR-T cells showed clear down regulation of *sell* (CD62L) and upregulation in a family of KIR genes e.g., *kir2dl1*, *kir2dl3*, and *kir3dl1*, associated with an exhausted CD8 phenotype (Bjorkstrom et al., 2012). Interestingly, *atp9a*, a phospholipid flippase that positively regulates GLUT1 recycling, was upregulated in rituximab CAR-T cells. GLUT1 recycling from endosomes to the plasma membrane is essential for cellular glucose

uptake. It has been reported that T cells which have undergone chronic viral infection show impaired function towards utilization of mitochondrial energy supply (OXPHOS) and thus depend on glycolysis, which leads to upregulation of the glucose transporter GLUT1 (Schurich et al., 2016). Increased glycolysis has been shown to associate with effector function in human T cells (Cretenet et al., 2016; Macintyre et al., 2014). ATAC-seq data further supported the observation of upregulation of *atp9a* and KIR family genes. Promoter regions of *atp9a* and *kir2dl3, kir2dl1 and kir3dl3* were highly accessible in rituximab CAR-T cells, supporting our observation in RNA-seq (Figure 3.7C).

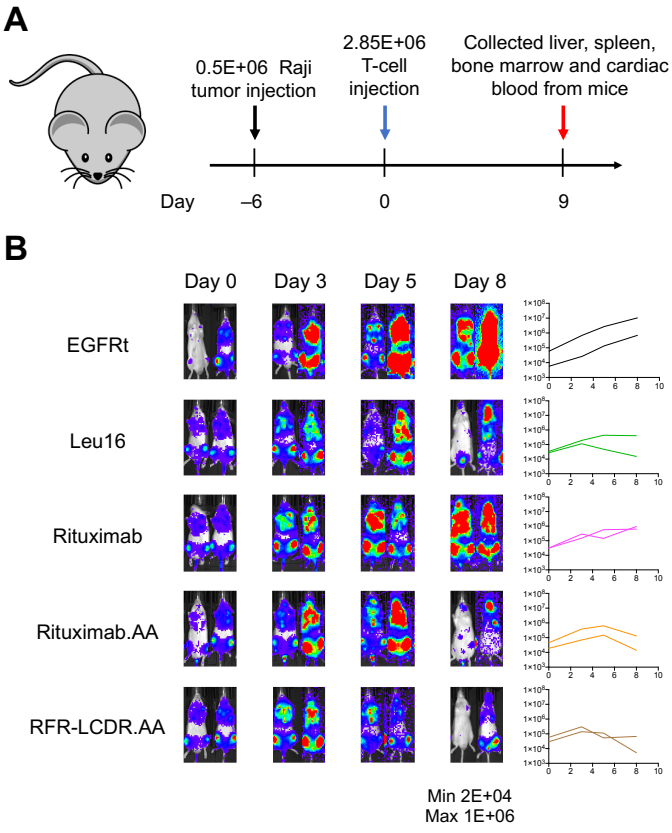

Figure 3.6 CAR-T cell harvested from tumor-bearing mice for transcriptomic and epigenetic profiling NSG mice were injected intravenously with 0.5 x 10^6 firefly-luciferase expressing Raji cells followed by 2.85 x 10^6 of CAR+ T cells 6 days later. CAR^+ T cells were collected from tumor-bearing mice 9 days after T-cell injection (n = 2 mice per group). Only a small number of mock-transduced (EGFRt-only) T cells were recovered from mice, consistent with lack of T-cell expansion in the absence of antigen recognition. However, this poor cell recovery led to low read counts in RNA-seq and ATAC-seq that precluded reliable data

analysis. As a result, these samples were excluded from the analyses shown in Figures 3.7 and 3.8.

(A) Schematic of *in vivo* experiment.

(B) Tumor progression as monitored by bioluminescence imaging.

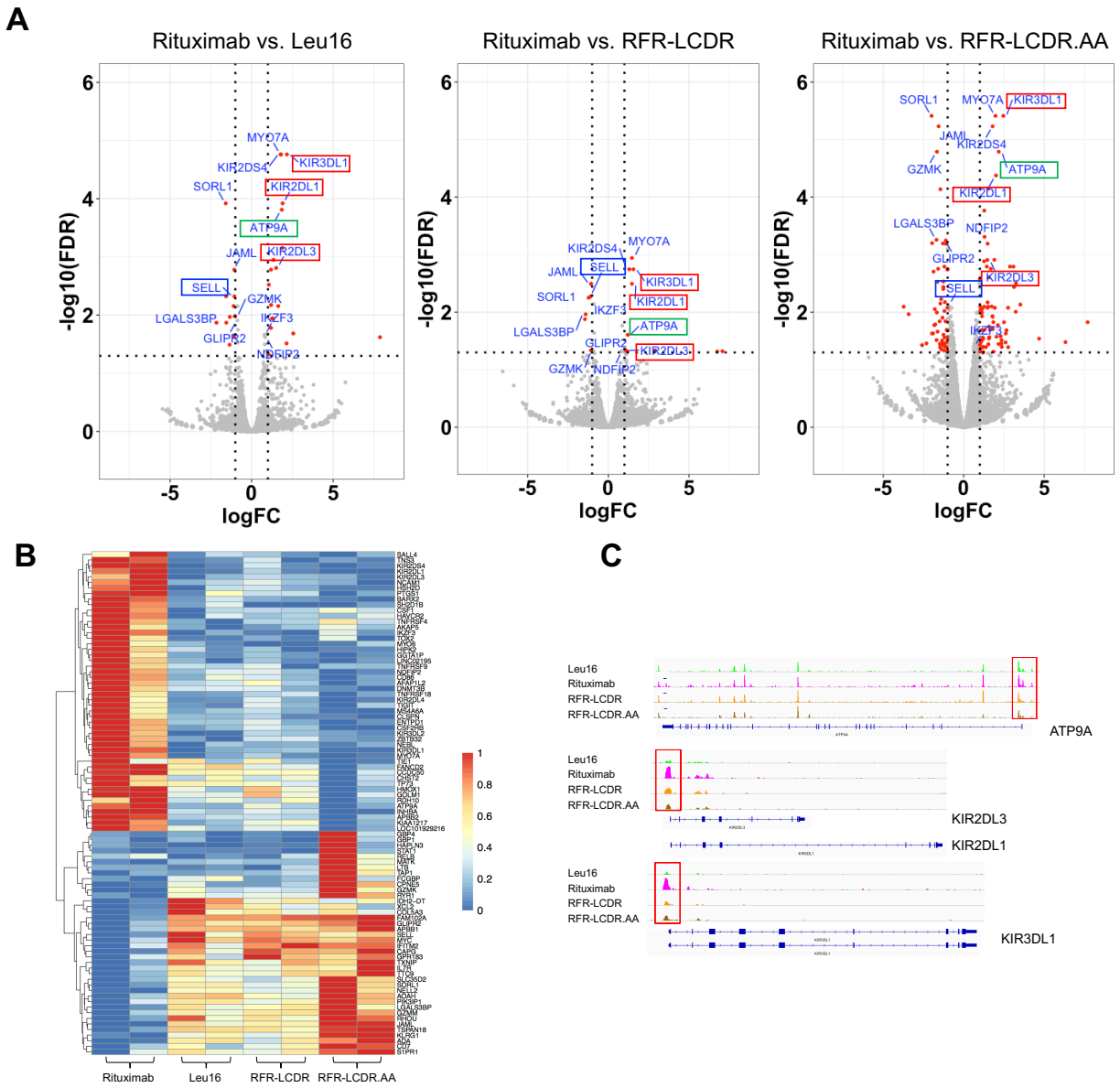

Figure 3.7 Transcriptomic and epigenetic analyses reveal CAR-dependent variations in T-cell phenotype

(A-C) NSG mice were injected i.v. with 0.5 x 10^6 firefly-luciferase–expressing Raji cells 6 days prior to treatment with 2.85 x 10^6 CAR+ T cells delivered i.v. Liver, spleen, cardiac blood, and bone marrow were collected from tumor-bearing mice 9 days after T-cell injection (n = 2 mice per group). CAR+ T cells were obtained by enriching for huCD45$^+$ EGFRt$^+$ populations, and subsequently analyzed by RNA-seq and ATAC-seq.

(A) Volcano plots of differentially expressed genes of Rituximab CAR-T cells versus Leu16 (left), RFR-LCDR (middle), or RFR-LCDR.AA (right) CAR-T cells based on RNA-seq. All differentially expressed genes are plotted in grey. Genes that have at least 2-fold upregulation or downregulation (log2FC > 1 or log2FC < -1) with FDR < 0.05 are shown as red dots. The names of genes that appear in all three sets of pair-wise comparisons with log2FC > 1 and FDR < 0.05 or log2FC < -1 and FDR < 0.05 are labeled.
(B) Heatmap of differentially expressed genes the 91 differentially expressed genes in ANOVA comparison of Leu16, Rituximab, RFR-LCDR, RFR-LCDR.AA CAR-T cells isolated from mice 9 days post infusion (cutoff: FDR in ANOVA <0.05). Each column represented one mouse (n=2). Normalized read count (Reads Per Kilobase of transcript, per Million mapped reads, RPKM) were scaled to [0,1].
(C) Genome browser files of differentially accessible regions in Leu16, Rituximab, RFR-LCDR, RFR-LCDR.AA CAR-T cells at the *atp9a, kir2dl3, kir2dl1, kir3dl1* loci.

Furthermore, we have looked into Gene Set Enrichment Analysis (GSEA) to evaluate the differences among CD20 CAR-T cells. Our results revealed that the most superior RFR-LCDR.AA CAR-T cells exhibited strong T-cell activation and memory phenotype and retained low cell-cycle activities (Figure 3.8A-D), contrary to the profile of rituximab CAR-T cells.

Through RNA-seq and ATAC-seq analysis, our data indicate that superior CAR-T cells exhibit strong anti-tumor effector function while sustaining memory phenotype to promote long-term persistence *in vivo.*

Tonically signaling CAR-T cell upregulates metabolic activity at rest

Our previous finding on *atp9a* upregulation in rituximab CAR-T cells implied elevated glycolytic activity in this tonically signaling CAR-T cell line. To study how metabolism regulates cell fate and function, we have looked into the metabolomic landscape of a panel of differentially performing CARs. We observed that CARs with tonic signaling behavior had elevated glucose and glutamine uptake, which resulted in accumulation of extracellular lactate, alanine and glutamine (Figure 3.9). Unlike the changes observed in antigen-dependent T-cell proliferation and TNF-α production (Figure 3.2B,C), alanine-insertion in the rituximab CAR did not alter the T-cell metabolic profile at rest (Figure 3.9; Supplementary Figure 3.S8). Similar to previous findings (Figure 3.3C, Figure 3.4A), both of the hybrid CAR-T cells with and without alanine

insertion had a calibrated level of T-cell activation and metabolic activity at rest (Figure 3.9; Supplementary Figure 3.S8)

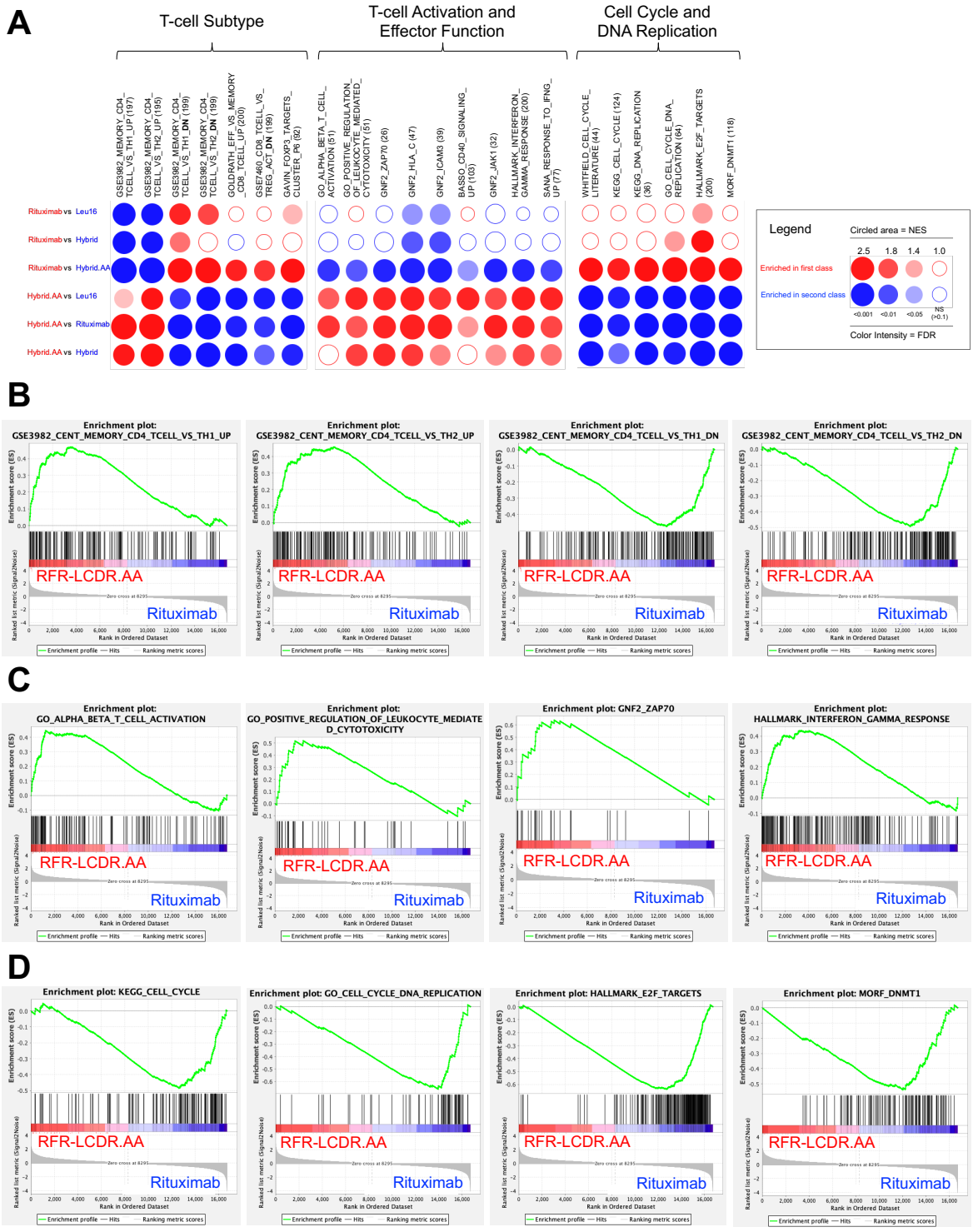

Figure 3.8. RFR-LCDR.AA CAR-T cells show robust T-cell activation coupled with memory phenotype
(A) Gene Set Enrichment Analysis (GSEA) was performed on RNA-seq data obtained as described in Figure 3.6A. A summary of results in pathways related to T-cell phenotype and function are shown in BubbleGUM map format (Spinelli et al., 2015).
(B) Mountain plots of pathways related to T-cell subtype.
(C) Mountain plots of pathways related to T-cell activation and interferon gamma signaling.
(D) Mountain plots of pathways related to cell cycle, DNA replication, and cell metabolism.

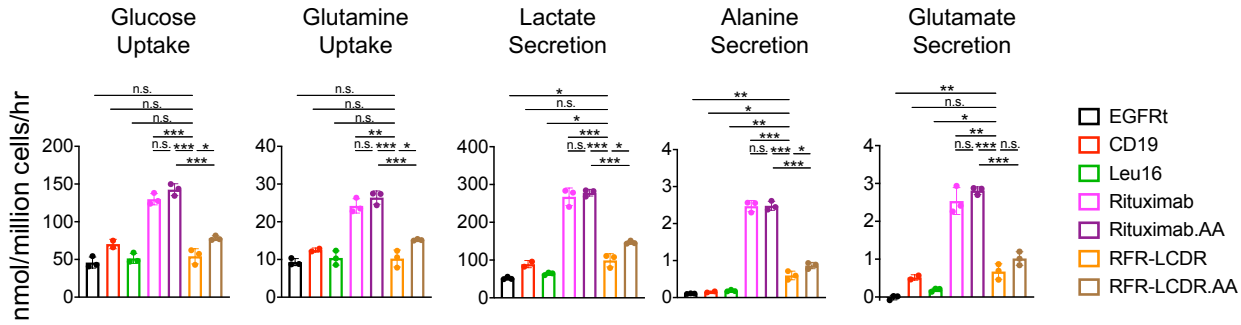

Figure 3.9 Metabolic activity at rest is associated with tonic signaling Metabolic analysis of CAR-T cells in culture in the absence of antigen stimulation. CAR-T cells were cultured for 72 hours in RPMI supplemented with 10% heat-inactivated, dialyzed fetal bovine serum (HI-dFBS), IL-2, and IL-15. Data bars indicate the means of technical triplicates ± 1 S.D. Data are representative of three independent experiments from three different healthy donors. *p<0.05, **p<0.01, ***p<0.001, n.s. not statistically significant.

In addition to metabolomic analysis, we also evaluated the transcriptomic profile of T cells *in vitro*. Sets of genes that associated with T-cell activation, exhaustion and memory phenotype were measured on T cells without stimulation and with one or four stimulations. Rituximab CAR-T cells upregulated some activation related (*ifng, gzmb, il2ra)* and exhaustion related (*lag3, ctla4, havcr2, prdm1, tbx21, jun, junb, fosb*, etc) genes indicating their basal T-cell signaling at rest (Figure 3.10) (Blackburn et al., 2009; Crawford et al., 2014; Fraietta et al., 2018; Long et al., 2015; Lynn et al., 2019; Mognol et al., 2017). Echoing previous findings on T cells retrieved from tumor-bearing mice, rituximab CAR-T cells downregulated memory associated genes (*il7r, tcf7, lef1, klf2, sell*) (Figure 3.10, Figure 3.7B). Alanine-insertion reduced the strong exhaustion phenotype of rituximab CAR-T cells. Being similar in their *in vitro* and *in vivo* function, both hybrid CAR-T cells exhibited similar gene expression profiles. There was not

a distinct phenotypic difference among different CD20 CAR-T cells with stimulation (regardless of the numbers of stimulation).

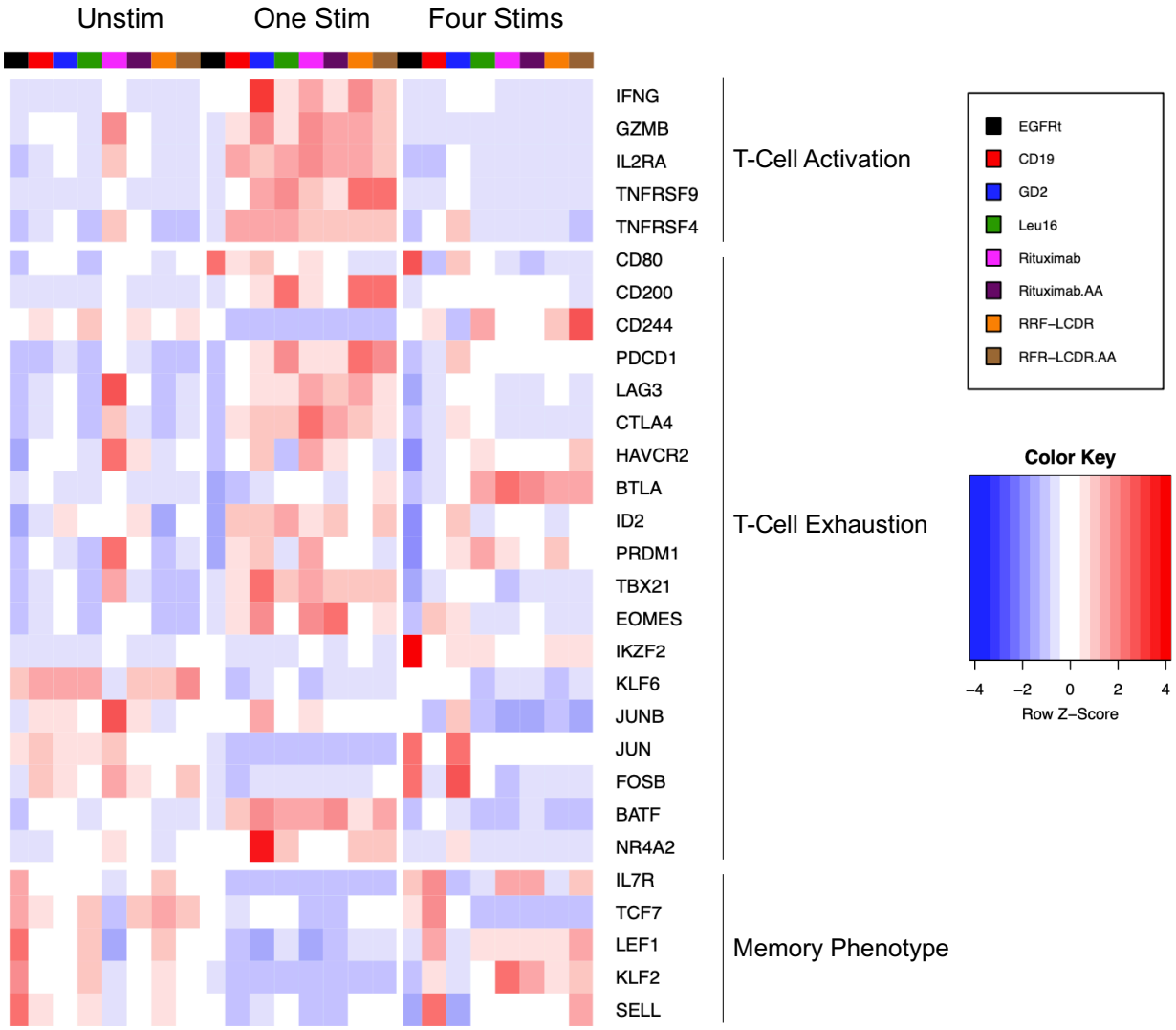

Figure 3.10 Rituximab CAR-T cells hav4 basal T-cell activation at rest coupled with reduction in memory associated genes CAR+ T cells with and without stimulation with Raji cells were enriched for EGFRt^{+} populations, and subsequently analyzed by RNA-seq. One stimulation was done fourteen hours post Raji addition. In four stimulations, Raji cells were added to the culture every two days. The heatmap of genes associated with T-cell activation and exhaustion as well as memory phenotype is shown. Data shows rpkm of genes. Data represented one donor.

Taken together, our results indicate that rituximab CAR-T cells exhibit elevated metabolic activity and downregulation of memory associated genes at rest and upon antigen stimulation *in vivo*. In contrast, RFR-LCDR.AA promotes rapid effector function and memory T-

cell phenotype while maintaining relatively low metabolic activity and long-term persistence. This study also underscores the positive correlation of tonic signaling and metabolic activity of cells. Both alanine insertion and scFv sequence hybridization calibrated tonic signaling phenotype indicated by transcriptomic profiling and metabolic activity at rest. In summary, non-zero, basal T-cell activation could be used to predict CAR-T cell function.

DISCUSSION

Previous studies have suggested that tonic signaling is detrimental to CAR-T cell function (Frigault et al., 2015; Gomes-Silva et al., 2017; Long et al., 2015; Watanabe et al., 2016). Many CAR studies have excluded candidates that exhibit tonic signaling behaviors (Bloemberg et al., 2020; Mirzaei et al., 2019; Smith et al., 2019). From the high-throughput screening study in Chapter 2, we found that the elimination of clones that exhibited tonic signaling phenotype did not reduce library diversity. This finding suggested the possibility that tonic signaling might not always have adverse effect on T-cell function.

In this study, we were particularly interested in evaluating the impact of tonic signaling on T-cell performance. We focused on the sequence-to-function effect of CARs and methods to calibrate CAR tonic signaling via extracellular and intracellular domain engineering. Our results indicated that a two amino acid insertion and slight changes in scFv sequences tune CAR signaling and dramatically redirect T-cell fate. Two alanines inserted in tonically signaling rituximab CAR-T cells successfully decreased their signaling intensities at rest and upon antigen stimulation, which yielded a CAR with superior *in vivo* performance. ScFv hybridization via combining FRs from tonically signaling CARs and CDRs from non-tonically signaling CARs resulted in a variant with a further improvement in anti-tumor efficacy, which even outperformed the well-established CD19 CAR. To our knowledge, this is the first study that suggested positive effect of tonic signaling and underscored a low-level activation at rest prepared engineered

CAR-T cells to launch a rapid anti-tumor response without compromising long-term T-cell persistence.

The alanine-insertion method indicates that there exists an optimal physical conformation of a given CAR. Each CAR molecule adopts a native protein conformation for optimal signal transduction. Alanine insertion in the signaling moiety of CARs represents a generalized strategy to tune CAR-T cells signaling both at rest and upon stimulation. Incorporation of two alanines proved to be the optimal conformation for multiple CARs – rituximab CAR and GD2 CAR – that resulted the best *in vivo* outcome. Thus, our strategy opens a new avenue of systematic CAR design.

In addition to alanine insertion, scFv hybridization indicated the possibility to improve CAR-T cell function by changing its FR sequence without abolishing tonic signaling. A hybrid RFR-LCDR generated by grafting the framework from rituximab to leu16 CDRs exhibited low-level tonic signaling and a significant improvement in CAR-T cell function compared to both of the parental CARs, suggesting that certain residues on the rituximab FRs contributed to tonic CAR signaling. The other hybrid LFR-RCDR CAR-T cells containing FRs from leu16 and CDRs from rituximab had complete loss of effector function. These results suggested that scFv hybridization provides useful insight towards optimization of CAR design, but the methodology still requires further improvement. In-depth analysis of amino acid residues on FRs is needed to identify critical residues that retain binding to cognate antigens as well as confer optimal CAR function.

Memory and effector T cells are very different in metabolism. Memory T cells have catabolic metabolism to break down nutrients to generate energy while activating/effector T cells have anabolic metabolism to build up biomass (Pearce and Pearce, 2013; Pearce et al., 2013). Unlike effector or activating T cells, memory T cells have distinct metabolic pathways and mainly engage in oxidative phosphorylation (OXPHOS) and fatty acid oxidation (FAO), with little involvement in glycolysis and pentose phosphate pathway (PPP) (Pearce and Pearce, 2013;

Pearce et al., 2013; Pearce et al., 2009; van der Windt et al., 2012). In our study, we investigated the uptake rate of the two main nutrient sources – glucose and glutamine – and observed the high consumption rate was tightly correlated with their tonic signaling behavior. The RFR-LCDR.AA CAR-T cells exhibiting calibrated, non-zero tonic signaling and metabolic activity at rest was strongly correlated with their functional superiority.

In this study, we established a modular protein engineering approach to calibrate CAR-T cell signaling with the presence and absence of stimulation, yielding functionally superior CARs against different antigens in B-cell lymphoma and metastatic neuroblastoma. Our work presents a highly adaptable method for optimization of CAR design for various disease types including both blood and solid malignancies.

REFERENCES

Bennett, B.D., Yuan, J., Kimball, E.H., and Rabinowitz, J.D. (2008). Absolute quantitation of intracellular metabolite concentrations by an isotope ratio-based approach. Nat Protoc *3*, 1299-1311.

Bjorkstrom, N.K., Beziat, V., Cichocki, F., Liu, L.L., Levine, J., Larsson, S., Koup, R.A., Anderson, S.K., Ljunggren, H.G., and Malmberg, K.J. (2012). CD8 T cells express randomly selected KIRs with distinct specificities compared with NK cells. Blood *120*, 3455-3465.

Blackburn, S.D., Shin, H., Haining, W.N., Zou, T., Workman, C.J., Polley, A., Betts, M.R., Freeman, G.J., Vignali, D.A., and Wherry, E.J. (2009). Coregulation of CD8+ T cell exhaustion by multiple inhibitory receptors during chronic viral infection. Nat Immunol *10*, 29-37.

Bloemberg, D., Nguyen, T., MacLean, S., Zafer, A., Gadoury, C., Gurnani, K., Chattopadhyay, A., Ash, J., Lippens, J., Harcus, D.*, et al.* (2020). A High-Throughput Method for Characterizing Novel Chimeric Antigen Receptors in Jurkat Cells. Mol Ther Methods Clin Dev *16*, 238-254.

Brown, R.J., Adams, J.J., Pelekanos, R.A., Wan, Y., McKinstry, W.J., Palethorpe, K., Seeber, R.M., Monks, T.A., Eidne, K.A., Parker, M.W.*, et al.* (2005). Model for growth hormone receptor activation based on subunit rotation within a receptor dimer. Nat Struct Mol Biol *12*, 814-821.

Buenrostro, J.D., Giresi, P.G., Zaba, L.C., Chang, H.Y., and Greenleaf, W.J. (2013). Transposition of native chromatin for fast and sensitive epigenomic profiling of open chromatin, DNA-binding proteins and nucleosome position. Nat Methods *10*, 1213-1218.

Chang, Z.L., Lorenzini, M.H., Chen, X., Tran, U., Bangayan, N.J., and Chen, Y.Y. (2018). Rewiring T-cell responses to soluble factors with chimeric antigen receptors. Nat Chem Biol *14*, 317-324.

Chothia, C., and Lesk, A.M. (1987). Canonical structures for the hypervariable regions of immunoglobulins. J Mol Biol *196*, 901-917.

Chothia, C., Lesk, A.M., Tramontano, A., Levitt, M., Smith-Gill, S.J., Air, G., Sheriff, S., Padlan, E.A., Davies, D., Tulip, W.R.*, et al.* (1989). Conformations of immunoglobulin hypervariable regions. Nature *342*, 877-883.

Clasquin, M.F., Melamud, E., and Rabinowitz, J.D. (2012). LC-MS data processing with MAVEN: a metabolomic analysis and visualization engine. Curr Protoc Bioinformatics *Chapter 14*, Unit14 11.

Constantinescu, S.N., Keren, T., Socolovsky, M., Nam, H., Henis, Y.I., and Lodish, H.F. (2001). Ligand-independent oligomerization of cell-surface erythropoietin receptor is mediated by the transmembrane domain. Proc Natl Acad Sci U S A *98*, 4379-4384.

Corces, M.R., Trevino, A.E., Hamilton, E.G., Greenside, P.G., Sinnott-Armstrong, N.A., Vesuna, S., Satpathy, A.T., Rubin, A.J., Montine, K.S., Wu, B.*, et al.* (2017). An improved ATAC-seq protocol reduces background and enables interrogation of frozen tissues. Nat Methods *14*, 959-962.

Crawford, A., Angelosanto, J.M., Kao, C., Doering, T.A., Odorizzi, P.M., Barnett, B.E., and Wherry, E.J. (2014). Molecular and transcriptional basis of CD4(+) T cell dysfunction during chronic infection. Immunity *40*, 289-302.

Cretenet, G., Clerc, I., Matias, M., Loisel, S., Craveiro, M., Oburoglu, L., Kinet, S., Mongellaz, C., Dardalhon, V., and Taylor, N. (2016). Cell surface Glut1 levels distinguish human CD4 and CD8 T lymphocyte subsets with distinct effector functions. Sci Rep *6*, 24129.

Feucht, J., Sun, J., Eyquem, J., Ho, Y.J., Zhao, Z., Leibold, J., Dobrin, A., Cabriolu, A., Hamieh, M., and Sadelain, M. (2019). Calibration of CAR activation potential directs alternative T cell fates and therapeutic potency. Nat Med *25*, 82-88.

Fraietta, J.A., Lacey, S.F., Orlando, E.J., Pruteanu-Malinici, I., Gohil, M., Lundh, S., Boesteanu, A.C., Wang, Y., O'Connor, R.S., Hwang, W.T.*, et al.* (2018). Determinants of response and resistance to CD19 chimeric antigen receptor (CAR) T cell therapy of chronic lymphocytic leukemia. Nat Med *24*, 563-571.

Frigault, M.J., Lee, J., Basil, M.C., Carpenito, C., Motohashi, S., Scholler, J., Kawalekar, O.U., Guedan, S., McGettigan, S.E., Posey, A.D., Jr.*, et al.* (2015). Identification of chimeric antigen receptors that mediate constitutive or inducible proliferation of T cells. Cancer Immunol Res *3*, 356-367.

Gomes-Silva, D., Mukherjee, M., Srinivasan, M., Krenciute, G., Dakhova, O., Zheng, Y., Cabral, J.M.S., Rooney, C.M., Orange, J.S., Brenner, M.K.*, et al.* (2017). Tonic 4-1BB Costimulation in Chimeric Antigen Receptors Impedes T Cell Survival and Is Vector-Dependent. Cell Rep *21*, 17-26.

Greiser, J.S., Stross, C., Heinrich, P.C., Behrmann, I., and Hermanns, H.M. (2002). Orientational constraints of the gp130 intracellular juxtamembrane domain for signaling. J Biol Chem *277*, 26959-26965.

Hartman, N.C., and Groves, J.T. (2011). Signaling clusters in the cell membrane. Curr Opin Cell Biol *23*, 370-376.

Hudecek, M., Sommermeyer, D., Kosasih, P.L., Silva-Benedict, A., Liu, L., Rader, C., Jensen, M.C., and Riddell, S.R. (2015). The nonsignaling extracellular spacer domain of chimeric antigen receptors is decisive for in vivo antitumor activity. Cancer Immunol Res *3*, 125-135.

Jensen, M., Tan, G., Forman, S., Wu, A.M., and Raubitschek, A. (1998). CD20 is a molecular target for scFvFc:zeta receptor redirected T cells: implications for cellular immunotherapy of CD20+ malignancy. Biol Blood Marrow Transplant *4*, 75-83.

Jones, P.T., Dear, P.H., Foote, J., Neuberger, M.S., and Winter, G. (1986). Replacing the complementarity-determining regions in a human antibody with those from a mouse. Nature *321*, 522-525.

Kabat, E.A., and Wu, T.T. (1971). Attempts to locate complementarity-determining residues in the variable positions of light and heavy chains. Ann N Y Acad Sci *190*, 382-393.

Klein, C., Lammens, A., Schafer, W., Georges, G., Schwaiger, M., Mossner, E., Hopfner, K.P., Umana, P., and Niederfellner, G. (2013). Epitope interactions of monoclonal antibodies targeting CD20 and their relationship to functional properties. MAbs *5*, 22-33.

Krauss, J., Arndt, M.A., Martin, A.C., Liu, H., and Rybak, S.M. (2003). Specificity grafting of human antibody frameworks selected from a phage display library: generation of a highly stable humanized anti-CD22 single-chain Fv fragment. Protein Eng *16*, 753-759.

Liu, W., Kawahara, M., Ueda, H., and Nagamune, T. (2008). Construction of a fluorescein-responsive chimeric receptor with strict ligand dependency. Biotechnol Bioeng *101*, 975-984.

Long, A.H., Haso, W.M., Shern, J.F., Wanhainen, K.M., Murgai, M., Ingaramo, M., Smith, J.P., Walker, A.J., Kohler, M.E., Venkateshwara, V.R.*, et al.* (2015). 4-1BB costimulation ameliorates T cell exhaustion induced by tonic signaling of chimeric antigen receptors. Nat Med *21*, 581-590.

Love, P.E., and Hayes, S.M. (2010). ITAM-mediated signaling by the T-cell antigen receptor. Cold Spring Harb Perspect Biol *2*, a002485.

Lynn, R.C., Weber, E.W., Sotillo, E., Gennert, D., Xu, P., Good, Z., Anbunathan, H., Lattin, J., Jones, R., Tieu, V.*, et al.* (2019). c-Jun overexpression in CAR T cells induces exhaustion resistance. Nature *576*, 293-300.

Macintyre, A.N., Gerriets, V.A., Nichols, A.G., Michalek, R.D., Rudolph, M.C., Deoliveira, D., Anderson, S.M., Abel, E.D., Chen, B.J., Hale, L.P.*, et al.* (2014). The glucose transporter Glut1 is selectively essential for CD4 T cell activation and effector function. Cell Metab *20*, 61-72.

Majzner, R.G., and Mackall, C.L. (2019). Clinical lessons learned from the first leg of the CAR T cell journey. Nat Med *25*, 1341-1355.

Martin, A.C., and Thornton, J.M. (1996). Structural families in loops of homologous proteins: automatic classification, modelling and application to antibodies. J Mol Biol *263*, 800-815.

Mirzaei, H.R., Jamali, A., Jafarzadeh, L., Masoumi, E., Alishah, K., Fallah Mehrjardi, K., Emami, S.A.H., Noorbakhsh, F., Till, B.G., and Hadjati, J. (2019). Construction and functional characterization of a fully human anti-CD19 chimeric antigen receptor (huCAR)-expressing primary human T cells. J Cell Physiol *234*, 9207-9215.

Mognol, G.P., Spreafico, R., Wong, V., Scott-Browne, J.P., Togher, S., Hoffmann, A., Hogan, P.G., Rao, A., and Trifari, S. (2017). Exhaustion-associated regulatory regions in CD8(+) tumor-infiltrating T cells. Proc Natl Acad Sci U S A *114*, E2776-E2785.

Mossner, E., Brunker, P., Moser, S., Puntener, U., Schmidt, C., Herter, S., Grau, R., Gerdes, C., Nopora, A., van Puijenbroek, E.*, et al.* (2010). Increasing the efficacy of CD20 antibody therapy through the engineering of a new type II anti-CD20 antibody with enhanced direct and immune effector cell-mediated B-cell cytotoxicity. Blood *115*, 4393-4402.

Niederfellner, G., Lammens, A., Mundigl, O., Georges, G.J., Schaefer, W., Schwaiger, M., Franke, A., Wiechmann, K., Jenewein, S., Slootstra, J.W.*, et al.* (2011). Epitope characterization and crystal structure of GA101 provide insights into the molecular basis for type I/II distinction of CD20 antibodies. Blood *118*, 358-367.

Notredame, C., Higgins, D.G., and Heringa, J. (2000). T-Coffee: A novel method for fast and accurate multiple sequence alignment. J Mol Biol *302*, 205-217.

Park, J.O., Tanner, L.B., Wei, M.H., Khana, D.B., Jacobson, T.B., Zhang, Z., Rubin, S.A., Li, S.H., Higgins, M.B., Stevenson, D.M.*, et al.* (2019). Near-equilibrium glycolysis supports metabolic homeostasis and energy yield. Nat Chem Biol *15*, 1001-1008.

Pearce, E.L., and Pearce, E.J. (2013). Metabolic pathways in immune cell activation and quiescence. Immunity *38*, 633-643.

Pearce, E.L., Poffenberger, M.C., Chang, C.H., and Jones, R.G. (2013). Fueling immunity: insights into metabolism and lymphocyte function. Science *342*, 1242454.

Pearce, E.L., Walsh, M.C., Cejas, P.J., Harms, G.M., Shen, H., Wang, L.S., Jones, R.G., and Choi, Y. (2009). Enhancing CD8 T-cell memory by modulating fatty acid metabolism. Nature *460*, 103-107.

Queen, C., Schneider, W.P., Selick, H.E., Payne, P.W., Landolfi, N.F., Duncan, J.F., Avdalovic, N.M., Levitt, M., Junghans, R.P., and Waldmann, T.A. (1989). A humanized antibody that binds to the interleukin 2 receptor. Proc Natl Acad Sci U S A *86*, 10029-10033.

Reff, M.E., Carner, K., Chambers, K.S., Chinn, P.C., Leonard, J.E., Raab, R., Newman, R.A., Hanna, N., and Anderson, D.R. (1994). Depletion of B cells in vivo by a chimeric mouse human monoclonal antibody to CD20. Blood *83*, 435-445.

Rufener, G.A., Press, O.W., Olsen, P., Lee, S.Y., Jensen, M.C., Gopal, A.K., Pender, B., Budde, L.E., Rossow, J.K., Green, D.J.*, et al.* (2016). Preserved Activity of CD20-Specific Chimeric Antigen Receptor-Expressing T Cells in the Presence of Rituximab. Cancer Immunol Res *4*, 509-519.

Scheller, L., Strittmatter, T., Fuchs, D., Bojar, D., and Fussenegger, M. (2018). Generalized extracellular molecule sensor platform for programming cellular behavior. Nat Chem Biol *14*, 723-729.

Schurich, A., Pallett, L.J., Jajbhay, D., Wijngaarden, J., Otano, I., Gill, U.S., Hansi, N., Kennedy, P.T., Nastouli, E., Gilson, R.*, et al.* (2016). Distinct Metabolic Requirements of Exhausted and Functional Virus-Specific CD8 T Cells in the Same Host. Cell Rep *16*, 1243-1252.

Smith, E.L., Harrington, K., Staehr, M., Masakayan, R., Jones, J., Long, T.J., Ng, K.Y., Ghoddusi, M., Purdon, T.J., Wang, X.*, et al.* (2019). GPRC5D is a target for the immunotherapy of multiple myeloma with rationally designed CAR T cells. Sci Transl Med *11*.

Smith-Garvin, J.E., Koretzky, G.A., and Jordan, M.S. (2009). T cell activation. Annu Rev Immunol *27*, 591-619.

Spinelli, L., Carpentier, S., Montanana Sanchis, F., Dalod, M., and Vu Manh, T.P. (2015). BubbleGUM: automatic extraction of phenotype molecular signatures and comprehensive visualization of multiple Gene Set Enrichment Analyses. BMC Genomics *16*, 814.

Swindells, M.B., Porter, C.T., Couch, M., Hurst, J., Abhinandan, K.R., Nielsen, J.H., Macindoe, G., Hetherington, J., and Martin, A.C. (2017). abYsis: Integrated Antibody Sequence and Structure-Management, Analysis, and Prediction. J Mol Biol *429*, 356-364.

Teeling, J.L., Mackus, W.J., Wiegman, L.J., van den Brakel, J.H., Beers, S.A., French, R.R., van Meerten, T., Ebeling, S., Vink, T., Slootstra, J.W.*, et al.* (2006). The biological activity of human CD20 monoclonal antibodies is linked to unique epitopes on CD20. J Immunol *177*, 362-371.

Uchiyama, S., Suzuki, Y., Otake, K., Yokoyama, M., Ohta, M., Aikawa, S., Komatsu, M., Sawada, T., Kagami, Y., Morishima, Y.*, et al.* (2010). Development of novel humanized anti-CD20 antibodies based on affinity constant and epitope. Cancer Sci *101*, 201-209.

van der Windt, G.J., Everts, B., Chang, C.H., Curtis, J.D., Freitas, T.C., Amiel, E., Pearce, E.J., and Pearce, E.L. (2012). Mitochondrial respiratory capacity is a critical regulator of CD8+ T cell memory development. Immunity *36*, 68-78.

Watanabe, N., Bajgain, P., Sukumaran, S., Ansari, S., Heslop, H.E., Rooney, C.M., Brenner, M.K., Leen, A.M., and Vera, J.F. (2016). Fine-tuning the CAR spacer improves T-cell potency. Oncoimmunology *5*, e1253656.

Willuda, J., Honegger, A., Waibel, R., Schubiger, P.A., Stahel, R., Zangemeister-Wittke, U., and Pluckthun, A. (1999). High thermal stability is essential for tumor targeting of antibody fragments: engineering of a humanized anti-epithelial glycoprotein-2 (epithelial cell adhesion molecule) single-chain Fv fragment. Cancer Res *59*, 5758-5767.

Ying, Z., Huang, X.F., Xiang, X., Liu, Y., Kang, X., Song, Y., Guo, X., Liu, H., Ding, N., Zhang, T.*, et al.* (2019). A safe and potent anti-CD19 CAR T cell therapy. Nat Med *25*, 947-953.

Zah, E., Lin, M.Y., Silva-Benedict, A., Jensen, M.C., and Chen, Y.Y. (2016). T Cells Expressing CD19/CD20 Bispecific Chimeric Antigen Receptors Prevent Antigen Escape by Malignant B Cells. Cancer Immunol Res *4*, 498-508.

Zettlitz, K.A., Tavare, R., Knowles, S.M., Steward, K.K., Timmerman, J.M., and Wu, A.M. (2017). ImmunoPET of Malignant and Normal B Cells with (89)Zr- and (124)I-Labeled Obinutuzumab Antibody Fragments Reveals Differential CD20 Internalization In Vivo. Clin Cancer Res *23*, 7242-7252.

SUPPLEMENTARY FIGURES

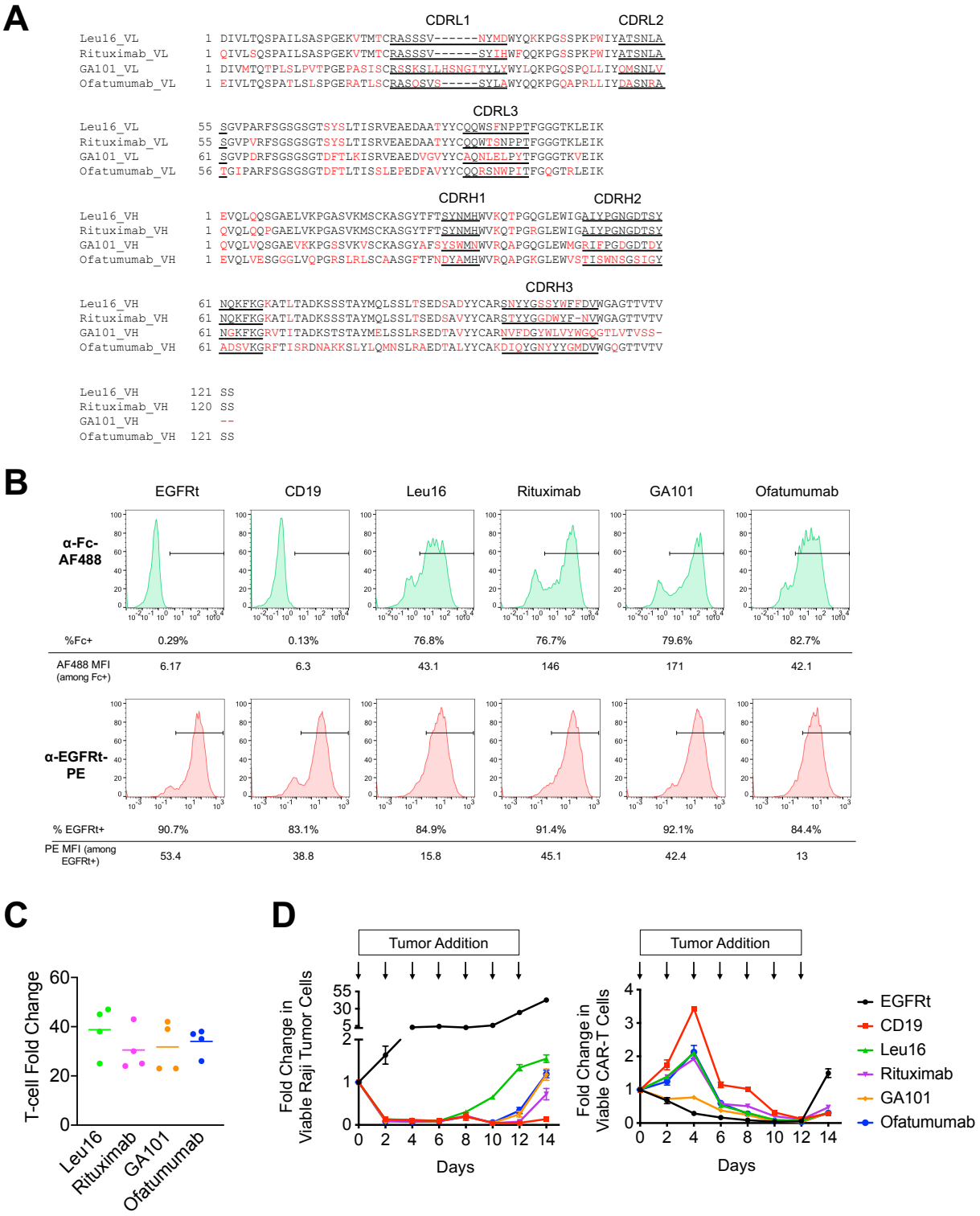

Supplementary Figure 3.S1. Panel of CD20 CARs exhibit similar characteristics *in vitro*
(A) Alignment of leu16, rituximab, GA101 and ofatumumab scFv sequences using T-Coffee (Notredame et al., 2000).

(B) CAR-T cell transduction efficiency as quantified by CAR surface expression (top) and transduction-marker expression (bottom), which were detected via antibody staining of the CAR's IgG4 extracellular spacer (Fc) and EGFRt, respectively. Median florescence intensity (MFI) and % positive of each antigen staining were noted below flow cytometry histograms. Results are representative of three independent experiments from three different healthy donors.
(C) CD20 CAR-T cell proliferation during *ex vivo* culture with exogenous cytokine IL-2 and IL15. Fold change in total viable cell count between Day 2 and Day 14 are shown. Each data point represents one donor; data for 4 donors per construct are shown. No statistical difference between any of the donors was detected by unpaired, two-tailed, two-sample Student's *t* test.
(D) CAR-T cell cytotoxicity and proliferation upon repeated antigen challenge. CD20 CAR-T cells were challenged with Raji tumor cells at a 2:1 effector-to-target (E:T) ratio every two days, and the number of viable Raji and CAR-T cell was quantified by flow cytometry. Data shown are the means of technical triplicates with error bars indicating ± 1 standard deviation (S.D.). Results are representative of three independent experiments from three different healthy donors.

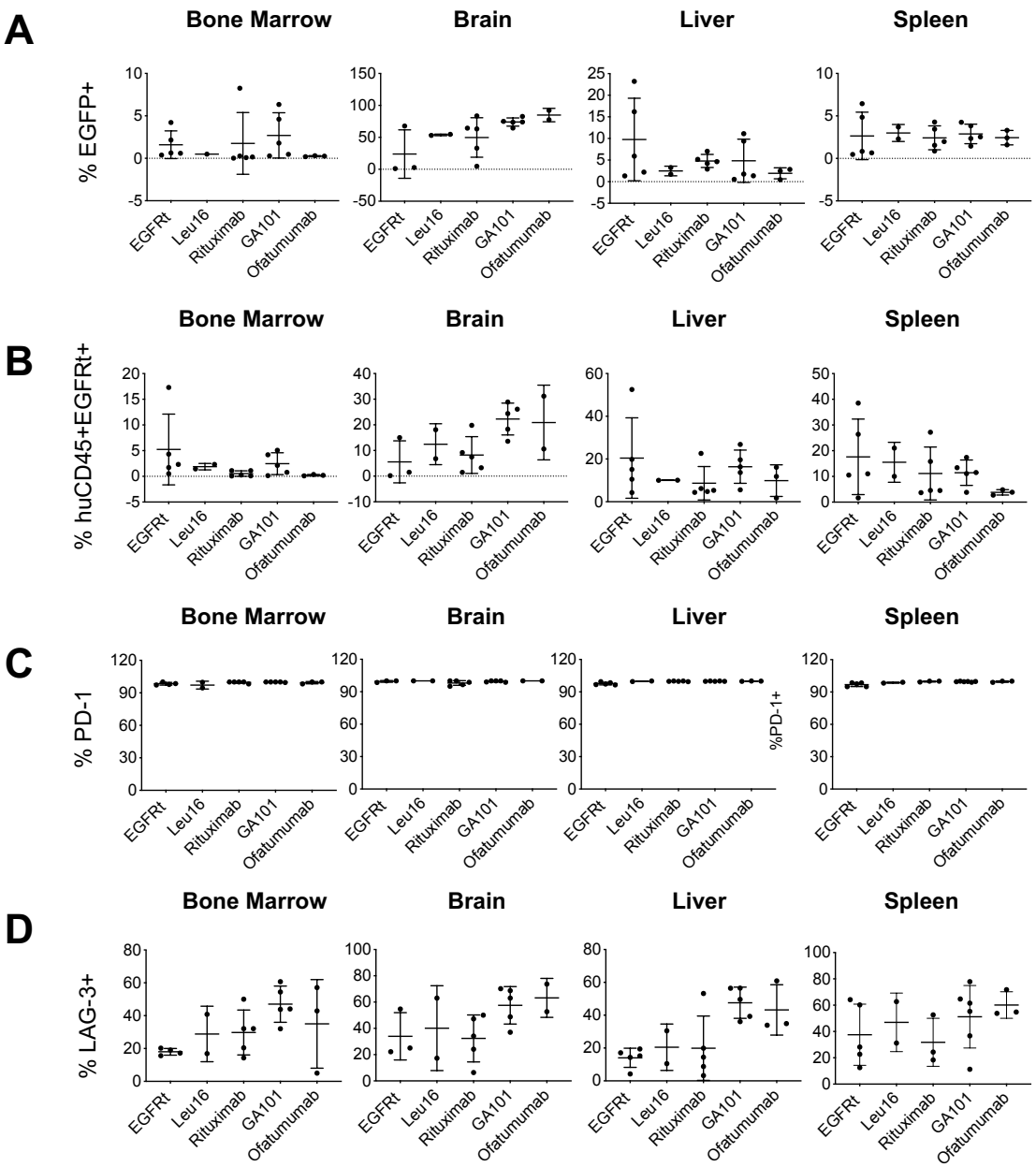

Supplementary Figure 3.S2. Tumor progression and post-mortem CD20 CAR-T cell characterization in Raji xenograft model

(A, B) Frequency of tumor cells (B) and human $CD45^{+}EGFRt^{+}$ cell (B) in bone marrow, brain, liver, and spleen collected from mice at the time of euthanasia, as quantified by flow cytometry. (C,D) Frequency of PD-1^{+} (C) and LAG-3^{+} (D) cells among human $CD45^{+}EGFRt^{+}$ cell in bone marrow, brain, liver, and spleen collected from mice at the time of euthanasia, as quantified by flow cytometry. No statistical difference between any of the donors was detected by unpaired, two-tailed, two-sample Student's *t* test for all data shown in panels (A) through (D).

Supplementary Figure 3.S3. CD20 CARs express uniformly on cell surface. Jurkat cells transduced with CAR-HaloTag fusion proteins were stained with the red fluorescent dye tetramethylrhodamine (TMR) and imaged by confocal microscopy. CAR molecules are uniformly distributed on cell surface in the absence of antigen stimulation.

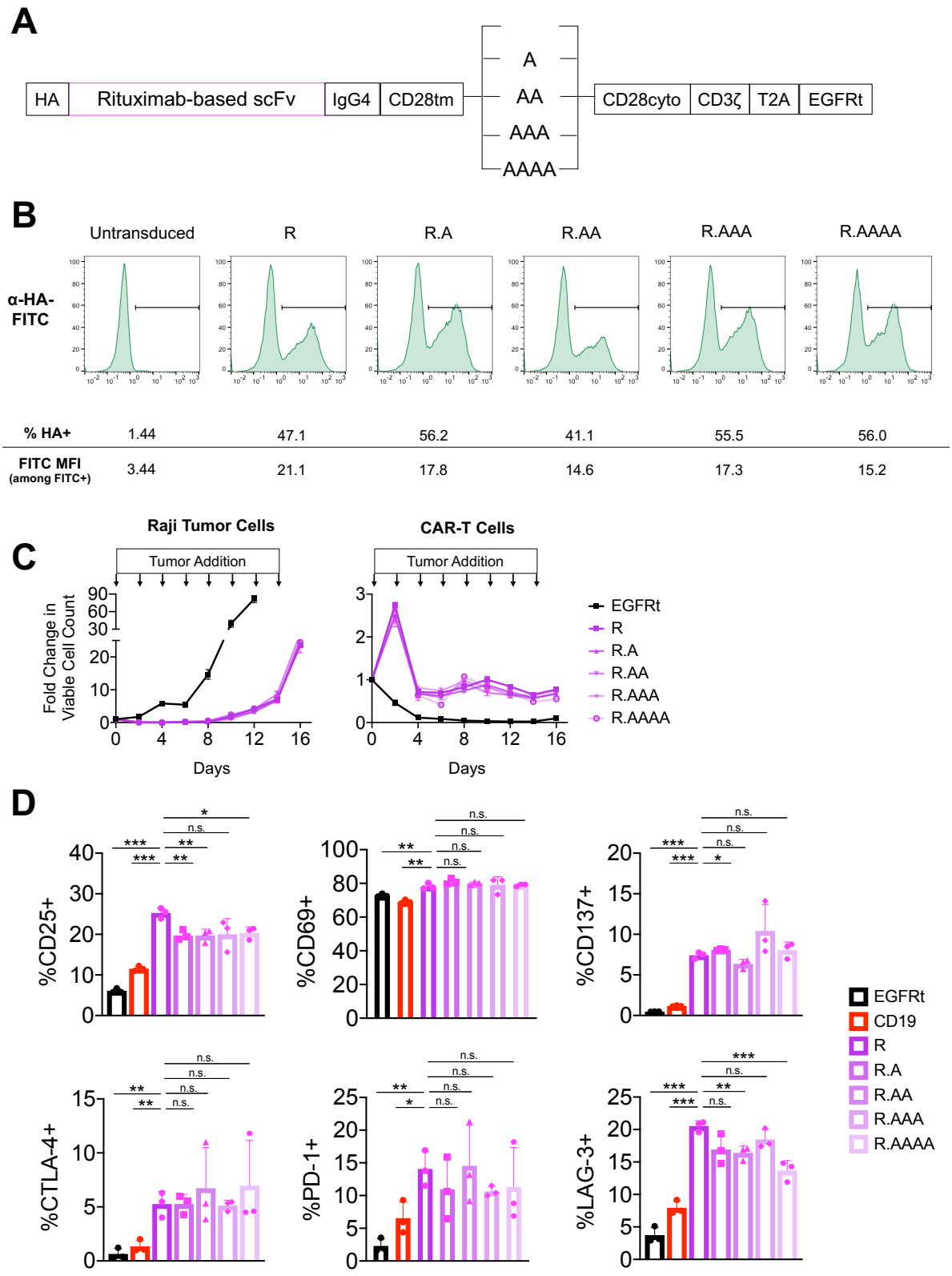

Supplementary Figure 3.S4. Rituximab CAR-T cells with torsional reorientation exhibit similar *in vitro* cytotoxicity and antigen-independent activation-marker expression

(A) Schematic of rituximab-based CAR constructs with zero to four alanines inserted between the CD28 transmembrane and cytoplasmic domains.
(B) CAR surface expression was quantified by antibody staining of HA tag fused to the N-terminus of each CAR. Data are representative of three independent experiments from three different healthy donors.
(C) CAR-T cell cytotoxicity and proliferation upon repeated antigen challenge. CD20 CAR-T cells were challenged with Raji tumor cells at a 2:1 E:T ratio every two days, and the number of viable Raji and CAR-T cell was quantified by flow cytometry. Data shown are the means of technical triplicates with error bars indicating ± 1 standard deviation (S.D.). Results are representative of three independent experiments from three different healthy donors.
(D) Activation- and exhaustion-maker expression were evaluated 11 days post Dynabead removal, without CD20 antigen stimulation. Data bars indicate the means of technical triplicates ± 1 S.D. Results are representative of three independent experiments from three different healthy donors. Unless otherwise noted, p values were determined by unpaired two-tailed Student's t test; *$p<0.05$, **$p<0.01$, ***$p<0.001$, n.s. not statistically significant.

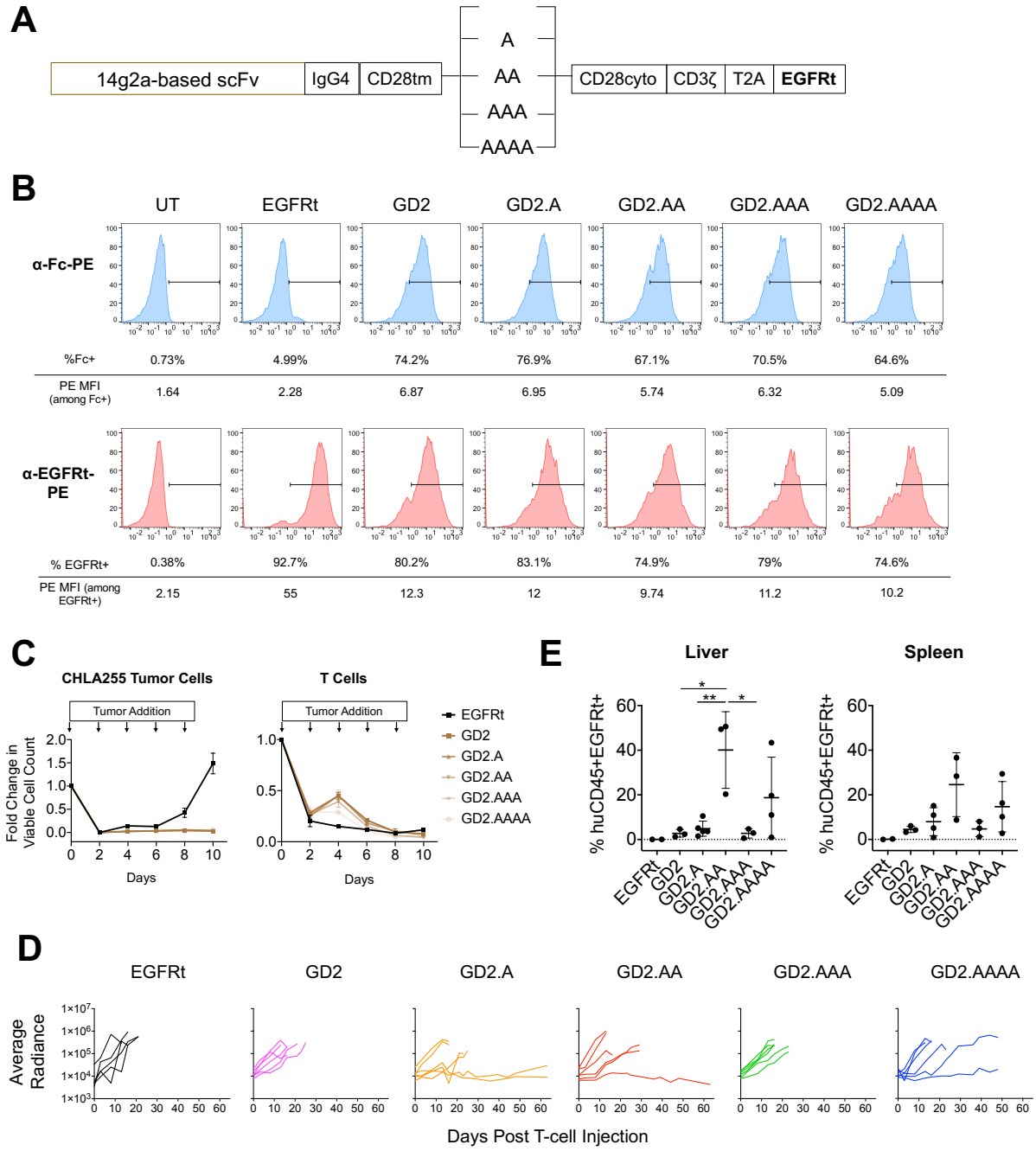

Supplementary Figure 3.S5. GD2 CAR-T cells with torsional reorientation exhibit differential tumor control *in vivo* despite same *in vitro* performance

(A) Schematic of GD2 CAR constructs with zero to four alanines inserted between the CD28 transmembrane and cytoplasmic domains.

(B) CAR surface expression (top) and transduction efficiency (bottom) were quantified by antibody staining of Fc and EGFRt.

(C) CAR-T cell cytotoxicity and proliferation upon repeated antigen challenge. GD2 CAR-T cells were challenged with CHLA-255 tumor cells at a 2:1 E:T ratio every two days, and the number of viable Raji and CAR-T cell was quantified by flow cytometry. Data shown are the means of technical triplicates with error bars indicating ± 1 standard deviation (S.D.).

(D,E) NSG mice were injected intravenously with 3.5 x 106 firefly-luciferase expressing CHLA-255 cells followed by 2 x 10^6 GD2 CAR-T cells 17 days later.
(D) Tumor progression was monitored by bioluminescence imaging.
(E) Frequency of human CD45+EGFRt+ cell in liver and spleen collected from mice at the time of euthanasia was quantified by flow cytometry. *p<0.05, **p<0.01, ***p<0.001, n.s. not statistically significant.

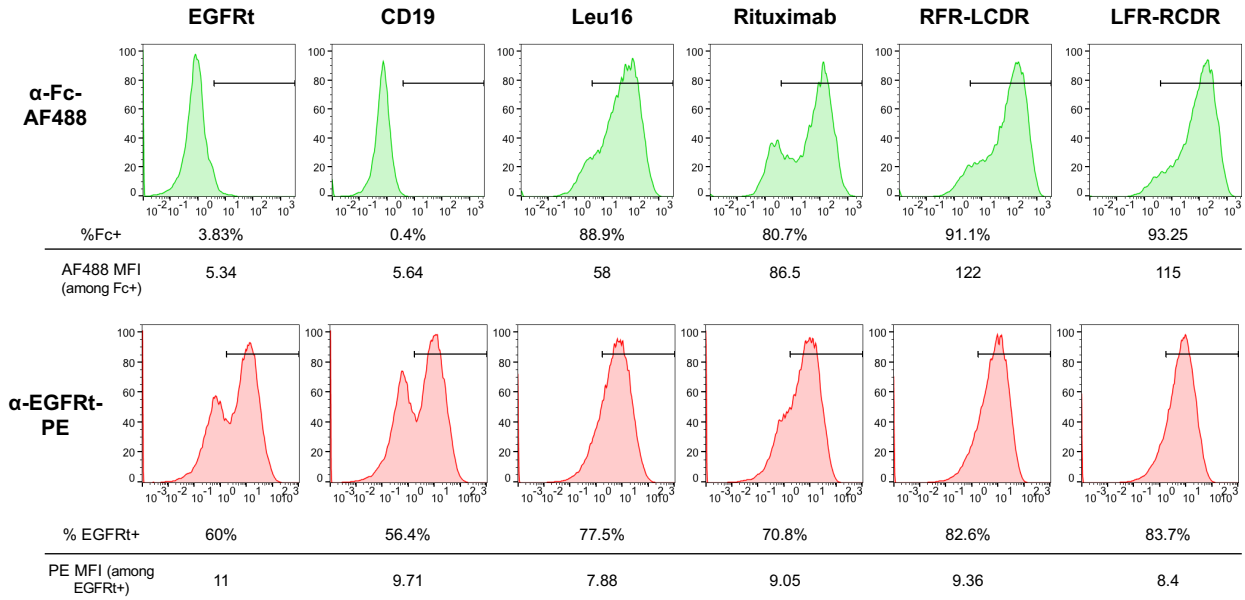

Supplementary Figure 3.S6. Hybrid CARs have similar expression level as other CD20 CARs on T cells
CAR surface expression (top) and transduction efficiency (bottom) were quantified by antibody staining of Fc and EGFRt. Results are representative of three independent experiments from three different healthy donors.

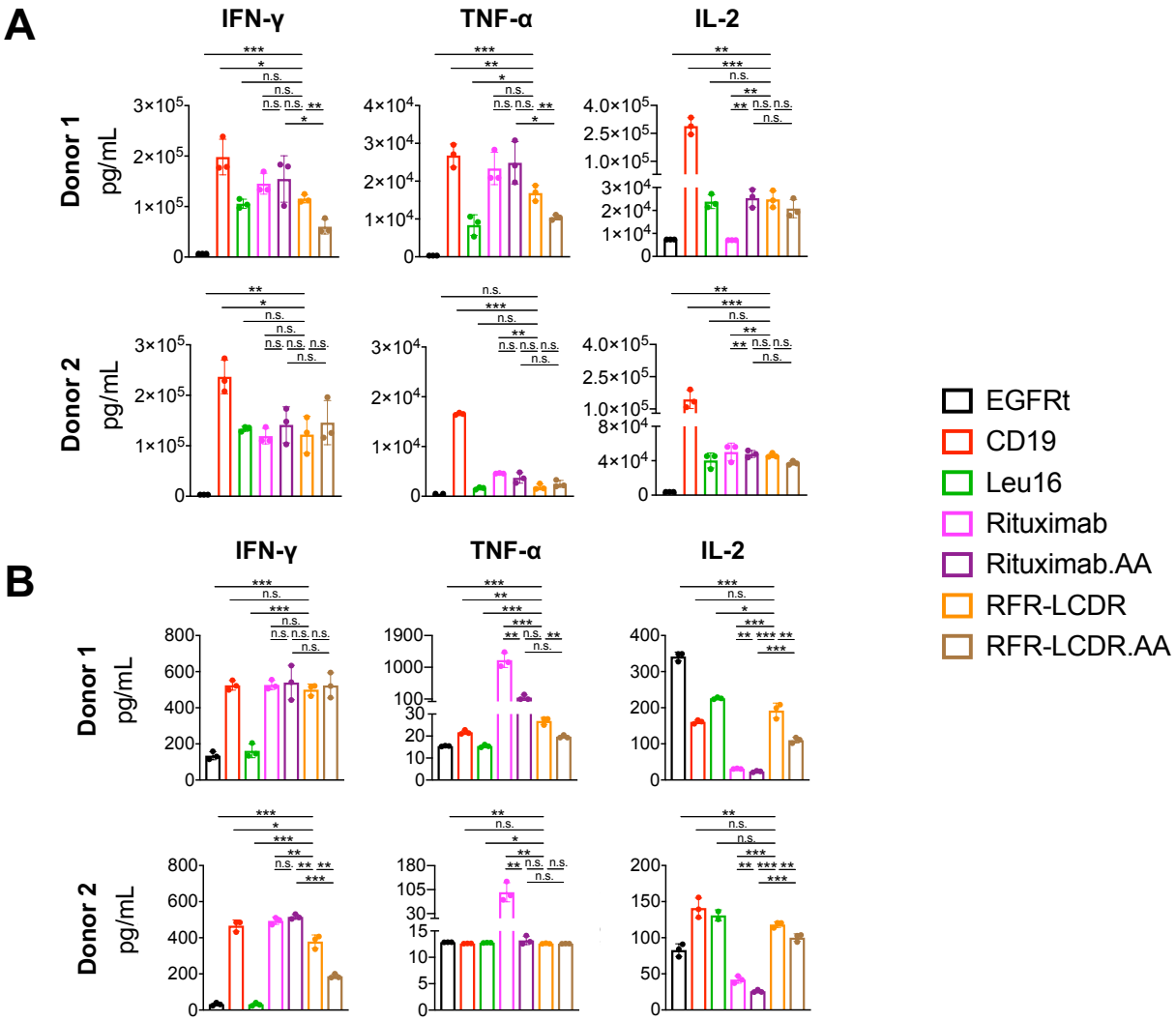

Supplementary Figure 3.S7 ***In vitro*** **characterization of hybrid CAR-T cells**
(A-B) IFN-γ, TNF-α, IL-2 production in the presence (A) and absence (B) of CD19+/CD20+ K562 target cells. *p<0.05, **p<0.01, ***p<0.001, n.s. not statistically significant.

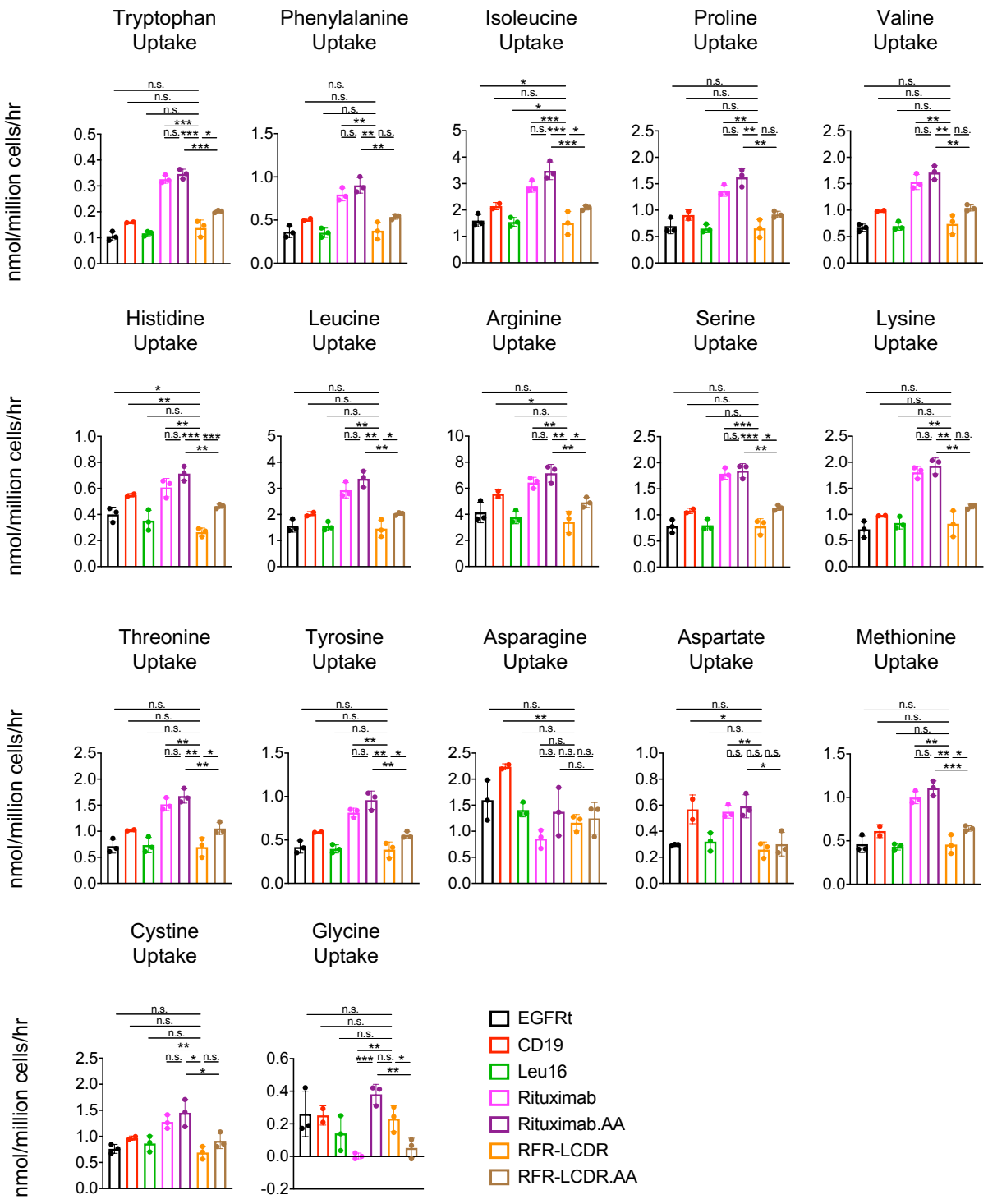

Figure 3.S8 Metabolic activity at rest is strongly associated with tonic signaling Metabolic analysis of CAR-T cells in culture in the absence of antigen stimulation. CAR-T cells were cultured for 72 hours in RPMI supplemented with 10% heat-inactivated, dialyzed fetal bovine serum (HI-dFBS), IL-2, and IL-15. Data bars indicate the means of technical triplicates ± 1 S.D. Data are representative of three independent experiments from three different healthy donors. **p*<0.05, ***p*<0.01, ****p*<0.001, n.s. not statistically significant.

Supplementary Table 3: Amino acid sequences of all anti-CD20 scFvs

Construct Name	Sequences
Leu16 scFv	DIVLTQSPAILSASPGEKVTMTCRASSSVNYMDWYQKKPGSSPKPWI YATSNLASGVPARFSGSGSGTSYSLTISRVEAEDAATYYCQQWSFNP PTFGGGTKLEIKGSTSGGGSGGGSGGGGSSEVQLQQSGAELVKPGA SVKMSCKASGYTFTSYNMHWVKQTPGQGLEWIGAIYPGNGDTSYNQ KFKGKATLTADKSSSTAYMQLSSLTSEDSADYYCARSNYYGSSYWFF DVWGAGTTVTVSS
Rituximab scFv	QIVLSQSPAILSASPGEKVTMTCRASSSVSYIHWFQQKPGSSPKPWIY ATSNLASGVPVRFSGSGSGTSYSLTISRVEAEDAATYYCQQWTSNPP TFGGGTKLEIKGSTSGGGSGGGSGGGGSSQVQLQQPGAELVKPGAS VKMSCKASGYTFTSYNMHWVKQTPGRGLEWIGAIYPGNGDTSYNQK FKGKATLTADKSSSTAYMQLSSLTSEDSAVYYCARSTYYGGDWYFNV WGAGTTVTVSS
GA101 scFv	DIVMTQTPLSLPVTPGEPASISCRSSKSLLHSNGITYLYWYLQKPGQS PQLLIYQMSNLVSGVPDRFSGSGSGTDFTLKISRVEAEDVGVYYCAQ NLELPYTFGGGTKVEIKGSTSGGGSGGGSGGGGSSQVQLVQSGAEV KKPGSSVKVSCKASGYAFSYSWMNWVRQAPGQGLEWMGRIFPGDG DTDYNGKFKGRVTITADKSTSTAYMELSSLRSEDTAVYYCARNVFDG YWLVYWGQGTLVTVSS
Ofatumumab scFv	EIVLTQSPATLSLSPGERATLSCRASQSVSSYLAWYQQKPGQAPRLLI YDASNRATGIPARFSGSGSGTDFTLTISSLEPEDFAVYYCQQRSNWPI TFGQGTRLEIKGSTSGGGSGGGSGGGGSSEVQLVESGGGLVQPGRS LRLSCAASGFTFNDYAMHWVRQAPGKGLEWVSTISWNSGSIGYADS VKGRFTISRDNAKKSLYLQMNSLRAEDTALYYCAKDIQYGNYYYGMD VWGQGTTVTVSS
RFR-LCDR scFv	QIVLSQSPAILSASPGEKVTMTCRASSSVNYMDWFQQKPGSSPKPWI YATSNLASGVPVRFSGSGSGTSYSLTISRVEAEDAATYYCQQWSFNP PTFGGGTKLEIKGSTSGGGSGGGSGGGGSSQVQLQQPGAELVKPGA SVKMSCKASGYTFTSYNMHWVKQTPGRGLEWIGAIYPGNGDTSYNQ KFKGKATLTADKSSSTAYMQLSSLTSEDSAVYYCARSNYYGSSYWFF DVWGAGTTVTVSS
LFR-RCDR scFv	DIVLTQSPAILSASPGEKVTMTCRASSSVSYIHWYQKKPGSSPKPWIY ATSNLASGVPARFSGSGSGTSYSLTISRVEAEDAATYYCQQWTSNPP TFGGGTKLEIKGSTSGGGSGGGSGGGGSSEVQLQQSGAELVKPGAS VKMSCKASGYTFTSYNMHWVKQTPGQGLEWIGAIYPGNGDTSYNQK FKGKATLTADKSSSTAYMQLSSLTSEDSADYYCARSTYYGGDWYFNV WGAGTTVTVSS

Chapter 4 – Summary and Future Work

SUMMARY

In a matter of decades, CAR-T cell therapy has achieved unprecedented success as one of the most promising upcoming modalities in the treatment of cancer (MacKay et al., 2020; Majzner and Mackall, 2019; Yamamoto et al., 2019). However, the consistent clinical success in CARs targeting CD19 has not been replicated in CARs targeting other tumor associated antigens. In this dissertation, our goal was to understand the design parameters that are conducive to CAR-T cell function and investigate protein engineering strategies to optimize CAR design. In Chapter 2, we attempted to develop a high-throughput screening platform that enabled rapid characterization and identification of lead CAR candidates. In our effort to find parameters that allowed screening CAR variants in a pooled culture, we investigated CAR signaling in the presence and absence of antigen stimulation. Antigen-independent signaling, i.e., tonic signaling, has drawn a lot of attention lately and the unique potency of CD19 CAR-T cells might be attributed to its lack of tonic signaling (Frigault et al., 2015; Gomes-Silva et al., 2017; Long et al., 2015; Watanabe et al., 2016). Antigen-dependent T-cell expansion is also an important metric for evaluating efficacy of CARs. In our screening platform, we proposed to incorporate both negative selection of tonic signaling and positive selection of T-cell expansion as functional readouts to enrich for superior CAR variants. This two-step screening platform allowed enrichments of certain CAR candidates. However, contrary to our expectation, elimination of tonically signaling clones did not reduce the library diversity, suggesting that tonic signaling might not be detrimental to CAR-T cell function. Thus, we were particularly interested in evaluating the impact of tonic signaling on CARs as one of the design parameters to generate novel CAR candidates.

In Chapter 3, we demonstrated that a calibrated, non-zero level of tonic signaling was required to promote robust CAR-T cell function. The level of tonic signaling could be tuned by two protein engineering approaches – structure alteration of the CAR's intracellular domain by incorporation of one to four alanines, and scFv sequence hybridization from two CARs. The alanine insertion of a rituximab based, anti-CD20 CAR with strong a tonic signaling phenotype had yielded functionally superior variants that exhibited a calibrated level of tonic signaling and improved *in vivo* function. Furthermore, we proved that the alanine insertion approach was generalizable to a 14g2a, anti-GD2 CAR. In addition to structural alteration, we established that minute changes in the scFv resulted in disparate tonic signaling behavior and the hybridization of two scFvs could generate a CAR with improved *in vivo* anti-tumor function. We hybridized scFvs from leu16 and rituximab to construct a hybrid CAR consisting of the FRs from a tonically signaling rituximab CAR and the CDRs from a non-tonically signaling leu16 CAR. This newly generated CD20 CAR alone and with the alanine-insertion variant exhibited low tonic signaling behavior and improved anti-tumor effect *in vivo*. In particular, the scFv sequence hybridization approach synergized with alanine-insertion to yield an anti-CD20 CAR that outperformed the CD19 CAR *in vivo*. In our effort to evaluate the driving forces of tonic signaling and CAR superiority, we found that elevated metabolic activity at rest was strongly associated with tonic signaling. Functionally superior CARs triggered a calibrated level of metabolic activity and T-cell signaling at rest as well as sustained strong anti-tumor function along with a long-term memory phenotype *in vivo*. This work gives insight on the impact of structure and sequence on CAR-T cell function and the understanding of molecular signatures that are conducive to CAR-T cell function, and provides a robust engineering strategy for generating next-generation CARs.

FUTURE WORK

Elucidating the mechanism of functionally superior CARs

In Chapter 3, we have shown that minute changes in scFv sequences led to disparate tonic signaling profiles and *in vivo* outcome (Figure 3.1B-F). Given that leu16 and rituximab have 91% sequence identity, variation on those limited positions could lead to differential signaling kinetics. Therefore, we would like to further investigate the combinatorial effect of those residues. In addition, we generated a hybrid CAR from scFv sequence hybridization of leu16 and rituximab CARs, which exhibited superior functional performance in Raji xenograft. We attributed the functional superiority of the hybrid CAR to its calibrated, non-zero tonic signaling effect. To eliminate confounding factors in the system, such as differences in scFv binding affinity, we plan to evaluate the binding affinity of leu16, rituximab and the hybrid scFv to the CD20 peptide epitope (INIYNCEPANPSEKNSPSTQYCYSIQS). We have successfully generated CAR variants by tuning their signaling in the presence and absence of stimulation. However, the mechanism of the alteration of signaling transduction, phosphorylation status of CD3ζ, and adaptor proteins remains elusive. Previous studies have shown that each ITAM on CD3ζ has a different contribution to signal transduction (Feucht et al., 2019; Love and Hayes, 2010). Therefore, we are interested in studying the phosphorylation patterns of CAR CD3ζ and their impact on *in vivo* performance.

Improving CAR function for solid tumors by structural manipulation

Despite remarkable successes in treating hematological malignancies, the clinical results of CAR-T cell therapy for solid tumor have been far less encouraging. The challenges of treating solid tumors include the limited persistence of CAR-T cells and the immunosuppressive tumor microenvironments that inhibit CAR-T cell function (Castellarin et al., 2018; Guedan et al., 2018;

Li et al., 2018). To improve CAR-T cell function for solid tumors, extensive efforts have been made to target the immunosuppressive tumor microenvironment and combining CAR-T cells with other therapeutics modalities, e.g., checkpoint blockade, delivery of payload, etc. (Castellarin et al., 2018; Newick et al., 2017; Ribas and Wolchok, 2018). Our study focused on optimizing the CAR sequence and structure to improve therapeutic efficacy. In Chapter 3, we demonstrated a robust, generalizable method to tune T-cell signaling by imposing structural changes on intracellular domain of CAR via alanine insertion. A 14g2a-based GD2 CAR with one, two or four alanine insertions demonstrated improved anti-tumor function in a metastatic neuroblastoma xenograft with the two-alanine insertion yielding the best T-cell persistence *in vivo* (Supplementary Figure 3.S5D-E). Since GD2 is expressed on tumors of multiple disease types, e.g., glioblastoma, osteosarcoma, melanoma, sarcoma, etc., the new GD2 CAR variants could be applied to $GD2^{+}$ solid malignancies as a monotherapy or a combination therapy. We will work on utilizing the robust alanine-insertion strategy to design new CAR variants to improve treatment of solid tumors.

REFERENCES

Castellarin, M., Watanabe, K., June, C.H., Kloss, C.C., and Posey, A.D., Jr. (2018). Driving cars to the clinic for solid tumors. Gene Ther *25*, 165-175.

Feucht, J., Sun, J., Eyquem, J., Ho, Y.J., Zhao, Z., Leibold, J., Dobrin, A., Cabriolu, A., Hamieh, M., and Sadelain, M. (2019). Calibration of CAR activation potential directs alternative T cell fates and therapeutic potency. Nat Med *25*, 82-88.

Frigault, M.J., Lee, J., Basil, M.C., Carpenito, C., Motohashi, S., Scholler, J., Kawalekar, O.U., Guedan, S., McGettigan, S.E., Posey, A.D., Jr*., et al.* (2015). Identification of chimeric antigen receptors that mediate constitutive or inducible proliferation of T cells. Cancer Immunol Res *3*, 356-367.

Gomes-Silva, D., Mukherjee, M., Srinivasan, M., Krenciute, G., Dakhova, O., Zheng, Y., Cabral, J.M.S., Rooney, C.M., Orange, J.S., Brenner, M.K*., et al.* (2017). Tonic 4-1BB Costimulation in Chimeric Antigen Receptors Impedes T Cell Survival and Is Vector-Dependent. Cell Rep *21*, 17-26.

Guedan, S., Ruella, M., and June, C.H. (2018). Emerging Cellular Therapies for Cancer. Annu Rev Immunol *37*, 145-171.

Li, J., Li, W., Huang, K., Zhang, Y., Kupfer, G., and Zhao, Q. (2018). Chimeric antigen receptor T cell (CAR-T) immunotherapy for solid tumors: lessons learned and strategies for moving forward. J Hematol Oncol *11*, 22.

Long, A.H., Haso, W.M., Shern, J.F., Wanhainen, K.M., Murgai, M., Ingaramo, M., Smith, J.P., Walker, A.J., Kohler, M.E., Venkateshwara, V.R*., et al.* (2015). 4-1BB costimulation ameliorates T cell exhaustion induced by tonic signaling of chimeric antigen receptors. Nat Med *21*, 581-590.

Love, P.E., and Hayes, S.M. (2010). ITAM-mediated signaling by the T-cell antigen receptor. Cold Spring Harb Perspect Biol *2*, a002485.

MacKay, M., Afshinnekoo, E., Rub, J., Hassan, C., Khunte, M., Baskaran, N., Owens, B., Liu, L., Roboz, G.J., Guzman, M.L.*, et al.* (2020). The therapeutic landscape for cells engineered with chimeric antigen receptors. Nat Biotechnol *38*, 233-244.

Majzner, R.G., and Mackall, C.L. (2019). Clinical lessons learned from the first leg of the CAR T cell journey. Nat Med *25*, 1341-1355.

Newick, K., O'Brien, S., Moon, E., and Albelda, S.M. (2017). CAR T Cell Therapy for Solid Tumors. Annu Rev Med *68*, 139-152.

Ribas, A., and Wolchok, J.D. (2018). Cancer immunotherapy using checkpoint blockade. Science *359*, 1350-1355.

Watanabe, N., Bajgain, P., Sukumaran, S., Ansari, S., Heslop, H.E., Rooney, C.M., Brenner, M.K., Leen, A.M., and Vera, J.F. (2016). Fine-tuning the CAR spacer improves T-cell potency. Oncoimmunology *5*, e1253656.

Yamamoto, T.N., Kishton, R.J., and Restifo, N.P. (2019). Developing neoantigen-targeted T cell-based treatments for solid tumors. Nat Med 25, 1488-1499